PROGRAMME
FOR
ATMOSPHERIC WATER SUPPLY
(PAWS)

PHASE 1
1983 - 1986 FINAL REPORT

VOLUME 2
Natural Clouds and Rain in Nelspruit

Report to the
Water Research Commission
Pretoria, South Africa

by

Simpson Weather Associates, Inc
Charlottesville Va., USA

Cansas International Corp. (Pty) Ltd
Nelspruit, South Africa

DECEMBER 1986

ISBN : 0 947447 05 9
Set No : 0 947447 08 3

VOLUME II

Natural Clouds and Rain in Nelspruit

Table of Contents

NATURAL CLOUDS AND RAIN IN NELSPRUIT

1.0 INTRODUCTION

The PAWS project has one goal - water.

The project exists only because water is an increasingly valuable resource. The central effort is weather modification; the artificial enhancement of rainfall from cumulus clouds.

PAWS however was designed not only to evaluate the feasibility of making more rain, but also to illuminate the processes which create the natural rainfall along the Drakensberg escarpment. This is a proper mix of two opposing schools of thought on weather modification: one school says that we must understand the natural systems completely before we can attempt to modify them; the other says that we need only to proceed empirically, say by performing randomized tests of cloud treatments. The first is clearly wrong; we would have no medical technology at all if this were so. And the second, though undoubtedly being of greater merit, is a bit too extreme and would lead to mindless and expensive probing in the dark. In fact, the more scientific learning that one builds into weather modification evaluations, the more focussed each succeeding step becomes.

PAWS was set up with equipment and personnel capable of navigating this middle ground of research, and as a result has produced a vast pool of information on which to base a first, tentative description of the rainfall processes of the Eastern Transvaal Escarpment.

It is proper to present these results in a volume of their own, because they are expected to have a value of their own, independent of the results of our efforts at modifying the clouds for economic benefit. They are also expected to be of interest to a wider audience than that concerned with weather modification. A knowledge of the structure and composition of clouds and of the factors determining their behaviour must benefit the fields of aviation, forecasting, climatology, hydrology, agricultural meteorology, to name only a few.

We follow a scheme based on the instrument systems employed in the research: first the rainfall is described as it appears to instruments on the ground; then the associated meteorological influences are dealt with; then the storms are described as seen through the eyes of radar and, from within, by the instrumented aircraft.

2.0 A DESCRIPTION OF PAWS STUDY AREA RAINFALL (Garstang and Emmitt)

In this section we describe the rainfall in the Paws study area in terms of :

* rainfall amounts
* rainfall rates
* temporal distributions, e.g. climatic, annual/seasonal diurnal

Current raingauge networks are not adequate for resolving seeding reponses - the nonrecording gauges have long periods of record (about 50 years) but lack temporal resolution; the recording gauges have just the reverse. At this time, the seeding response is sought in the aircraft microphysical data (Volume 3, Section 2), and the PAWS 5 cm radar data (Volume 3, Section 3). The radar estimated rain volume (RERV) and area time integral (ATI) come closest to providing an estimate of rainfall response to seeding. However, the radar data is biased towards daytime rainfall on days that presented seeding opportunities. Therefore, our description of rainfall relies primarily upon the raingauges for most of the statistics dealing with climate, annual, seasonal and diurnal variations. Spatial rainfall variations and storm characteristics are documented with both the raingauges and the radar.

2.1 Data Base

Rainfall in the PAWS study area is described in terms of data obtained from the following sources:

a. South African national raingauge network (1931-1985). Nearly 80 gauges providing daily total rainfall data in and near the PAWS study area are available for this time period. Seventeen of these gauges have records that are sufficient to use in describing the rainfall in the primary operations area (Fig. 2.1.0)

b. PAWS Badplaas Valley recording raingauge network (1982-1986). Sixteen recording (5 minute totals) raingauges were deployed in a 30 x 30 km area shown in Fig. 2.1.0

c. PAWS meso-network recording raingauges (1984-1986). Nine recording (5 minute totals) gauges were co-located with 10 metre meteorological towers distributed over the escarpment region (Fig. 2.1.1)

d. PAWS 5 cm radar located at Nelspruit (1982-1985). The radar has been operating since 1971. However only the data for this abbreviated time period is available in the format needed for the rainfall analysis.

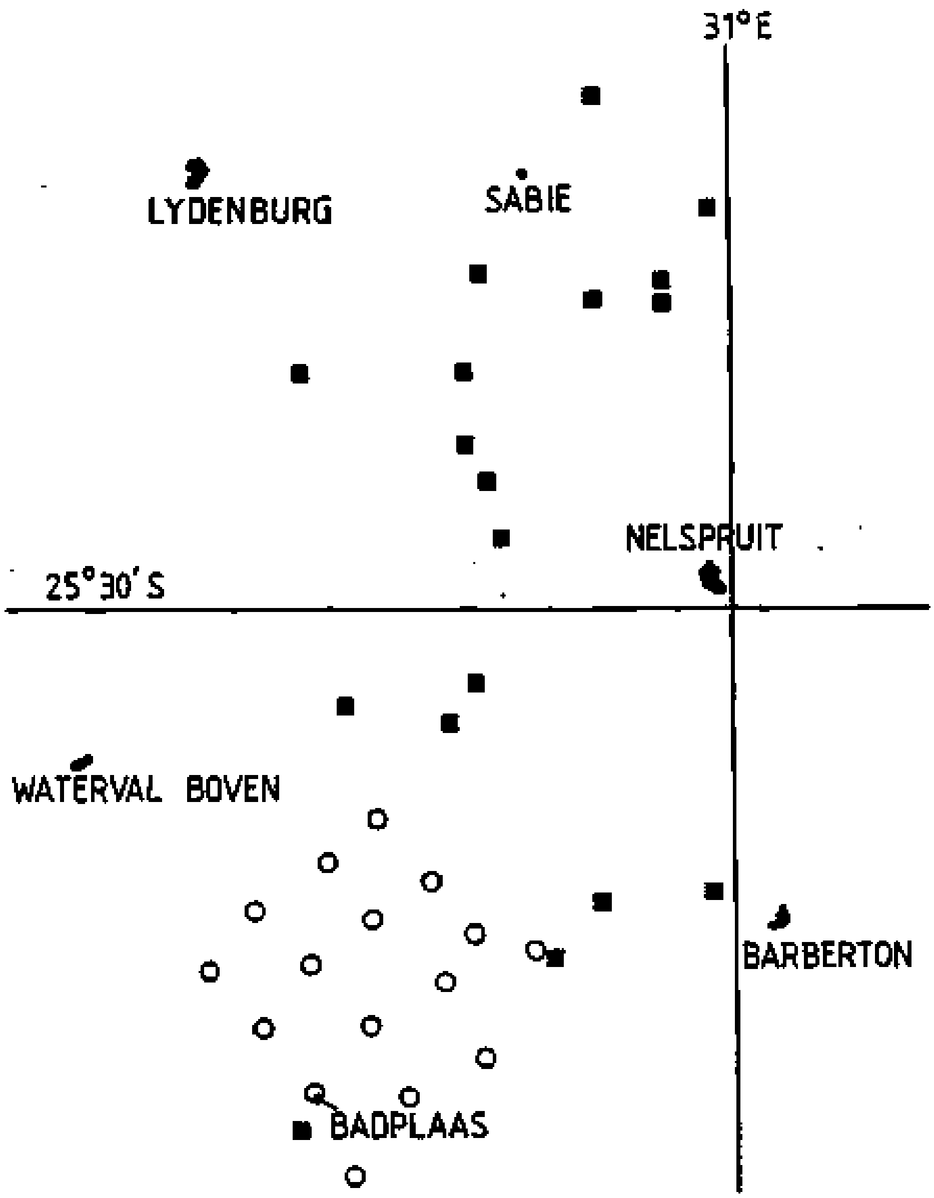

Figure 2.1.0. Distribution map for 18 National rain gauges (■) and 16 PAWS recording rain gauges (O) used in describing rainfall patterns in the PAWS study area (1 cm = 8 km).

2.2 Climatic and annual variations in rainfall

The general description of rainfall in the PAWS study is obtained from the national gauges located in the region outlined in Fig. 2.2.0 The PAWS area is enclosed primarily by blocks 517, 518, 519, 554, 555, and 556. The annual average rainfall (mm) shown in Fig. 2.2.1 depicts:

a. general rainfall maximum (1000 mm/yr) aligned N/S along the escarpment,

b. a local maximum of 1100 mm/yr in an area near Sabie just north of Nelspruit, and

c. strong E/W gradients of annual rainfall amounts to the east of Nelspruit.

Temporal variations in annual rainfall amounts are characterized by wet and dry sequences of years which have a dominant period near 18-20 years (Fig. 2.2.2). Other shorter periods of 26-36 months and 13-14 months have been resolved by Kelbe, et al., 1983. The 50 year length of record used precludes the detection of longer periodicities or trends. Longer periods or trends have been detected elsewhere at these latitudes and are probably present in the eastern Transvaal. The wet and dry periods seen in the eastern Transvaal show marked variation in amplitude depending upon the location, size of area, and portion of the rainfall record examined. In general, the annual rainfall totals vary more over the escarpment and lowveld than over the highveld that lies above 1500 metres (Fig. 2.2.3).

Using the 18 gauges that provide data covering the period 1930-1985, we see a somewhat noisier time series (Fig. 2.2.4) than those in Fig. 2.2.2 which were based upon many more gauges. However, the rainfall variation conforms to the wet-dry cycles described by Tyson (1980) and suggests that the PAWS study (82-86) was conducted during a generally dry period. Data after March 1985 have not been obtained at this time. The possible significanbe of having conducted the experiment in either drier or wetter than normal seasons is examined in Section 2.4.

2.3 Monthly and seasonal variations in rainfall

Based upon 55 years of data from the rain gauges in Fig. 2.1.0 summer (October-March) rainfall accounts for approximately 85% of the annual total. The monthly distribution of summer rainfall (Table 2.1) shows:

a. a maximum in December (175 mm) and January (181 mm)
b. maximum rainfall variability occurring in February, minimum in December.

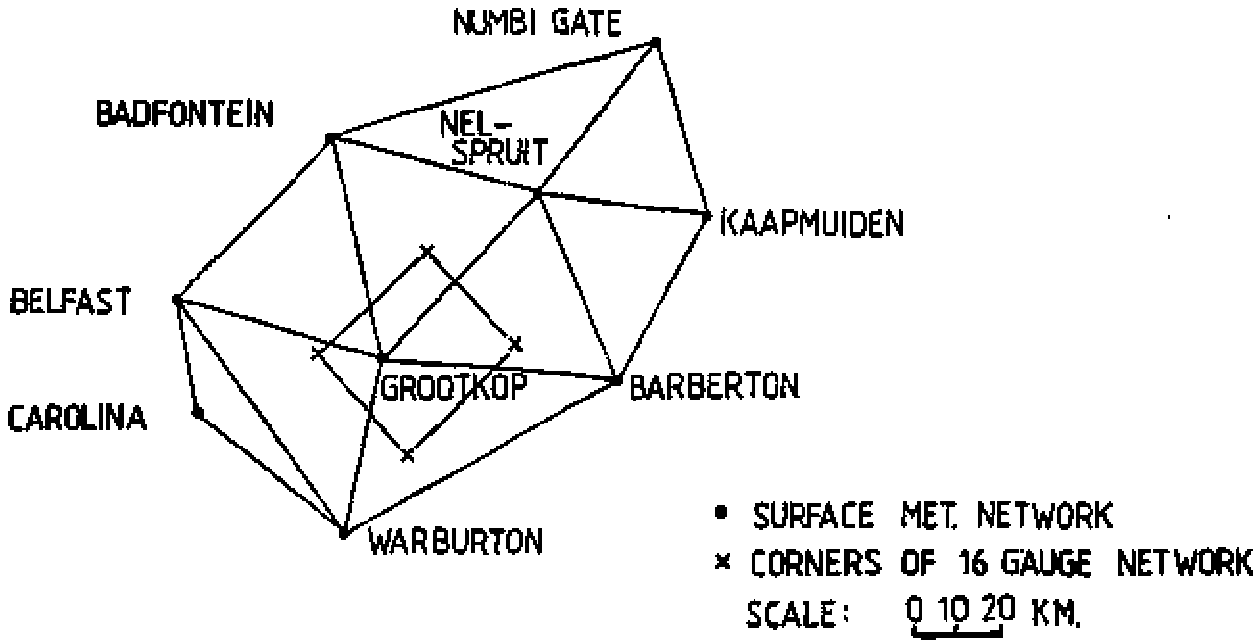

Figure 2.1.1. Distribution map for the nine stations in the PAWS mesoscale surface network. The (x) marks the corners of the 16 gauge Badplaas network.

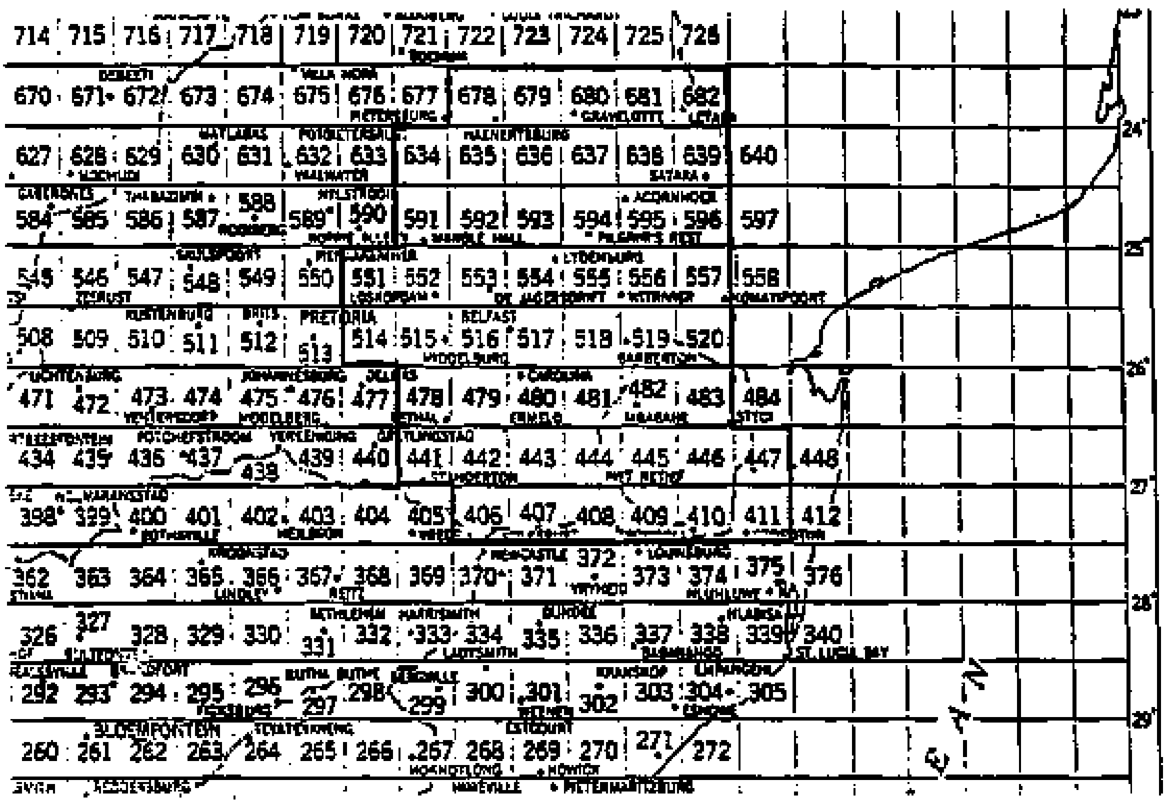

Figure 2.2.0. Map of a portion of the national rain gauge network reporting blocks (30' long x 30' lat).

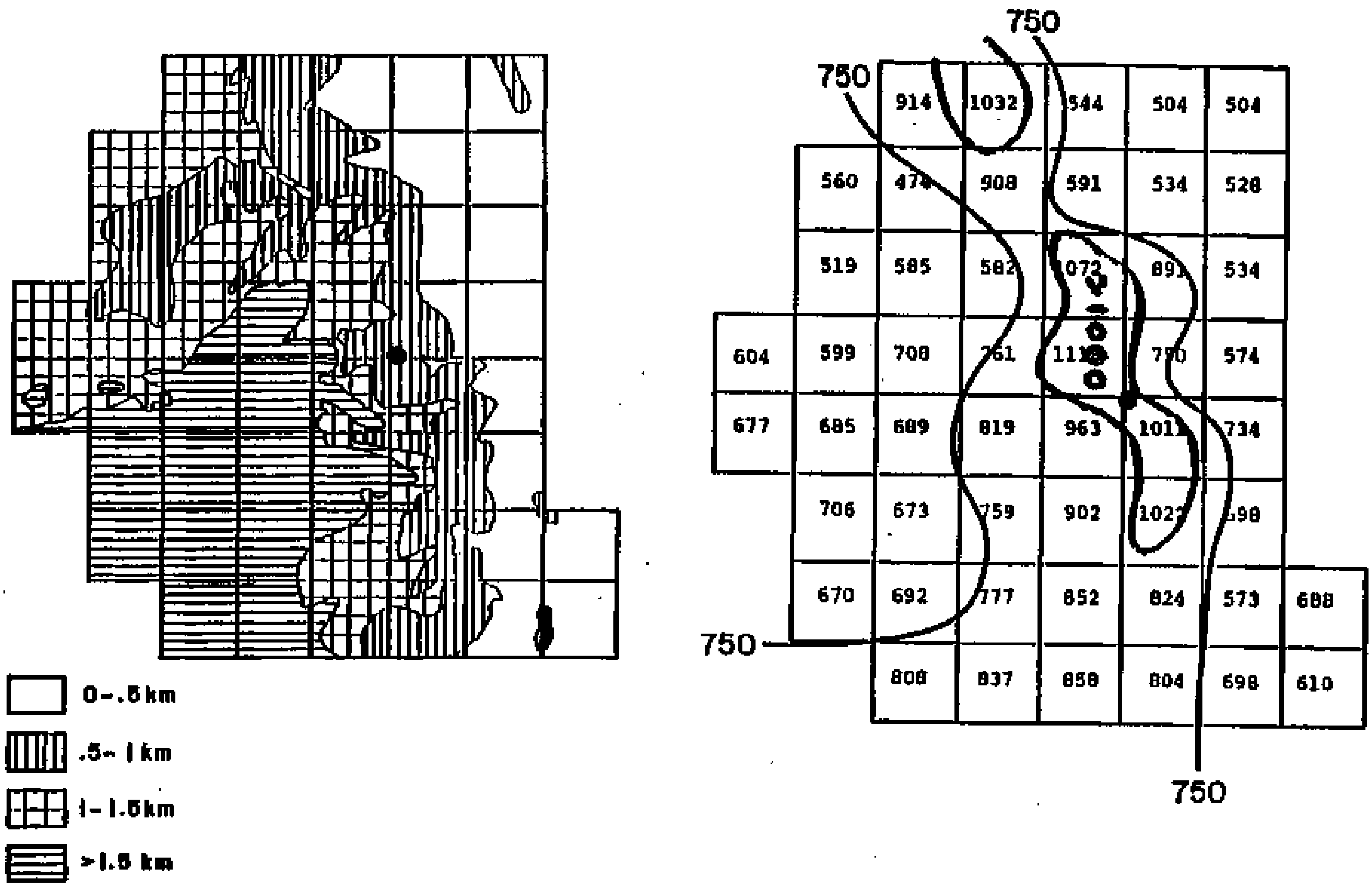

Fig. 2.2.1. Overlay of national raingage reporting blocks on topographical contour map (left); isohets for 750 and 1000 mm/year overlaid on 50 year (1930-1979) average rainfall (mm) for each recording block. ● denotes location of Nelspruit.

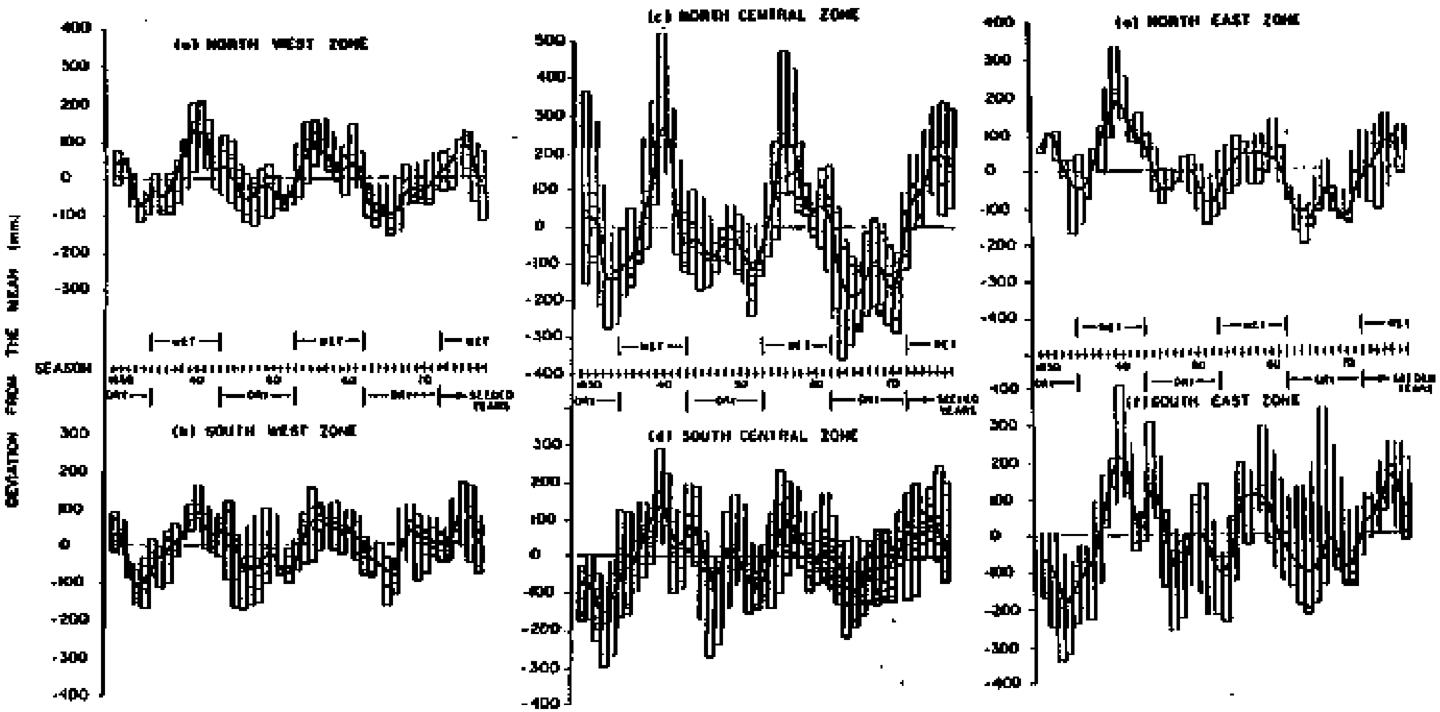

Fig. 2.2.2.The superimposed, smooth departures of the annual block rainfall values from the block means; for the six zones within the outlined area in Figure 2.3. Each horizontal bar in the overall envelope represents one block's departure. Smoothing was accomplished using a 5-term, low pass, binomial filter. The wet and dry period annotation is based upon Tyson (1980) (from Kelbe, et al., 1983).

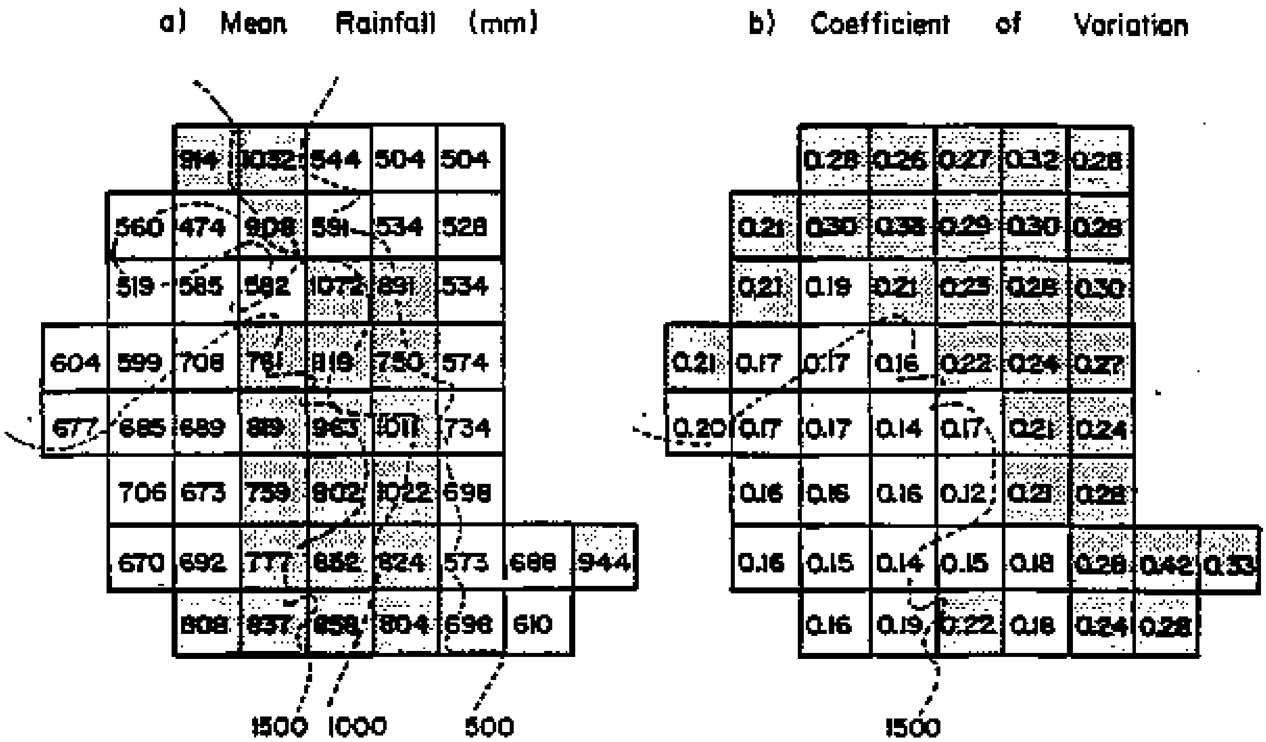

Fig. 2.2.3. (a) The 48-year mean annual rainfall for the 30' latitude by 30' longitude blocks. The 1500, 1000 and 500 m surface elevation contours are also shown. Shaded blocks > 750 mm.

(b) The coefficient of variation ($C_v = \sigma_x/\bar{x}$) for the 48 year series of each block. Also shown is the 1500 m surface elevation contour. Shaded blocks C_v > 20%.

TIME SERIES OF MEAN SUMMER RAINFALL OVER 18 ESCARPMENT GAGES

MEAN = 811 mm

STD DEV = 175 mm

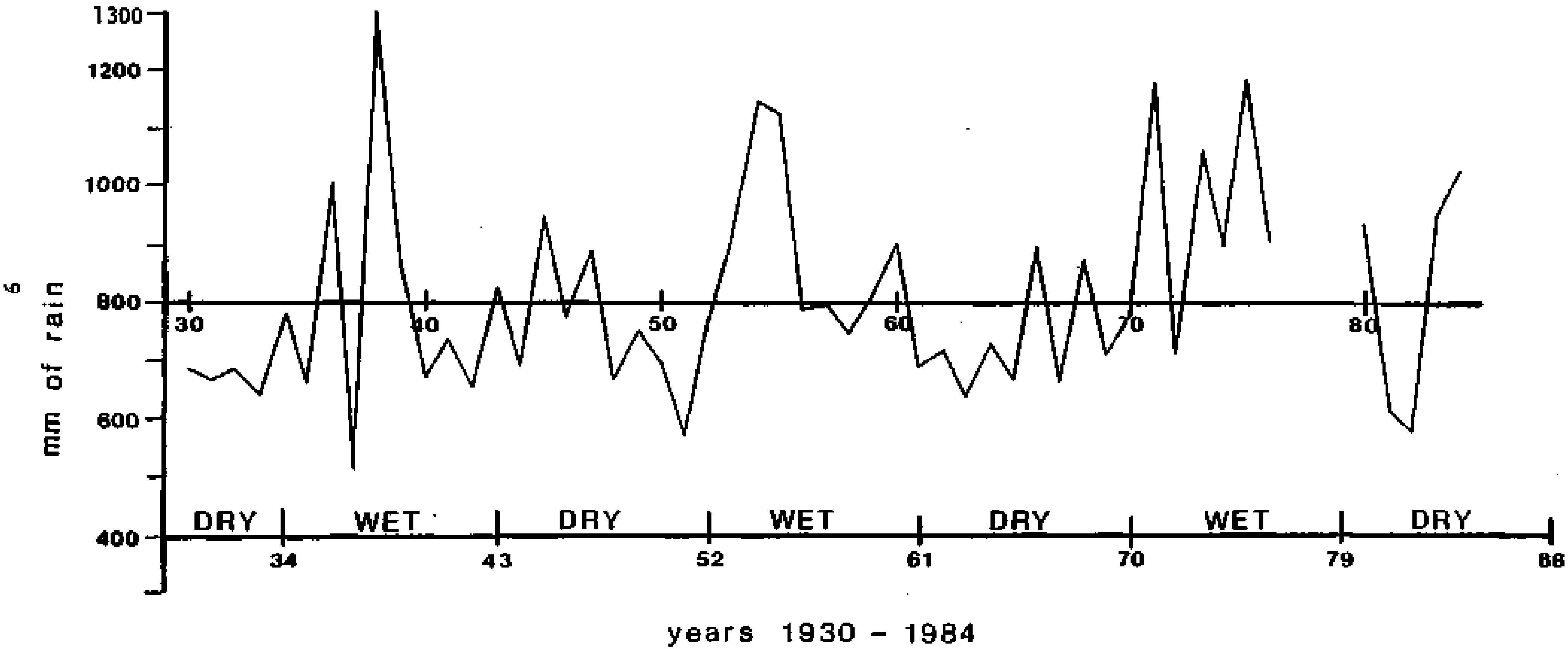

Fig. 2.2.4. Time series (1930-1984) of mean summer (1 Oct to 31 Mar) rainfall over 18 of the national network gages (see Fig. 2.1). Dry and wet periods are those described by Tyson (1980) and Kelbe et al. (1983).

Table 2.1 Summer monthly rainfall based on 55 years of data

	Mean (mm)	Standard Deviation (mm)	Dispersion
Oct	83.4	35.7	.43
Nov	154.3	59.8	.39
Dec	175.0	63.9	.37
Jan	181.1	78.0	.43
Feb	159.2	95.0	.60
Mar	112.7	47.9	.42

2.4 Daily rainfall variation

To answer the question "What are the differences in the manner in which rain falls between wet and dry years?" a 31 gauge subset of the non-recording national gauges was used to characterize the rain that fell on any given day. The 31 stations were chosen because they had a record of sufficient length (30 years) and were all near the same elevation (1000 m). Wet and dry years were defined as +- 100 mm/year deviations from the 30 year average.

By looking at the cumulative rainfall vs. the number of raindays we find very little difference between wet and dry years (Fig. 2.4.0). Regardless of the annual rainfall, it appears that:

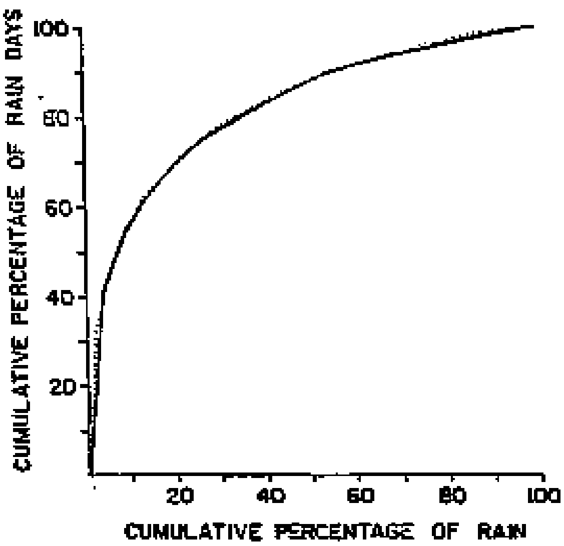

Figure 2.4.0. Cumulative percentage rain days and amount of rain for wet years (mean summer season rainfall greater than 800 mm, solid) and dry years (mean summer season rainfall less than 600 mm, dotted).

a. the top 12% of the raindays (ranked by mm/day) produce 50% of the annual rainfall, and

b. the lowest 50% of the raindays produce only 8% of the rainfall.

If we look at rainfall in terms of rainfall per station per day a very significant difference in wet and dry years is revealed. Two basic types of raindays were defined: Class I, a day when the rainfall was 15 mm/day or greater averaged over 31 gauges; Class II, a day when the rainfall was 7.5 mm/day or greater averaged over the 31 gauges. A summary of the statistics for all raindays, Class I and Class II raindays is provided in Table 2.2. From this table we conclude that:

a. the total number of raindays (greater than .1 mm) does not vary significantly from wet (157.5) to dry (148.6) years;

b. a more significant difference is in the number of Class I and Class II raindays, i.e. there are half the number of these days in dry years as in wet years;

c. the month of February has the greatest difference (wet to dry years) in the occurrence of significant raindays;

d. the month of March has the least difference between wet and dry years.

Another way of expressing the relationship between wet and dry years and the number of Class I days is given in Fig. 2.4.1. It is clear that the larger the deviation of annual rainfall, the greater the change in the number of Class I raindays.

Examination of the daily contributions to seasonal rainfall without reference to Class I or Class II days indicates that dry years are distinctly different from wet years in terms of rain days of 10 mm/day or greater (Fig. 2.4.2).

Perhaps most significant for hydrologic interests, is the result that dry and wet years are quite different in the number of consecutive Class I and Class II rainfall days (Fig. 2.4.3).

From the above we conclude that the primary difference between wet and dry years is not the number of raindays but the number and sequences of days with more than 7.5 mm/station.

Table 2.2. Number of stations out of 31 reporting average rainfall ≥ 0.1 mm, ≥ 7.5 mm and ≥ 15 mm per day based on 13 wet years and 11 dry years for each season and summer month for wet and dry years. The numbers in parentheses are the ratio of the dry versus wet years for rain days and for number of stations reporting rain.

	ALL RAIN DAYS					DAYS > 7.5 mm RAIN					DAYS > 15.0 mm RAIN				
	# of Rain Days		# of Stations Reporting	# of Stations Per Day		# of Rain Days		# of Stations Reporting	# of Stations Per Day		# of Rain Days		# of Stations Reporting	# of Stations Per Day	
WET YEAR	157.5		1897	12.0		39.6		925	23.4		18.2		443	24.3	
		(.94)			(.75)		(.56)			(.88)		(.40)			(.86)
DRY YEAR	148.6		1340	9.0		22.3		459	20.6		7.3		153	21.0	
WET OCT	23.9		266	11.1		3.5		83	23.7		1.0		25	25.0	
		(.86)			(.76)		(.57)			(.91)		(.50)			(.80)
DRY OCT	20.5		172	8.4		2.0		43	21.5		0.5		10	20.0	
WET NOV	26.0		336	12.9		6.8		157	23.1		2.5		63	25.2	
		(.97)			(.71)		(.54)			(.84)		(.44)			(.83)
DRY NOV	25.3		232	9.2		3.7		72	19.5		1.1		23	20.9	
WET DEC	28.1		339	12.1		6.8		179	26.3		3.8		105	27.6	
		(.98)			(.77)		(.56)			(.97)		(.37)			(.70)
DRY DEC	27.6		257	9.3		3.8		97	25.5		1.4		27	19.3	
WET JAN	27.8		332	11.9		8.5		187	22.0		4.2		99	23.6	
		(.98)			(.76)		(.55)			(.86)		(.31)			(.85)
DRY JAN	27.3		248	9.1		4.7		89	18.9		1.3		26	20.0	
WET FEB	24.8		336	13.5		9.1		209	23.0		4.4		108	24.5	
		(.95)			(.67)		(.35)			(.82)		(.32)			(.85)
DRY FEB	23.5		213	9.1		3.2		60	18.8		1.4		29	20.7	
WET MAR	26.8		289	10.8		4.8		111	23.1		2.5		59	23.6	
		(.91)			(.82)		(1.0)			(.89)		(.68)			(.95)
DRY MAR	24.5		218	8.9		4.8		99	20.6		1.7		38	22.4	

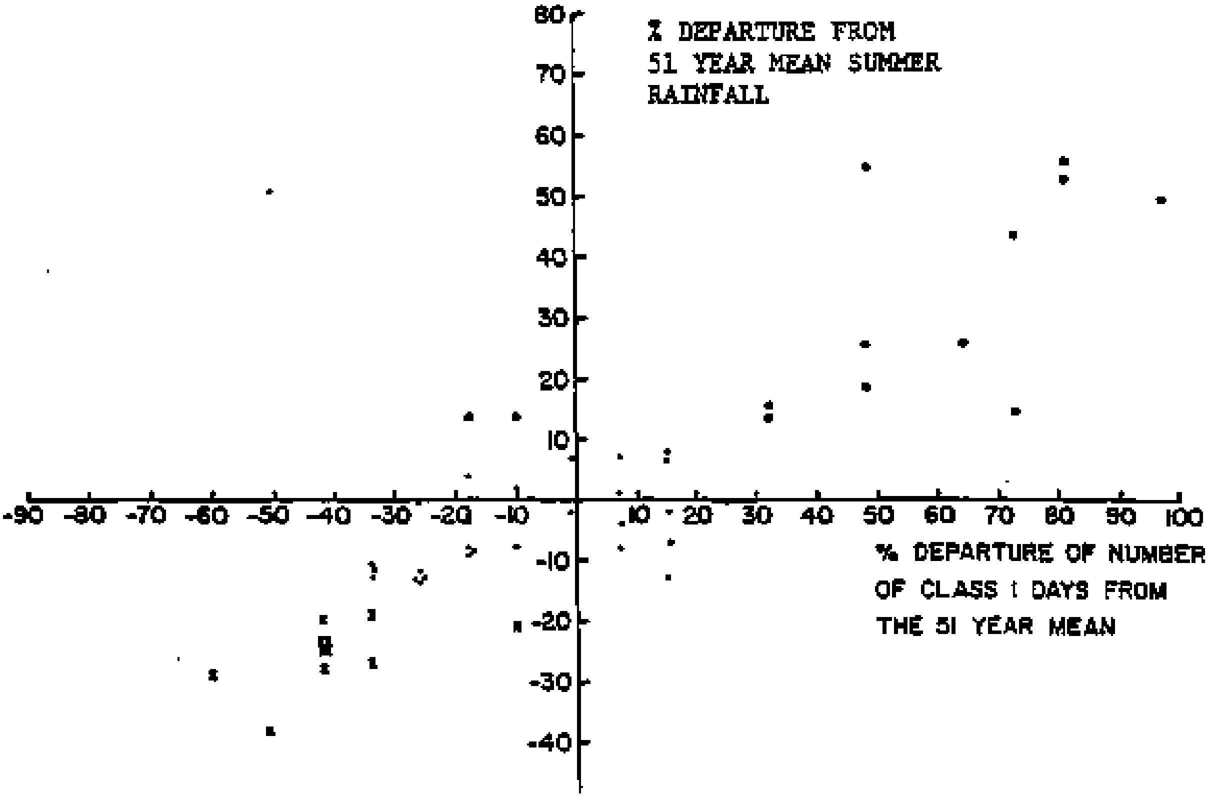

Figure 2.4.1. Percent departure of the summer rainfall from the 51 year annual mean rainfall and the percent departure of the number of Class 1 days from the 51 year mean number for dry (crosses), wet (circles) and normal (dots) for Class 1 days.

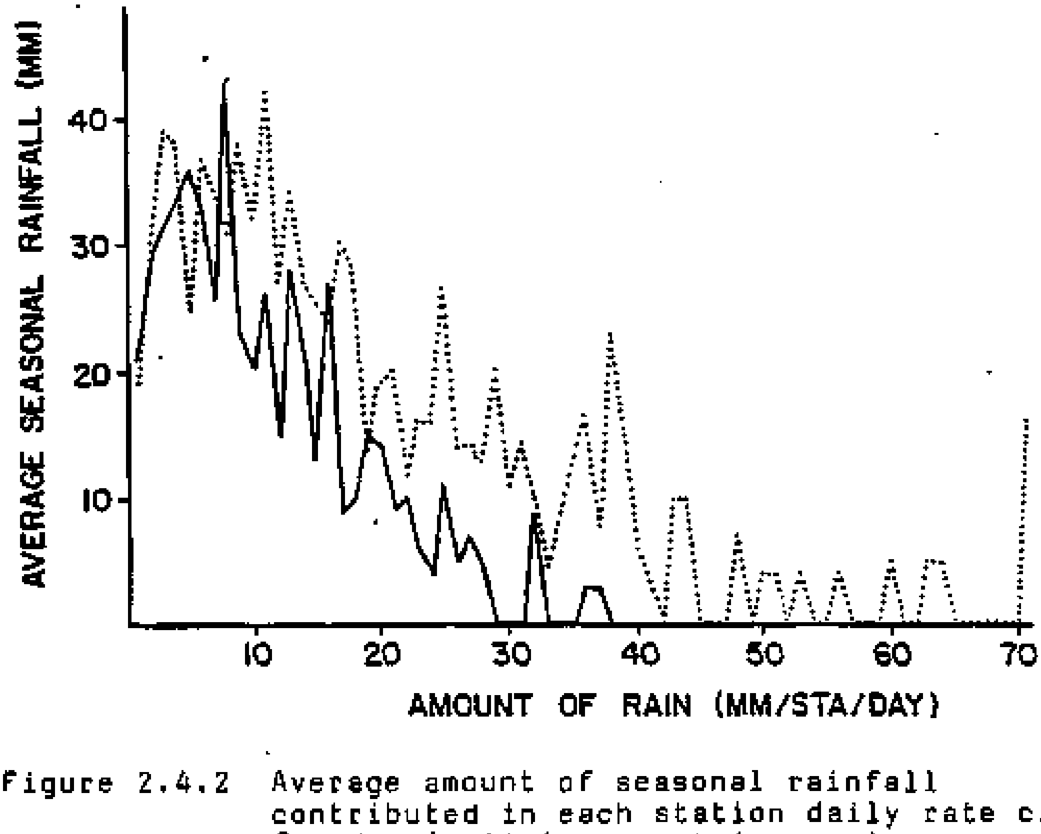

Figure 2.4.2 Average amount of seasonal rainfall contributed in each station daily rate class for dry (solid) and wet (dotted) years.

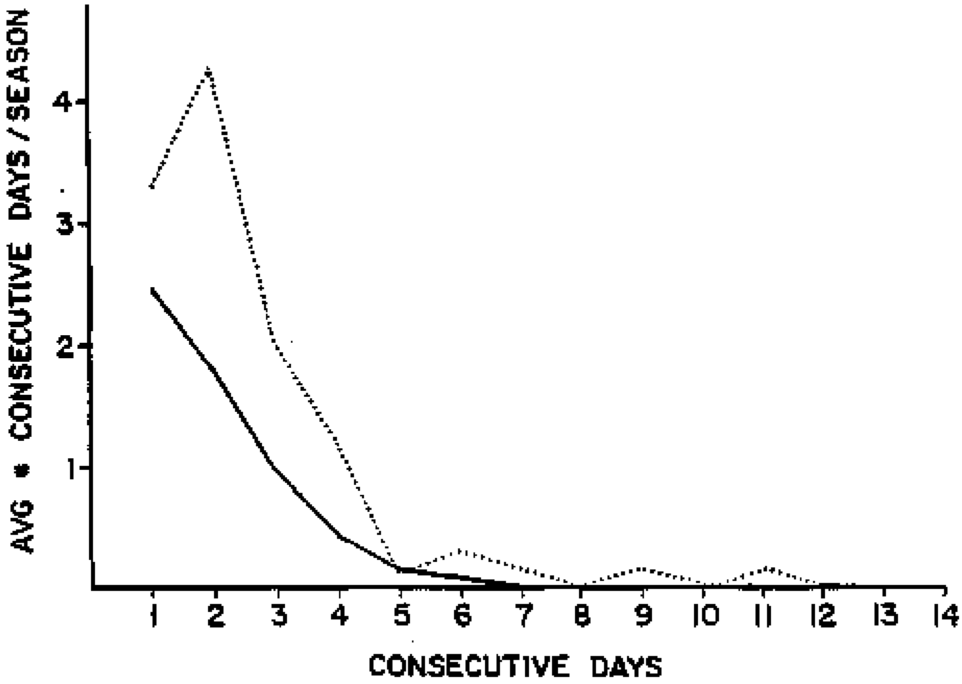

Fig. 2.4.3. Average number of consecutive days with rain per season where the consecutive days consist of clusters of Class I and Class II days as defined in the text. Wet years - dotted line; dry years - solid line.

2.5 Diurnal variations in rainfall

Both the 16 gauges clustered in the Badplaas valley and the 9 gauges spread over the PAWS study area show a clear diurnal pattern in the rainfall amounts and rainfall rates. Data from the Badplaas network and four seasons (82/83, 83/84, 84/85 and 85/86) are shown in Figs. 2.5.0 through 2.5.7. Several points can be made with these 8 figures:

a. 80% of the summer rain falls between noon and midnight

b. Three of the four seasons have two peaks in the rainfall, afternoon (1200-1600 LST) and early evening (1800-2200 LST). The two peaks are most clearly evident in the diurnal distribution of convective rain rates.

Examination of the diurnal rainfall distributions at the 9 meso-network stations indicates (only one good season of data - 85/86) that afternoon and evening rainfall maxima are common to all of the escarpment stations including Warburton and Belfast (Fig. 2.5.8). However, as one moves eastward the distributions show shifts of rain into the early morning hours (Nelspruit and Barberton) and eventually very little diurnal variations at the most eastern stations of Numbi and Kaapmuiden. This pattern is

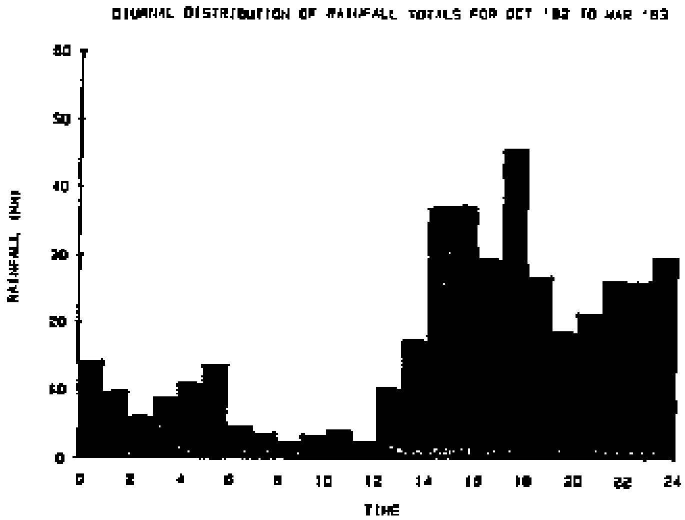

Fig. 2.5.0. Diurnal distribution of 82/83 summer rainfall in the 16 gauge PAWS network located in the Badplaas valley. Rainfall (mm) is the average over the gauge for each hour of the day.

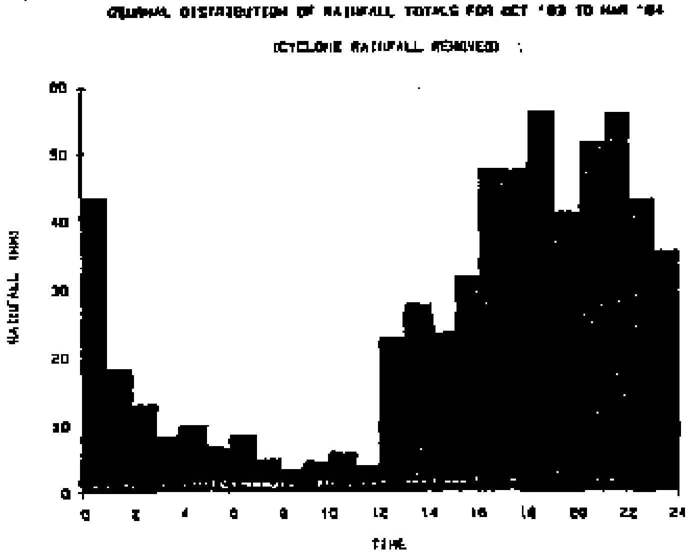

Fig. 2.5.1. Diurnal distribution of 83/84 summer rainfall in the 16 gauge PAWS network located in the Badplaas valley. Rainfall (mm) is the average over the gauges for each hour of the day.

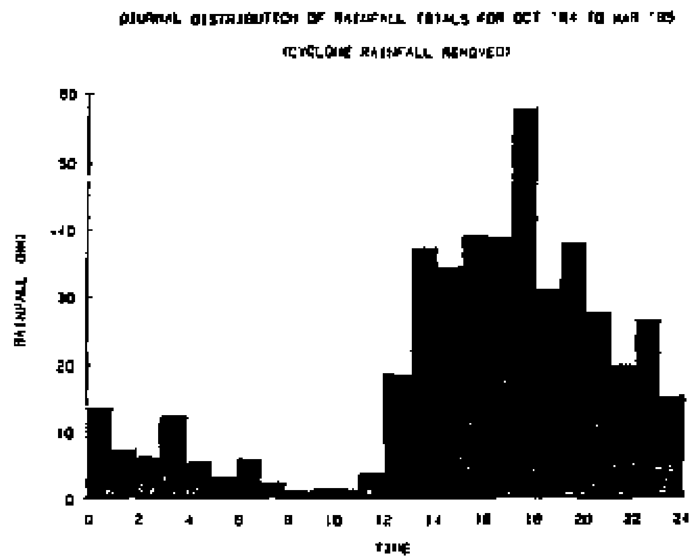

Fig. 2.5.2. Diurnal distribution of 84/85 summer rainfall in the 16 gauge PAWS network located in the Badplaas valley. Rainfall (mm) is the average over the gauges for each hour of the day.

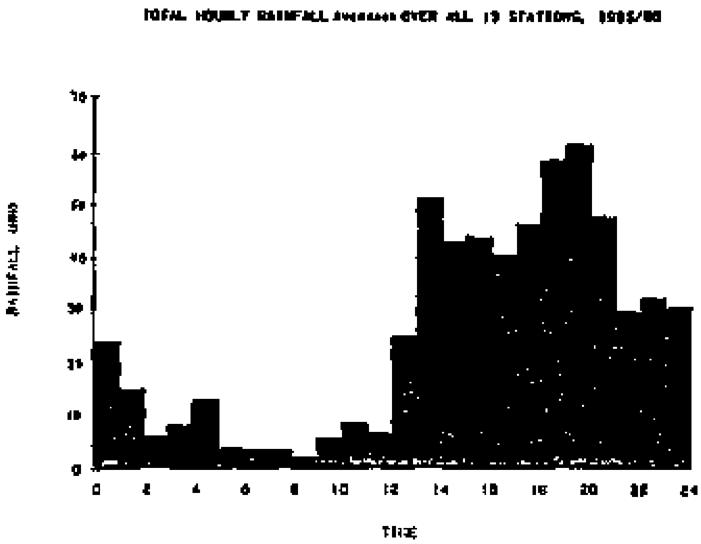

Fig. 2.5.3. Diurnal distribution of 85/86 summer rainfall in the 16 gauge PAWS network located in the Badplaas valley. Rainfall (mm) is the average over the gauges for each hour of the day.

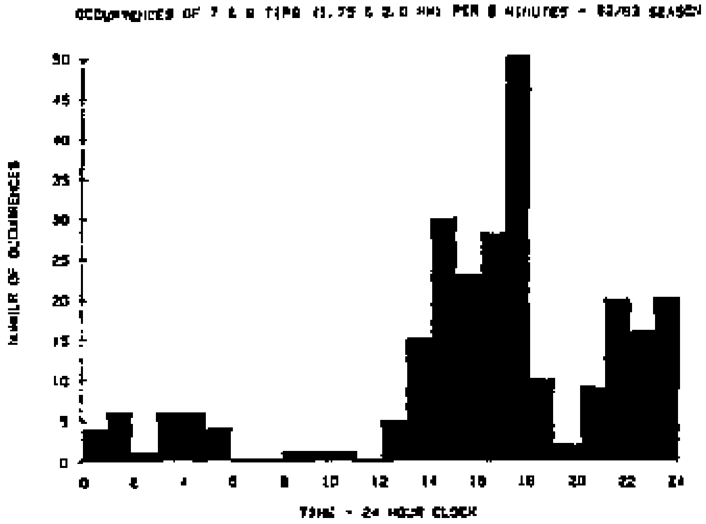

Fig. 2.5.4. Diurnal distribution of convective rain rates between 21 and 24 mm/hr for the 82/83 summer season. Number of occurrences is for the entire season.

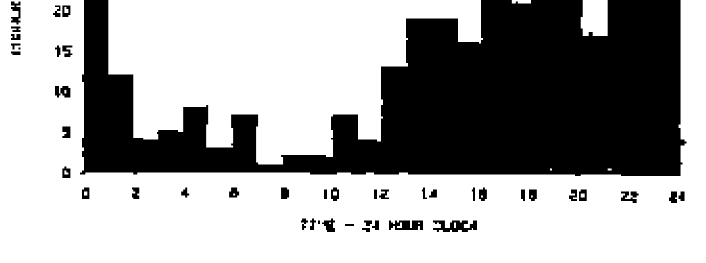

Fig. 2.5.5. Diurnal distribution of convective rain rates between 21 and 24 mm/hr for the 83/84 summer season. Number of occurrences is for the entire season.

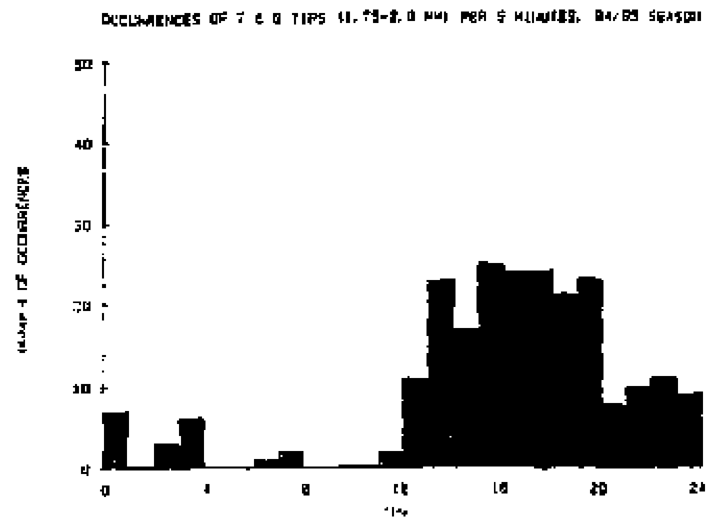

. Fig. 2.5.6. Diurnal distribution of convective rain rates between 21 and 24 mm/hr for the 84/85 summer season. Number of occurrences is for the entire season.

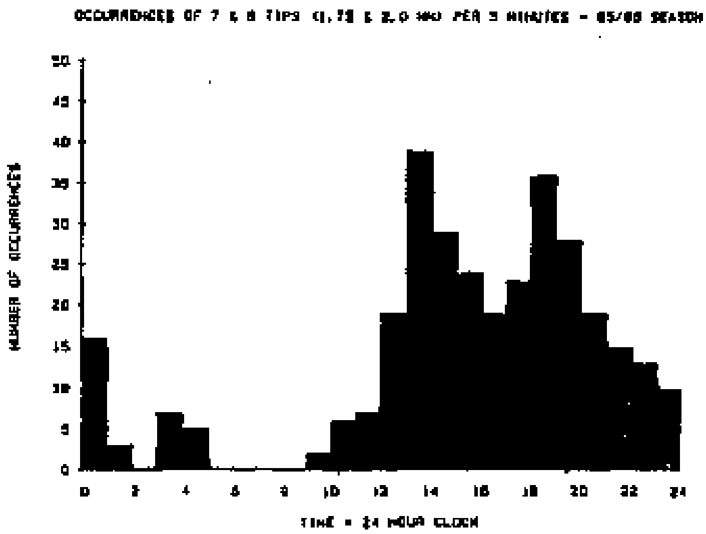

Fig. 2.5.7. Diurnal distribution of convective rain rates between 21 and 24 mm/hr for the 85/86 summer season. Number of occurrences is for the entire season.

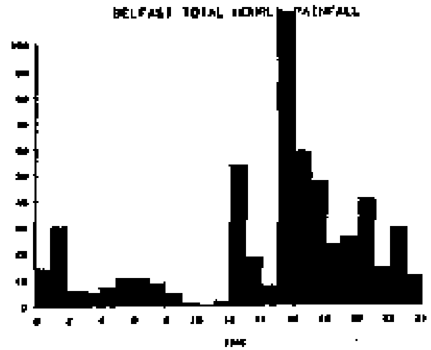

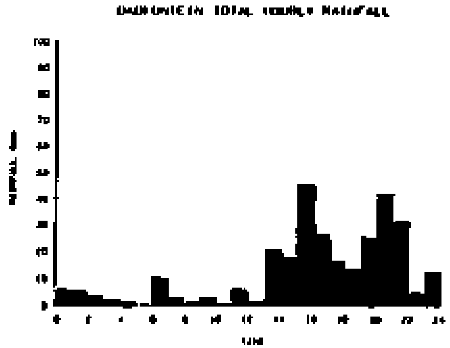

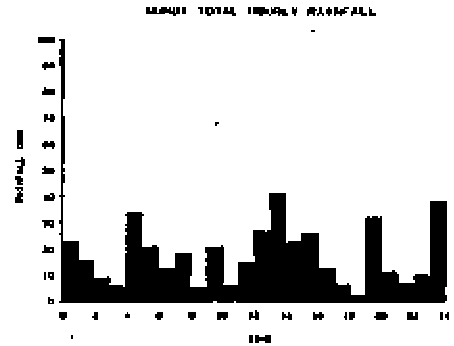

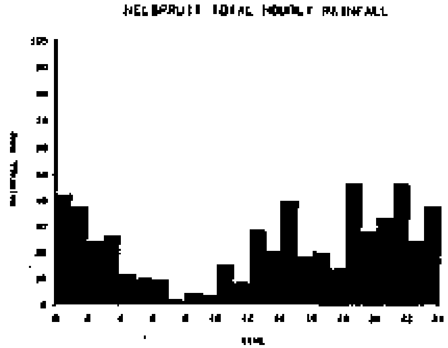

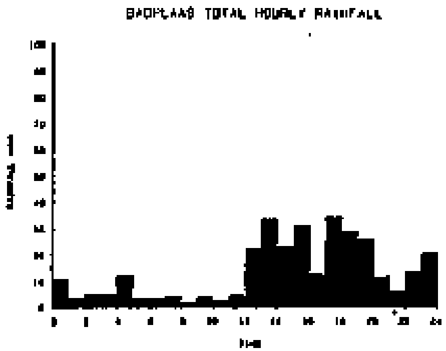

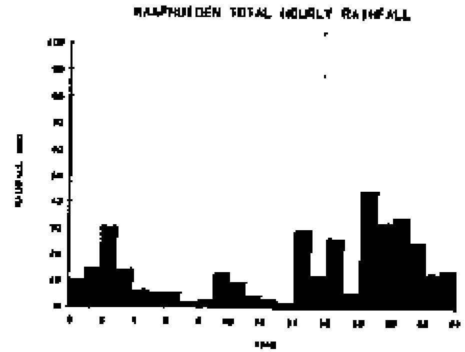

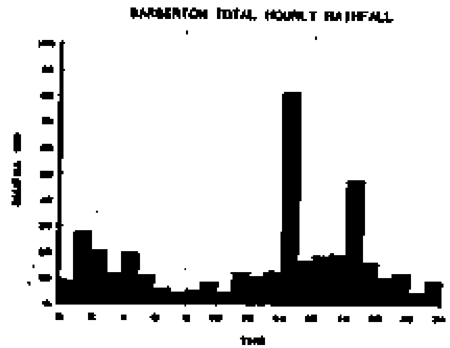

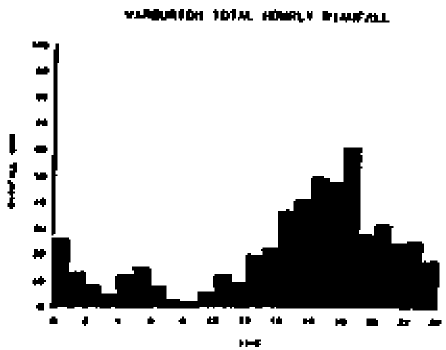

Fig.2.5.8. Diurnal distribution of rainfall at 8 of the PAWS surface network stations for the 85/86 season. Rainfall is in total mm per hour of the day. Plots are arranged to approximate the relative locations described in Figure 2.2.

consistent with the argument that the diurnal variations are primarily tied to mesoscale forcing along the eastern slopes of the escarpment (see Volume II, Section 3).

2.6 A description of rainfall over a dense raingauge network based on a biplot presentation (Mather)

One of the most efficient ways of plotting matrices of meteorological data is the biplot (Gabriel, 1972). A principal component analysis of the two seasons of rainfall data is performed using the covariance matrix. Since over 90 percent of the variance is explained by the first two components, a biplot of these components is a useful way of providing a visual display of the patterns existing in the data. The matrix used in the analysis is hourly rainfall averages from the 16 stations, a 16 by 24 matrix. The loadings were calculated on the stations and the scores on the hours. The data are biplotted in Fig. 2.6.0.

The following rainfall characteristics are displayed in this plot:

a. The length of the hour vector is a function of the standard deviation of the rainfall for that hour (a 14:00 hour vector represents the rainfall that fell between 13:00 and 14:00). Since a characteristic of convective rainfall is its variability, long hour vectors signify convective rainfall. The first significant fall of convective rainfall occurs between 13:00 and 14:00 (14:00 hour vector). Relatively long hour vectors persist through until about 22:00 after which rainfall over the network wanes.

This pattern suggests that most of the convection affecting the network is thermally forced and that this convection produces most of the rain. The diurnal cycle is also displayed on this plot since the component of the hour vector resolved along the x axis is directly proportional to the average network rainfall for that hour.

b. The stations are strung out along the y axis in roughly the same manner in which they are geographically grouped north to south. This seems to be a characteristic of these plots even though location information does not enter into the calculation. Rainfall increases from left to right on this diagram, so stations further to the right receive on average more rainfall. The fact that the stations are grouped in a narrow vertical column indicates that similar amounts of rainfall are received by all stations.

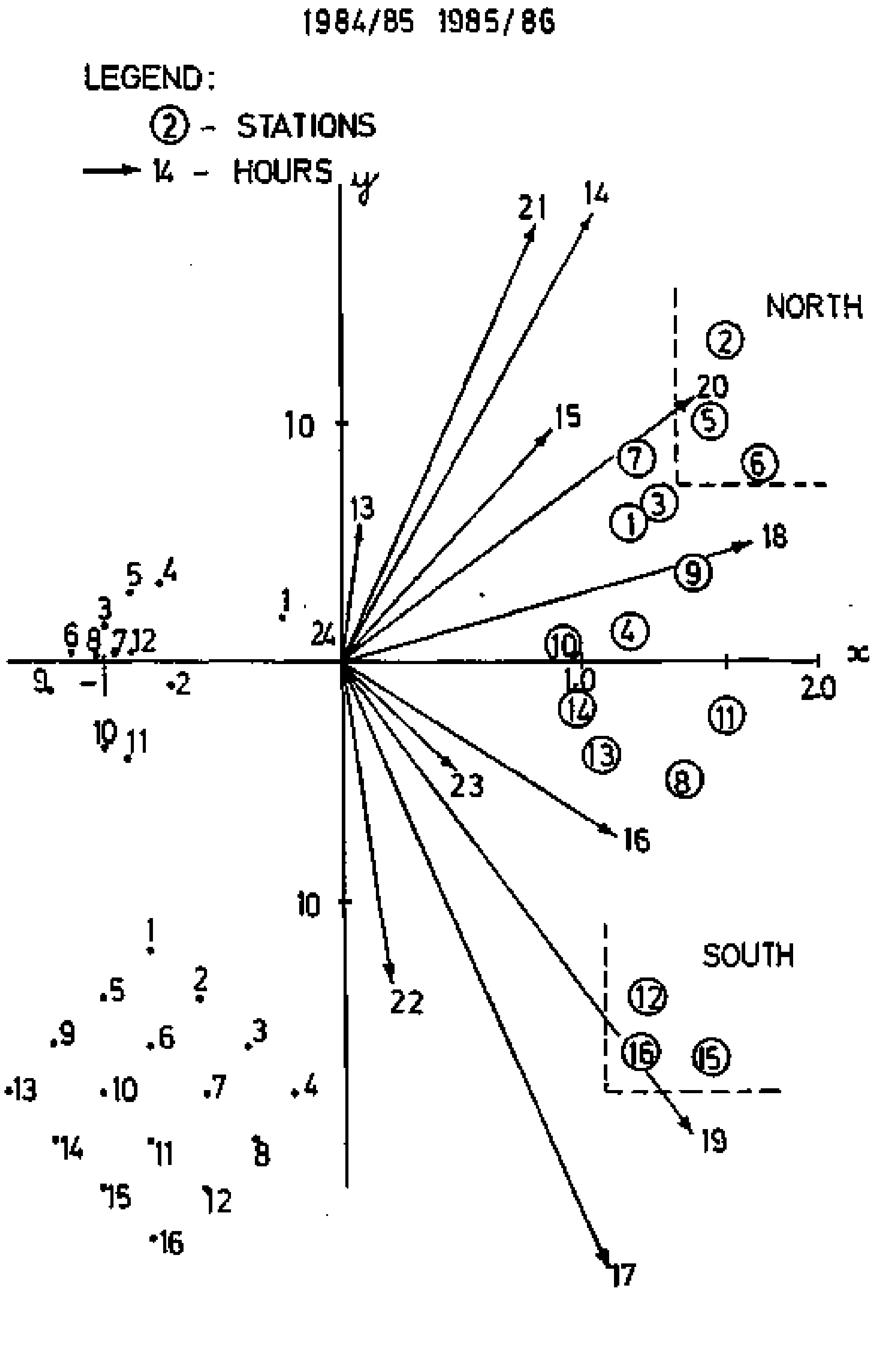

Figure 2.6.0. Biplot of average rainfall by hour and station, seasons 1984/85 and 1985/86 (see text for details).

c. The orthogonal projection from the station onto the hour vector reflects the relative amounts of rainfall received by each station in that hour. For example, between 13:00 and 14:00 hours, on average, most of the rain is falling over the northern stations. The converse is true between 15:00 and 17:00. Thus the elongation of station groups along the y axis reflects the timing of the precipitation over the network. There appear to be 3 convective surges over the network, commencing first over the northern stations, then swinging over the southern gauges.

FROM	TO
13:00 to 15:00	15:00 to 17:00
17:00 to 18:00	18:00 to 19:00
19:00 to 21:00	21:00 to 22:00

d. The cosine of the angle between the hour vectors approximates the correlations between hourly rainfall amounts. The adjacent hours are not always well correlated, another feature that can be attributed to the convective nature of the precipitation. Note that all the early morning precipitation over the network is light, but highly correlated, a characteristic of network-wide drizzle. The 14:00 and 21:00 hour vectors are strikingly similar. While it is reasonable to assume that the 14:00 rain event is thermally forced, some other mechanism must be responsible for the convection at 21:00 hours. As this late rain event swings over the network it becomes less convective as is indicated by the shrinking hour vectors (22.00 and 23.00).

If this analysis is climatically representative, seeding operations over this area would be planned to take advantage of the early and late afternoon storm surges across the area covered by these gauges. It would be interesting to gauge other areas of the Drakensberg escarpment to determine whether these surges are common to the whole ridge line.

3.0 RADAR DESCRIPTION OF RAIN AND STORM CHARACTERISTICS (Mather, Parsons, Wightman, Morgan and Emmitt)

The radar at Nelspruit has been systematically collecting data on convective storms for 4 consecutive seasons (each season runs from 1 October to 31 March). Radar analysis offers a description of the rainfall in the study area which is more than merely complementary to the description derived from rain gauges. Radar observations of rainfall are available at superior spatial and temporal resolutions than are the observations of raingauges, and the effort involved in obtaining the observations is incomparably reduced because of the single observation system. There are certain well known difficulties in deriving precise rainfall estimates from radar reflectivity, but these have been exhaustively debated in the scientific and technical literature (there exists a vast body of works published over the past 40 years from all over the world on this subject) and the radar has emerged as an indispensable tool for the study of rainfall.

Radar, properly employed, goes beyond the raingauge network in furnishing a description not only of the rainfall but also of the systems which produce it. In the case of thunderstorms these systems occupy deep layers of the atmosphere.

The characteristics of the Nelspruit radar, its volume scan mode, the limitations imposed by range effects and terrain shadowing, etc, are covered in detail in Vol. IV Section 3 of this report. Also described are the software analysis techniques which have been developed for processing, displaying and archiving the radar data.

Here we wish to impart an overall view of the nature of Nelspruit storms as observed by radar. This will cover a list of important characteristics:

- when they form
- where they form
- direction and speed of their movement
- how tall they are
- how much rain they produce
- geographical effects, etc.

3.1 Overall statistics

The following convective storm climatologies are constructed from 4 seasons of radar volume scan data. Table 3.1 shows the number of storm tracks between 10 and 80 km analysed each season. A storm track starts when a 30 dBz radar reflectivity volume exceeds 3 km^3 and ends when it drops below 3 km^3 (see Vol. IV, Section 3.9 for details of storm tracking algorithm). "Case tracks" in Fig. 3.1.0 (f) refers to the distributions of the rain volumes of those storms chosen for experiments.

Table 3.1 Number of Storm Tracks Analysed each Season

SEASON	1982/83	1983/84	1984/85	1985/86
NO OF STORM TRACKS	2270	1898	3033	3145

The storm track data for all 4 seasons are very similar indicating that, at least in the Nelspruit area, a representative climatic sample of convective clouds can be obtained in just a single season. Storm track times of origin, durations, directions and speeds, maximum echo heights, area-time integrals and radar-estimated rain volumes are depicted in Figs. 3.1.0 (a) through (f). Fig. 3.1.0 (a) also shows the hourly temperatures averaged over 9 stations and three months (December 1985, January and February 1986) measured by the mesoscale network. The shape closely approximates the time-of-origin histogram suggesting that

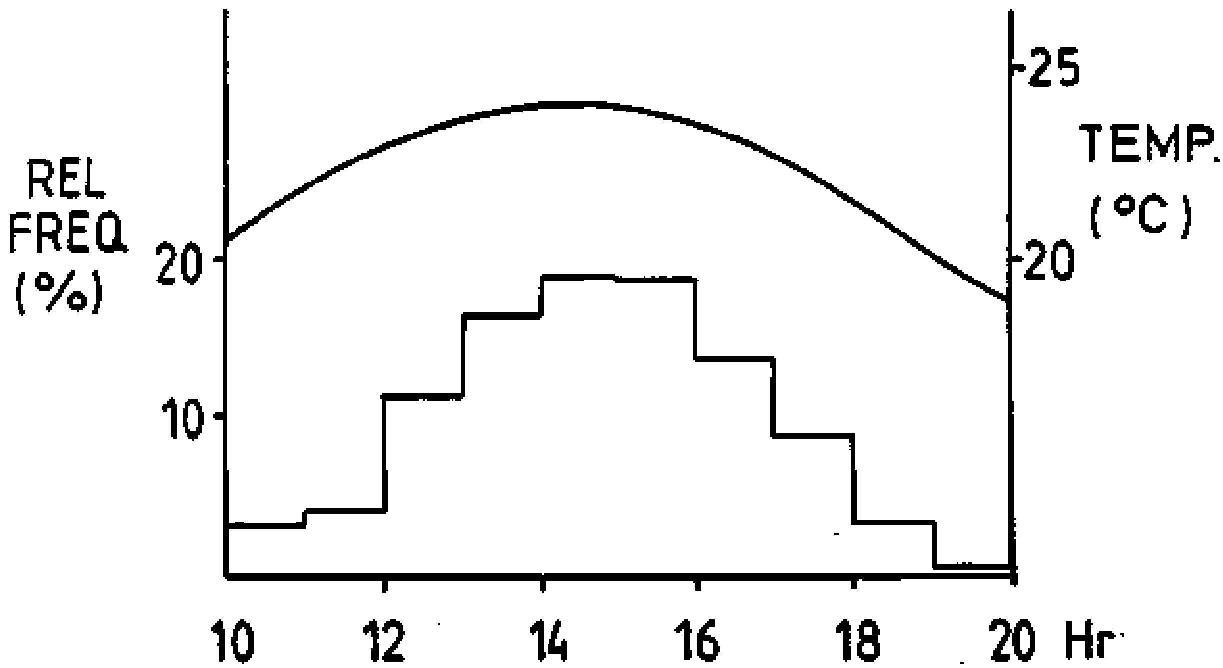

Fig. 3.1.0 (a) Time of storm track origin

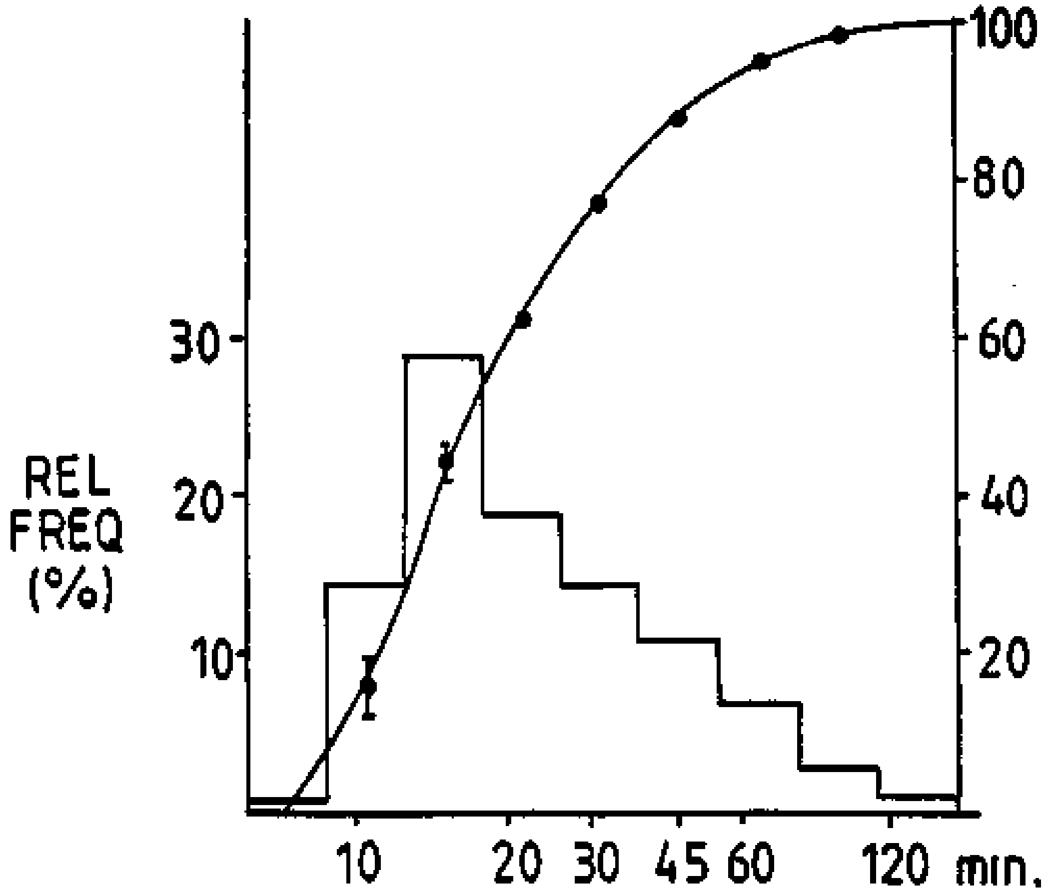

Fig. 3.1.0 (b) Storm durations

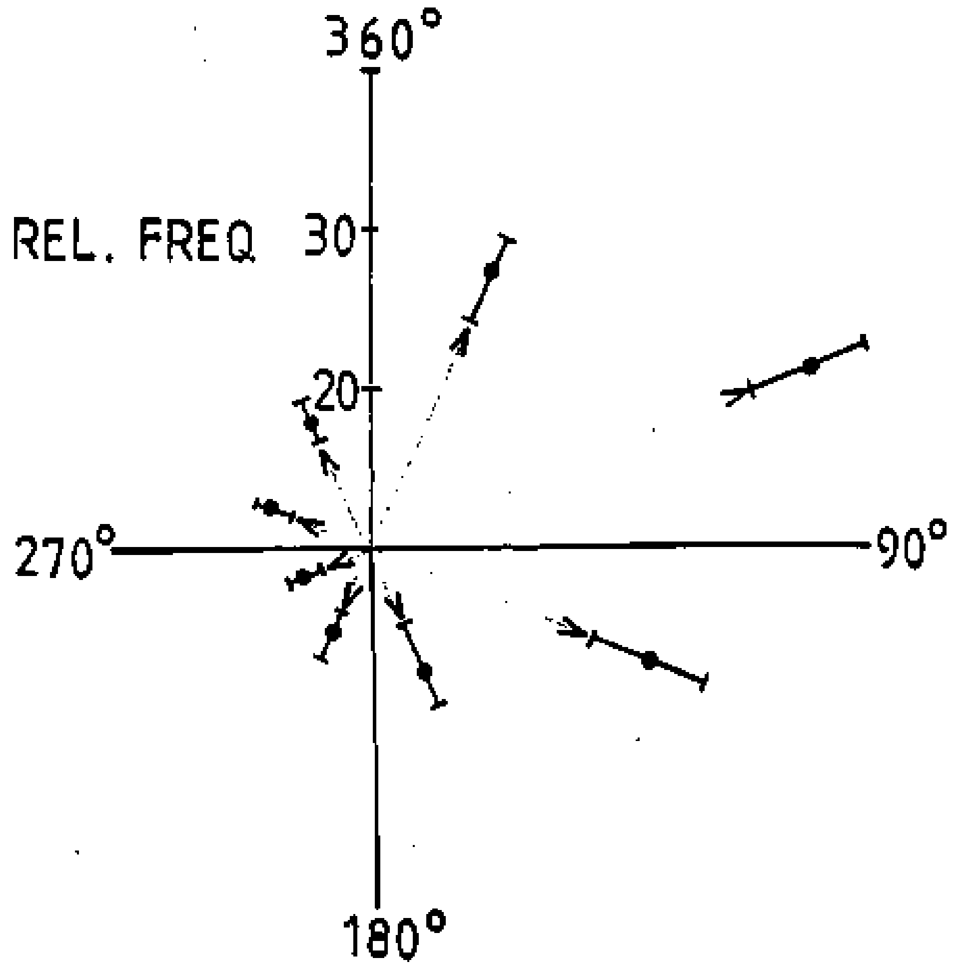

Fig. 3.1.0 (c) Storm directions

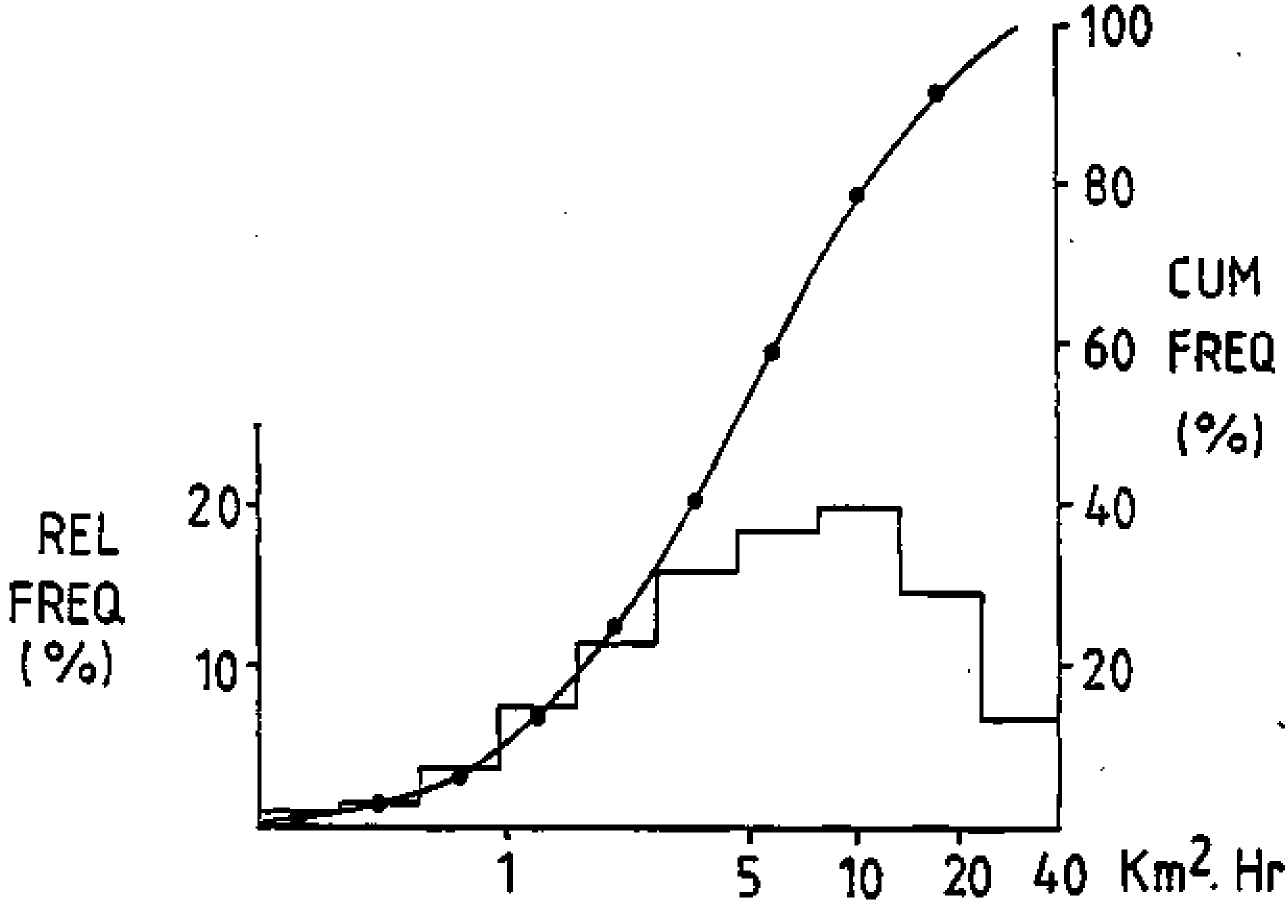

Fig. 3.1.0. (d) Storm speeds

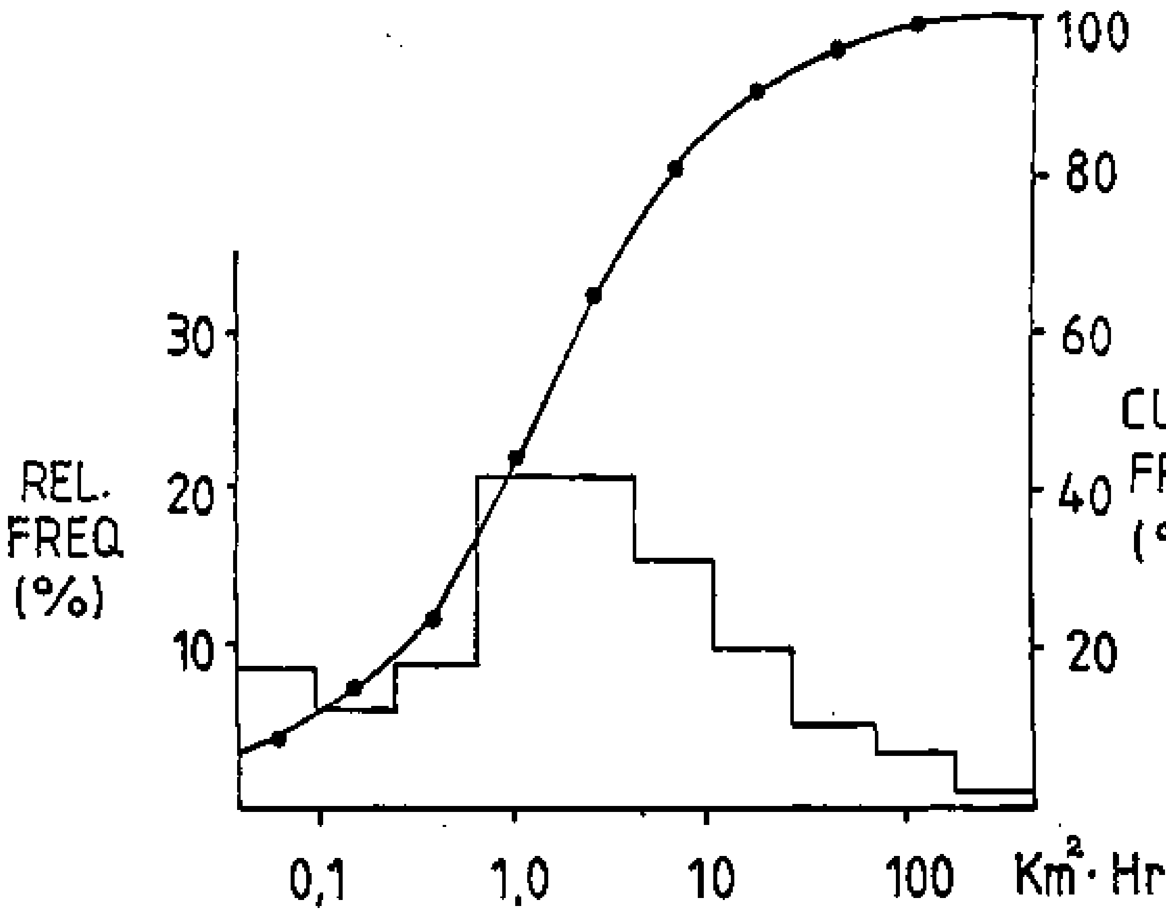

Fig. 3.1.0 (e) Storm Area-Time Integrals

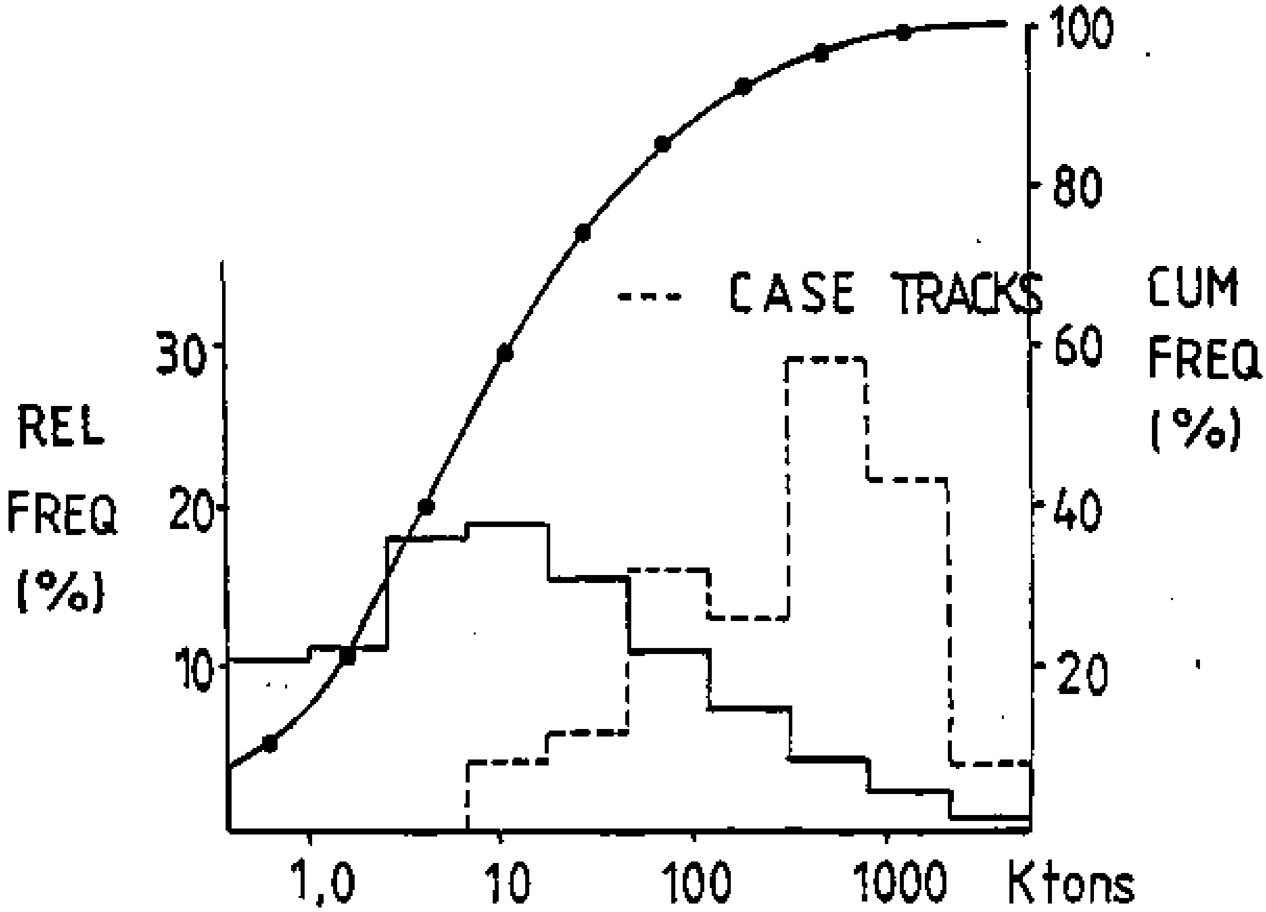

Fig. 3.1.0.(f) Storm radar-estimated
rain volumes

most of the storms in the data set are thermally forced. Comparison of these statistics with other analyses is somewhat difficult as the statistics are clearly a function of the storm tracking scheme.

3.2 Geographical patterns of radar echo frequency

The geographical dependence of storm echoes in the PAWS area is shown by dividing the area within radar range into 10 by 10 km squares and analysing the frequency of occurrence of selected storm track properties in these squares. Fig. 3.2.0 is a simple 3 contour map of the terrain surrounding the radar. Fig. 3.2.1 depicts the areal first detection frequencies and Fig. 3.2.2 the storm track frequencies per 10 by 10 km block summed over the 4 seasons. A storm track is logged each time a storm tracks into and out of a 10 x 10 km block. Both distributions are similar and are closely related to terrain features in the experimental area. Some seasonal detail is apparent when this same analysis is repeated for each season. In 2 out of the 4 seasons, storm track frequencies show a maximum southwest of radar (west of the Badplaas valley). In the remaining 2 seasons, this maximum shifts to a position northwest of the site. These inter-season differences are examined more fully in Volume IV of this report.

From geographical distributions of :

- track initiations
- track terminations
- track frequencies
- limited track frequencies, which are the distribution of tracks per block, allowing only a single count per block per storm track,

one can calculate areal storm "source-sink" distributions (see Volume IV for details of these calculations). The columns and rows of the 10 by 10 distributions of storm sources and sinks for the 4 seasons are summed and plotted as histograms in Fig. 3.2.3. The west-to-east profile shows a very clear pattern of storm sources to the west of Nelspruit and sinks to the east, underlining the importance of the storm generating effect of the escarpment. The north-south profile shows no clear pattern, other than perhaps a slight tendency for a storm source region south of the radar and a weak sink to the north.

Fig. 3.1.0 (c) whose vectors, if resolved onto the cardinal points of the compass (N,E, S and W), would show the west-to-east vector as the largest and the south-to-north as the next largest.

This type of analysis is important since one of the hypotheses of dynamic seeding is that treated storms should last longer (Woodley et al., 1982). If this hypothesis is correct, then large scale cloud seeding, as in an area experiment, might be expected to alter the west-east profile shown in Fig. 3.2.3 moving the "sink" trough eastwards.

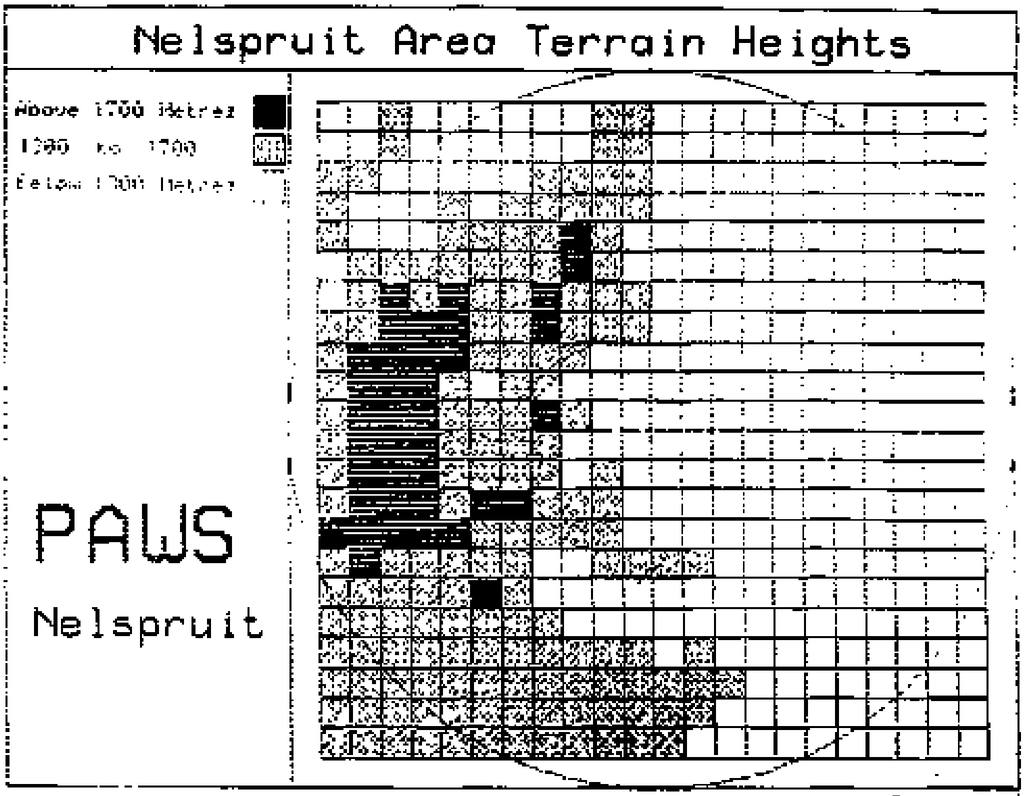

Fig. 3.2.0. Schematic of terrain in the PAWS experimental area.

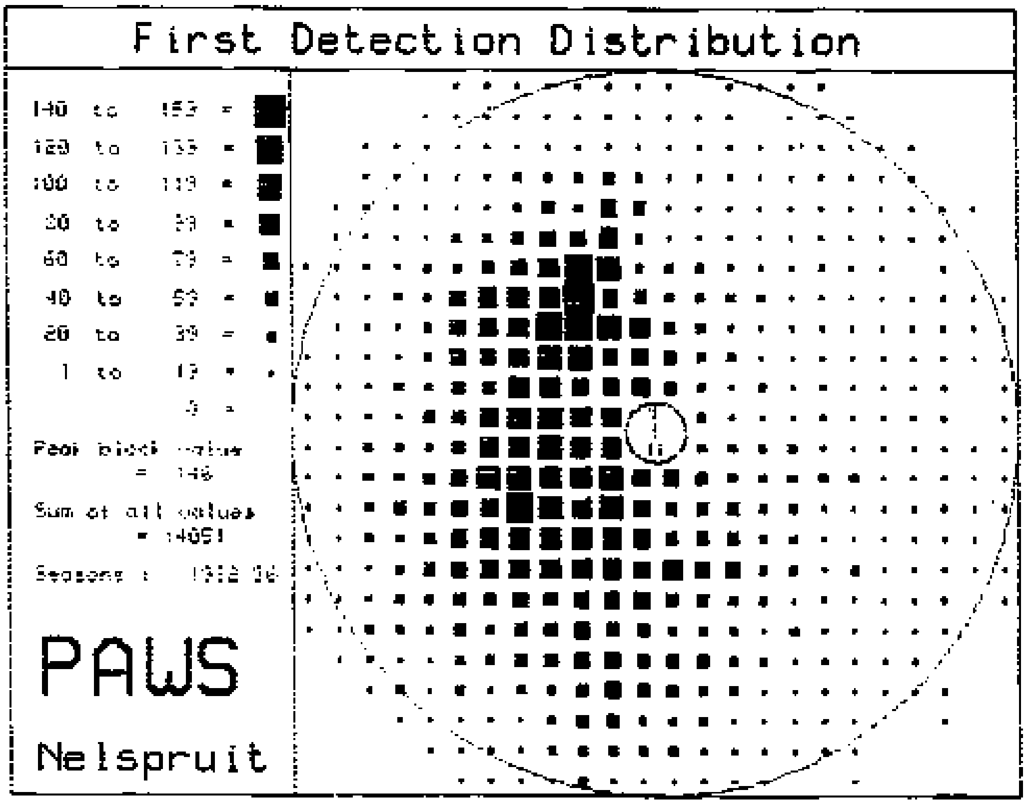

Fig. 3.2.1. First storm detection frequencies.

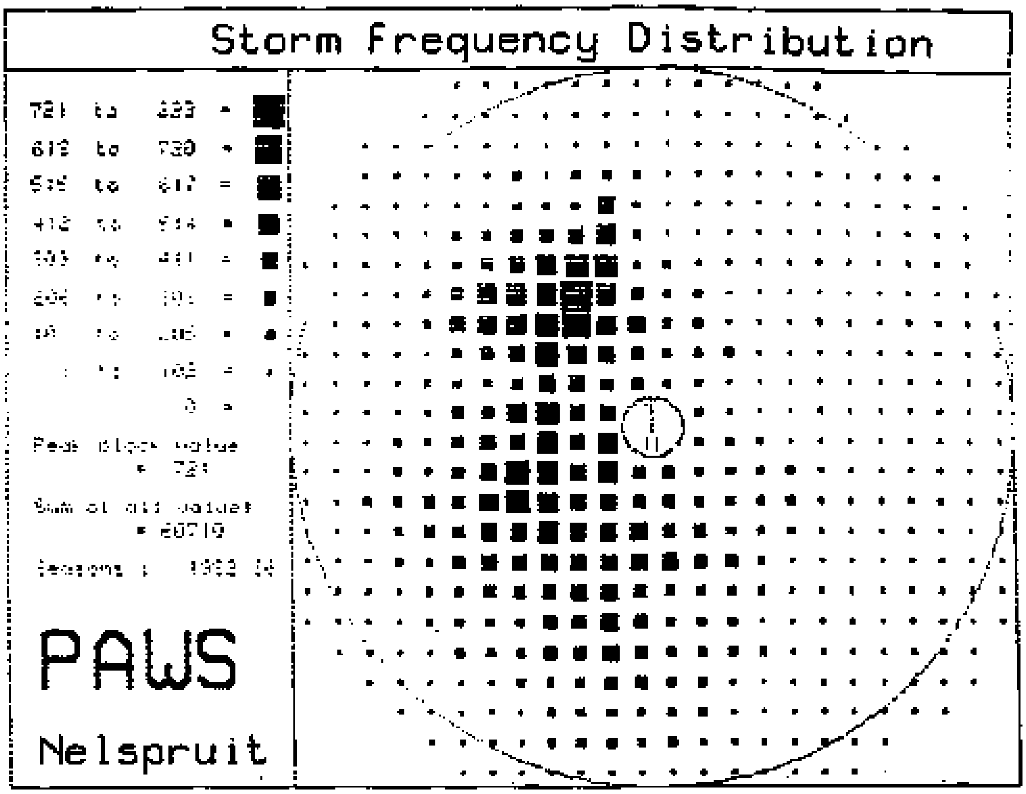

Fig. 3.2.2. Storm track frequency distributions.

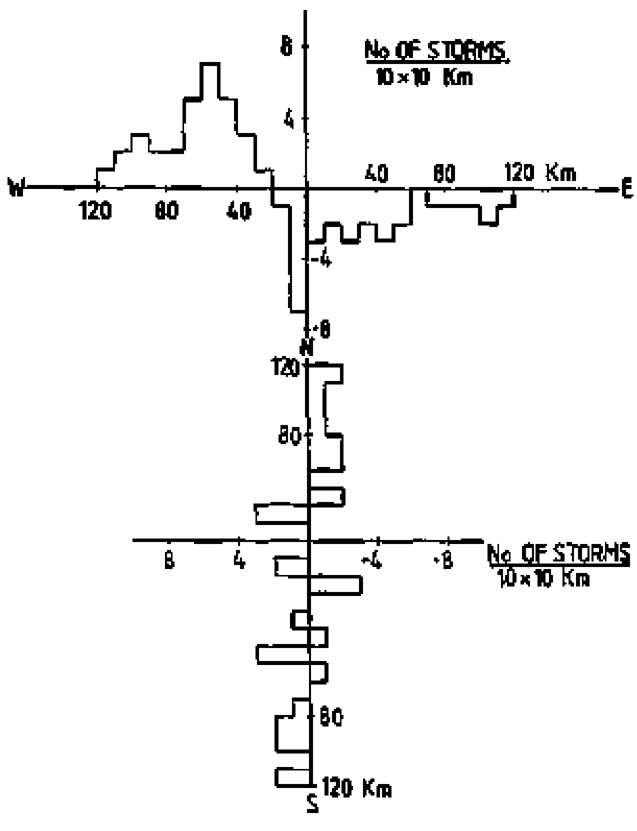

Fig. 3.2.3. N-S and E-W profiles of storm source/sink statistics.

Additional questions asked of the radar storm track data concern the sites where the sequence of radar echoes has specific temporal characteristics. From a hydrologic perspective, it may be important to know where rain tends to fall in an uninterrupted pattern leading to greater runoff/rainfall ratios.

In Fig. 3.2.4 the contours of continuous rainfall are presented. A continuous rainfall event is defined here as :

a. occurring within a 12 x 12 km area, and
b. having a radar echo of 35 dBz or greater occurring over the area for at least 60 minutes with no gaps in activity longer than 15 minutes.

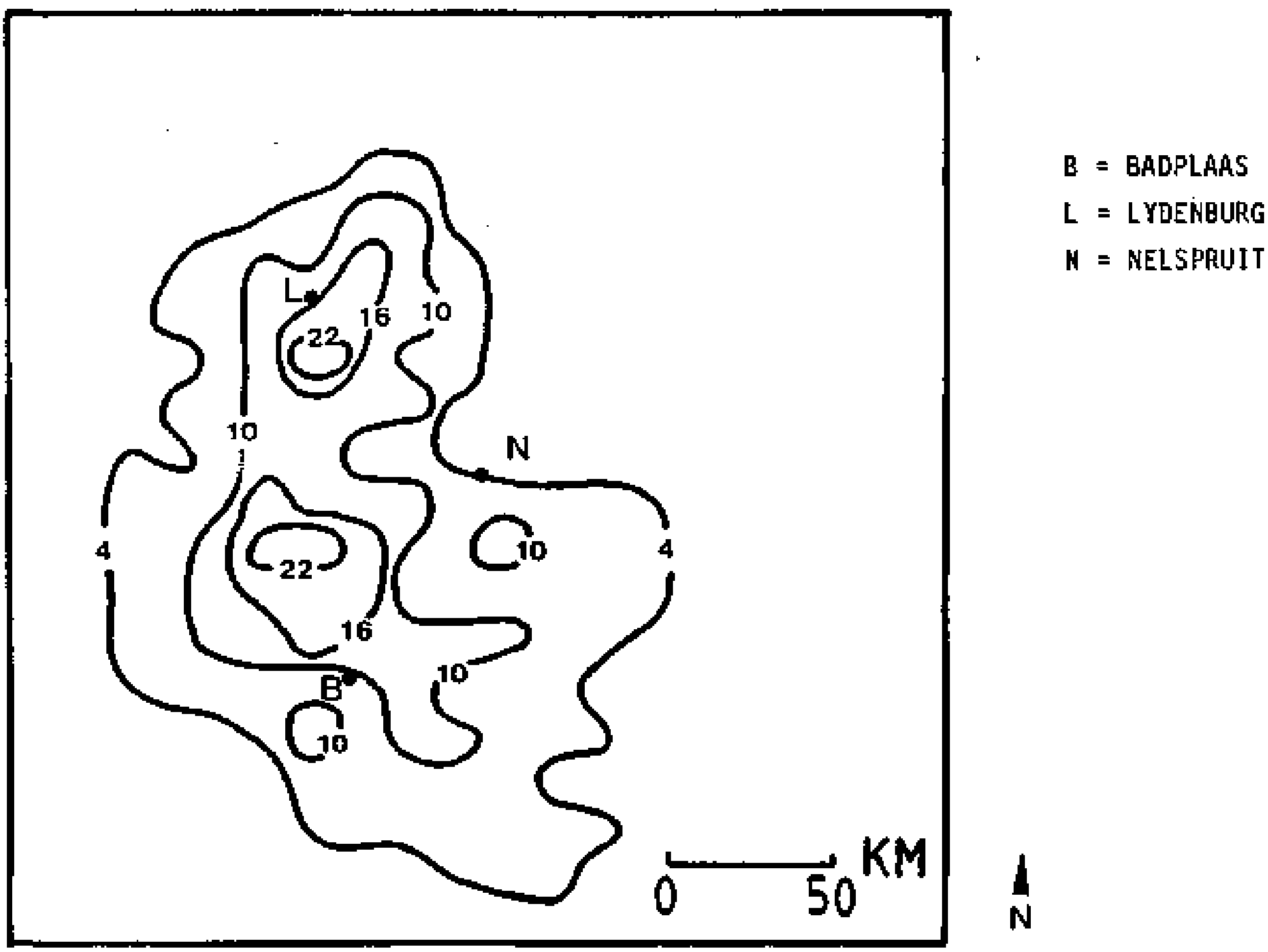

Figure 3.2.4. Contours of occurrence of continuous events as described in the text. For example, a value of 16 means that on 16 occasions radar echoes persisted over the area for more than 60 min.

The two primary areas for continuous rainfall events are the eastern slopes of the ridge along the northern edge of the Badplaas valley and the eastern slopes of the ridge to the northwest of Sabie.

Next, the geographical distribution of some of the key storm track properties that are related to gross radar-measured precipitation measurements are examined.

Average maximum echo tops.

Each storm reaches a maximum height during its lifetime. These maxima are summed and averaged over 10 by 10 blocks and plotted in Fig. 3.2.5. There is a tendency for storms to reach greater maximum heights to the west of radar. The outer ring of heights above 8000 m is thought to be at least partially a function of the tendency of the radar to overestimate cloud tops as distance from the radar increases.

Average maximum 3 degree areas.

Each storm reaches a maximum area during its lifetime. These 3 degree maximum areas are summed and plotted in Fig. 3.2.6. The most striking feature in this display is the minimum to the west of radar which corresponds to the radar shadow caused by Mataffin Kop. Maximum (greater than 40 km^2) areas occur more frequently east of the radar in this plot. This confirms a subjective impression long held at Nelspruit that storms that do form or continue to track east of radar are often more massive than those observed along the escarpment, presumably because the warmer and more moist air at these lower elevations gives rise to deeper and thus more massive storms.

Average of the maximum of the mean 3 degree reflectivities.

For each scan, a mean reflectivity at 3 degrees is calculated. The geographical location where the mean 3 degree reflectivities for each storm reaches a maximum is plotted in Fig. 3.2.7.

Again the gap to the west is evident, caused by terrain blocking the radar beam. Generally, the blocks in the immediate vicinity of the radar show higher reflectivities than the more distant blocks. There appear to be fewer higher reflectivities at far ranges to the southwest. This could be caused by partial blocking of the 3 degree scan or weaker storms on the highveld, or a combination of both of these factors.

Many of the other rainfall-related track parameters were analysed in a similar manner. The point that we want to emphasis here is that not one of these analyses showed a systematic grouping of storm track properties that could be related to the

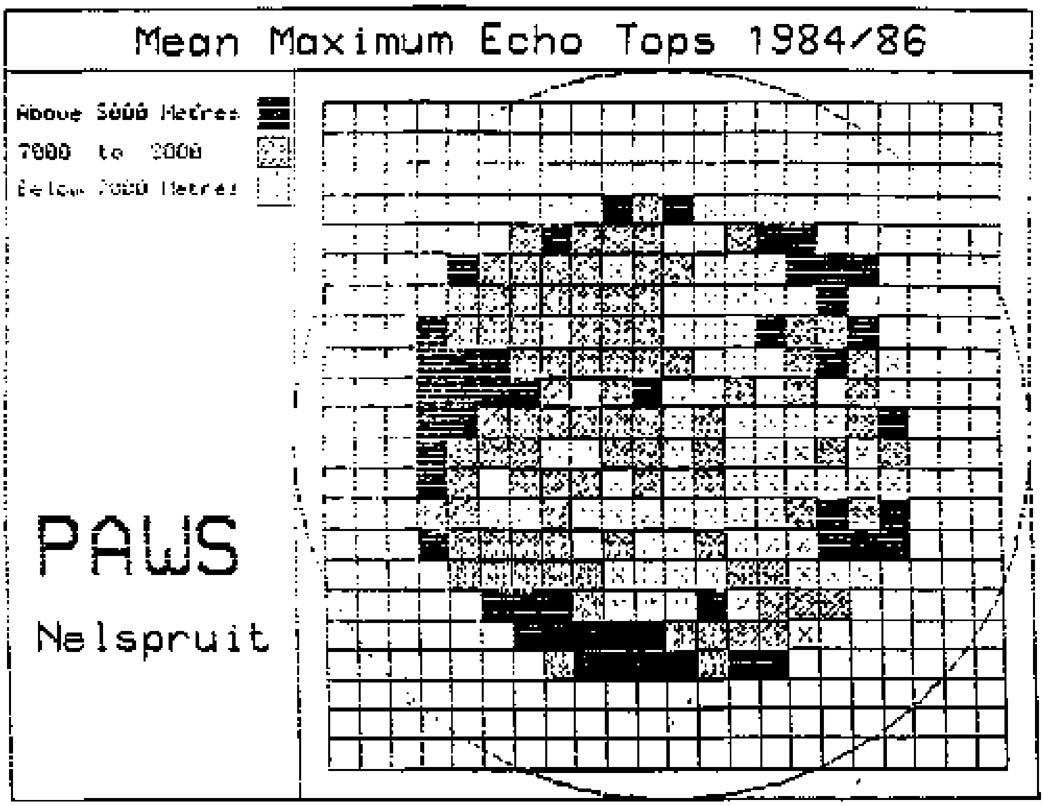

Fig. 3.2.5. Average maximum echo top distributions

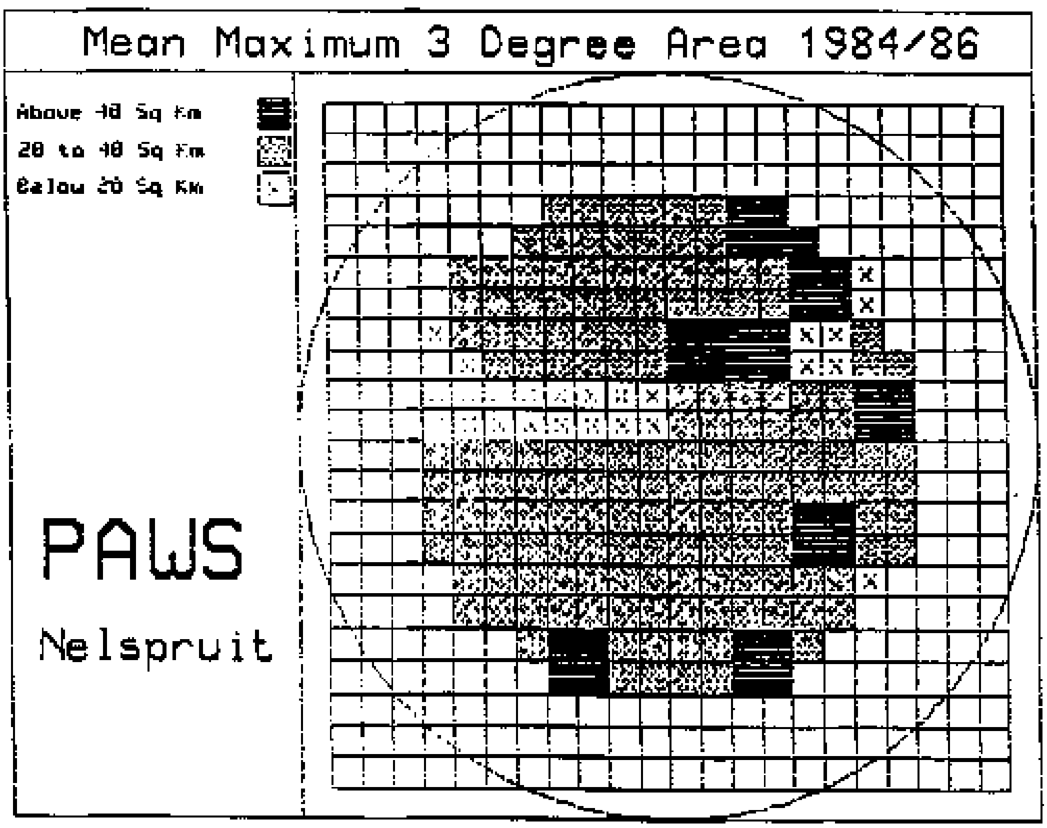

Fig. 3.2.6. Average maximum 3° area distributions.

underlying topography. Thus, while echo frequency and direction of movement can be closely tied to terrain, radar-measured storm characteristics cannot.

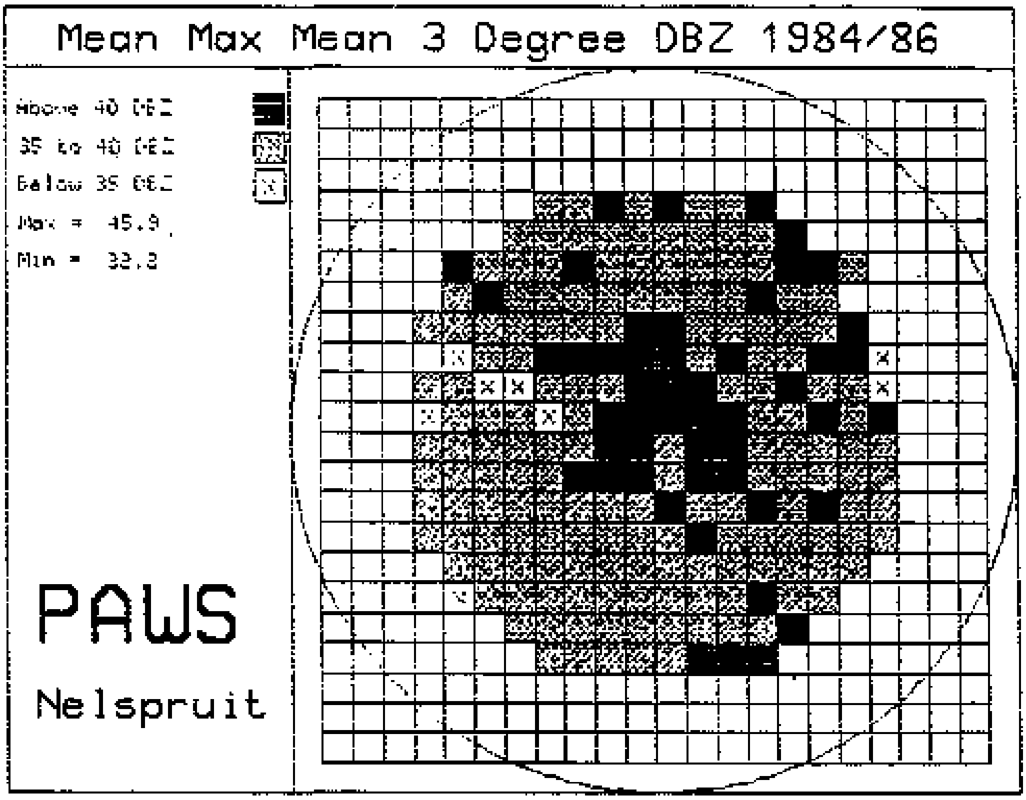

Figure 3.2.7. Average of the maximum of the mean 3 degree reflectivities.

4.0 THE METEOROLOGY OF NELSPRUIT RAINFALL

4.1 Large scale meteorological influences (Garstang and Cooper)

The above and below normal periods of rainfall illustrated in Section 2 appear increasingly to be tied to global circulation features. Tyson (1984) has pointed to the critical positioning of the south Atlantic anti-cyclone and for the role played by the Southern Oscillation and the Walker Circulation in governing summertime rainfall over southern Africa.

At least two aspects of these large scale controls are considered important to the PAWS findings:

a. the exploratory experiment conducted over the past 4 years, with most of the observations being obtained in the 1984/85 and 1985/86 summer seasons, took place during a dry period.

b. modulation of the rainfall in the Nelspruit region is in part dependent upon the relative contribution of temperate zone compared to tropical rain bearing systems.

The dry conditions prevailing during the early and mid-1980's may influence both the kind and frequency of rain bearing storms over the eastern Transvaal. Garstang and Emmitt (1983) and Garstang et al. (1983) show that wet years have approximately the same number of rain days and rain at approximately the same rate on the significant rain days (days with average station rainfall greater than 7.5 mm) as in dry years. The primary difference between wet years and dry years is the frequency of occurrence of significant rain days. In wet years significant rain days contribute 75% of the total seasonal rainfall with rain falling at about 50% more stations than in dry years. Days which receive a station average greater than 15.0 mm account for 50% of the rainfall in wet years and rain at 74% more stations in December, January and February than in dry years. Storms which yield more than 30 mm/day are confined to wet years and occur most frequently in late (January-March) summer. The most significant difference between wet and dry years is the frequency of occurrence of significant rain days.

Dry years have more days with low average rainfall per station (less than 2 mm) than do wet years. However, in both wet and dry years 12% of the days with rain yield 50% of the rain, alternatively 50% of the days with the lowest rainfall yield only 7.3% of the rain in both wet and dry years.

The large scale changes in the moist static energy field are illustrated in the time series for the 1985/86 season shown in Fig. 4.1. The departures in moist static energy of the daily Nelspruit sounding are from the seasonal mean. The period from December 6 to the end of March shows significant positive departures from the mean at the surface and through the atmospheric column. October, in contrast shows periods (1 to 4 days) of very dry conditions. A similar trend was noted for the latent heat content of the air. High values are frequent at and near the surface from early December onwards. Analyses of westerly/easterly and northerly/southerly flow in the troposphere revealed marked westerly incursions extending through most of the atmospheric column in October and early November. From mid-November onwards, westerlies are confined to levels mostly above 5 km while easterlies prevail in the lower troposphere (below 5 km). Meridional flow is strong with marked changes in sign from October to early December. From early December onwards meridional flows below 6 km are weak and mostly southerly.

Figure 4.1.1 shows the vertically integrated latent heat (LW) from the surface to 1 km and from the surface to 6 km for two seasons (1984/85 and 1985/86). Integration to intermediate (3 km) and higher (12 km) levels shows no additional information than is contained in the 0-6 km integration. In common with the previous figure, Fig. 4.1.1 (a) and (c) show that in the early part of the season integrated values of LW remain below 1.5×10^5 J kg^{-1} in the first kilometre and below 2.5×10^5 J kg^{-1} in the first 6 km. After the end of November extending to late March, Fig. 4.1.1 (b) and (d) show integrated values of LW in the two layers are mostly above these two levels.

There is, thus, little doubt that rain producing systems at Nelspruit change in character from early season (October-November) to mid and later season (December, January, February and March). These differences in the large scale atmosphere reflect changes in the rain producing synoptic systems from temperate to tropical back to temperate. Such distinct intraseasonal differences bear upon the question of weather modification through the possible differences in the microphysics and stability of the associated clouds. We deal with these implications in Volume III.

4.2 Synoptic-scale controls

Diab and Garstang (1985, 1986), Harrison (1984) and others have attempted to determine whether synoptic scale systems can be identified. If uniquely identified, then the synoptic class or category is likely to exhibit specific characteristics of say rainfall. Covariates have been developed to discriminate between five synoptic categories with significantly different rainfall characteristics (PAWS, 1984). Table 4.1 shows these differences, demonstrating that the tropical systems, TROPLINK and SUBTROP, while occurring only 13% of the time produce a combined total which accounts for more than 55% of the seasonal rainfall. Both tropical systems also yield the largest amount of rain per station. Heavy rain days (greater than 15 mm/station/day) occur most frequently in association with the TROPLINK category and account for 35% of the seasonal rainfall. Harrison (1984) showed an identical result for rainfall over the Orange Free State. In contrast, temperate zone fronts/troughs produce only 17% of the

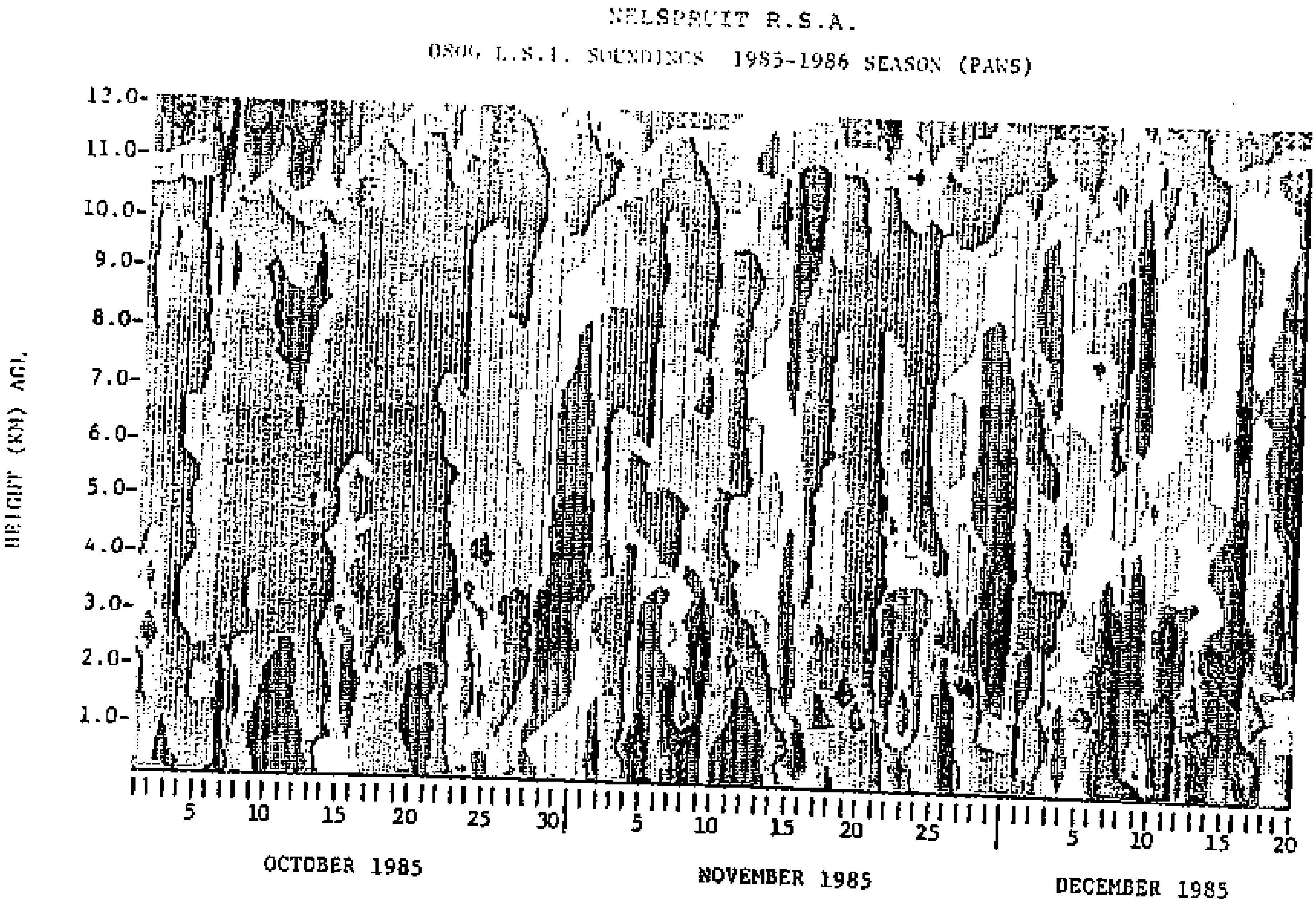

Fig.4.1.0(a) Departures of Moist Static Energy (1000 * J kg^{-1}) from Season Mean; Contours every 2.0 from -8.0 to 8.0.

Positive departures for shades from Yellow (small +) to Red (large +).
Negative departures for shades from Green (small -) to Blue (large -).

NELSPRUIT R.S.A.

0800 L.S.T. SOUNDINGS 1985-1986 SEASON (PAWS)

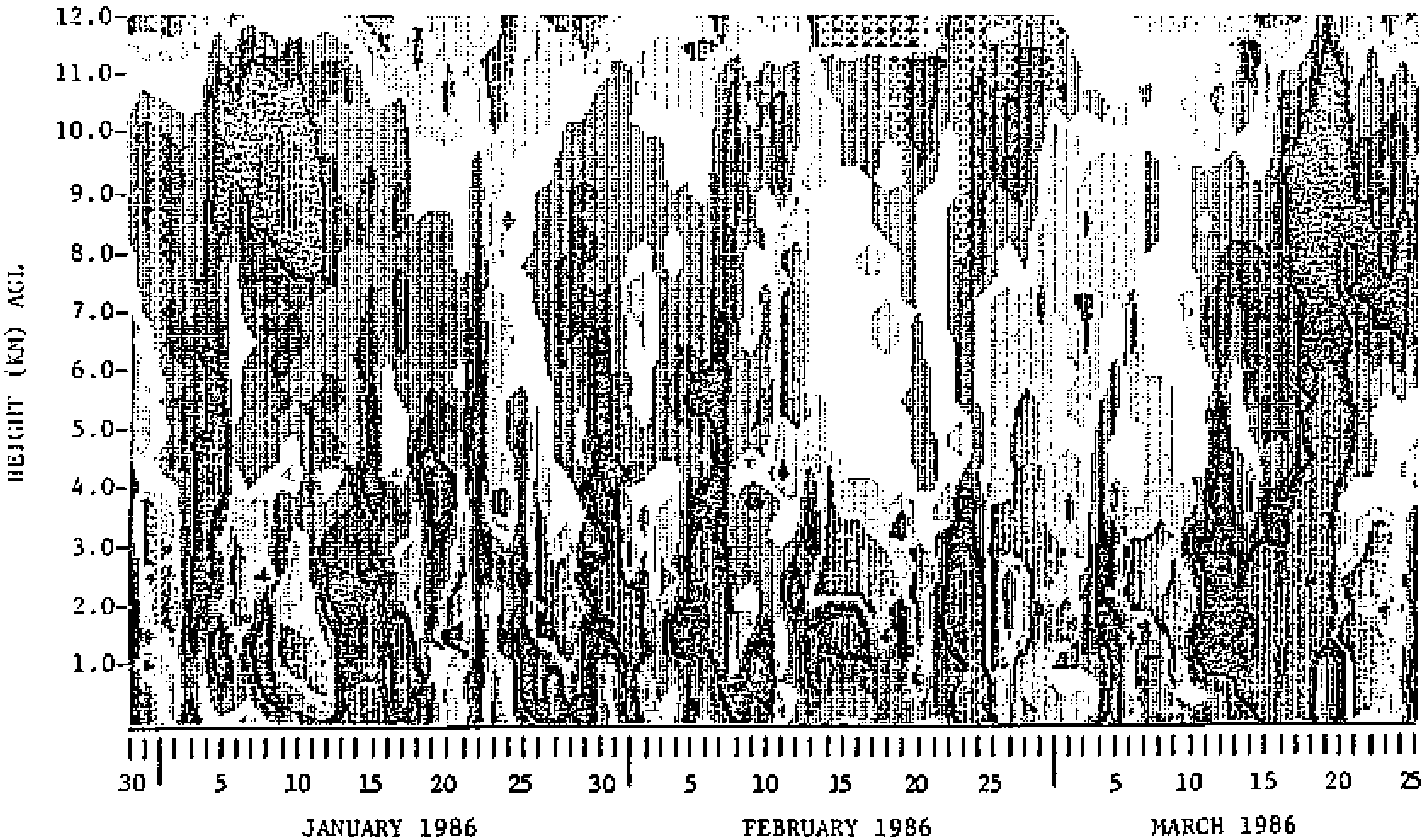

Fig.4.1.0(a)(cont.). Departures of Moist Static Energy (1000 * J kg^{-1}) from Season Mean; Contours every 2.0 from -8.0 to 8.0.

Positive departures for shades from Yellow (small +) to Red (large +).
Negative departures for shades from Green (small -) to Blue (large -).

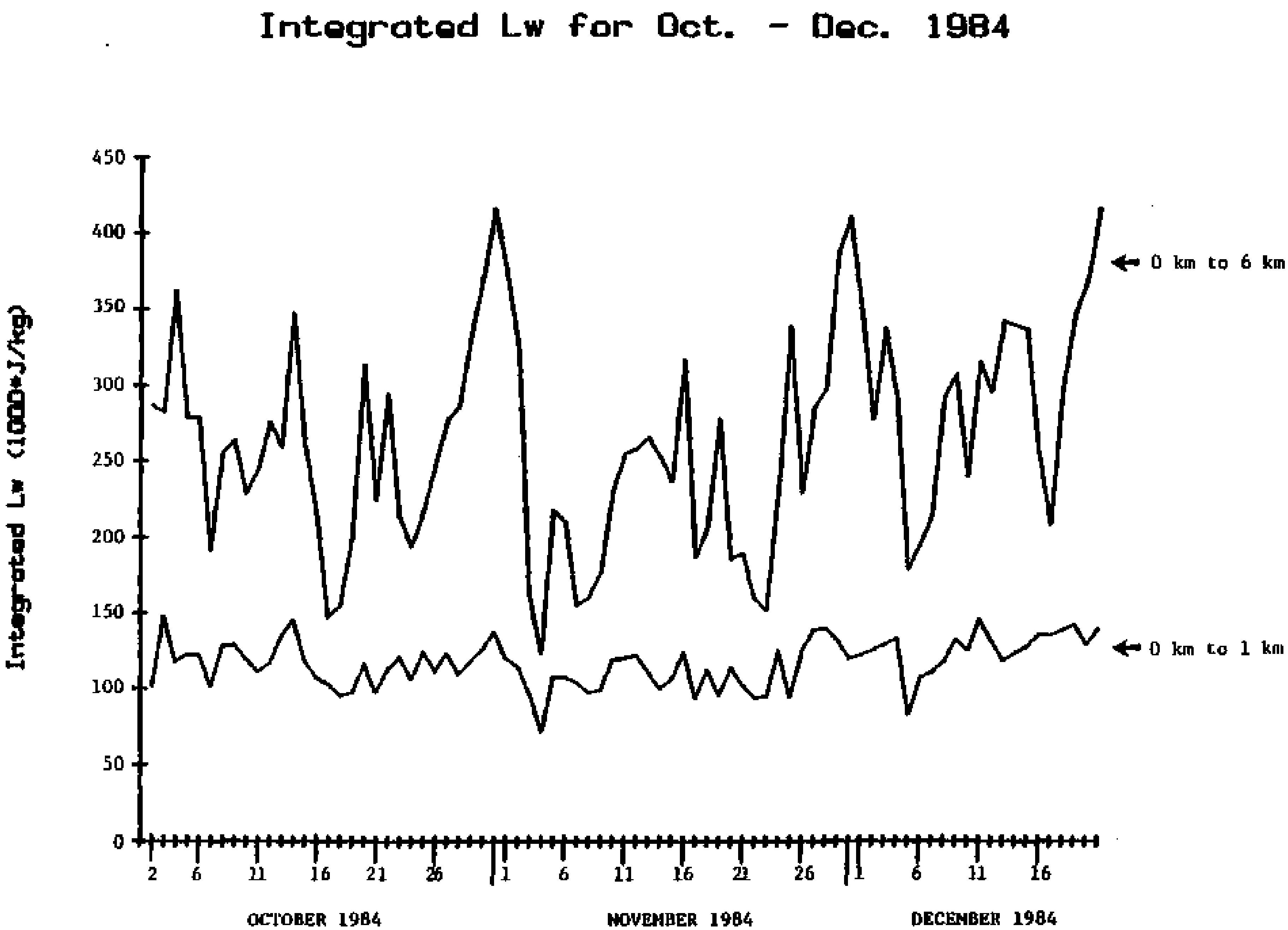
Integrated Lw for Oct. - Dec. 1984
Integrated Lw (1000*J/kg)
450
400
350
300
250
200
150
100
50
0
2
6
11
16
21
26
1
6
11
16
21
26
1
6
11
16
OCTOBER 1984
NOVEMBER 1984
DECEMBER 1984
0 km to 6 km
0 km to 1 km

Fig. 4.1.1.(a)

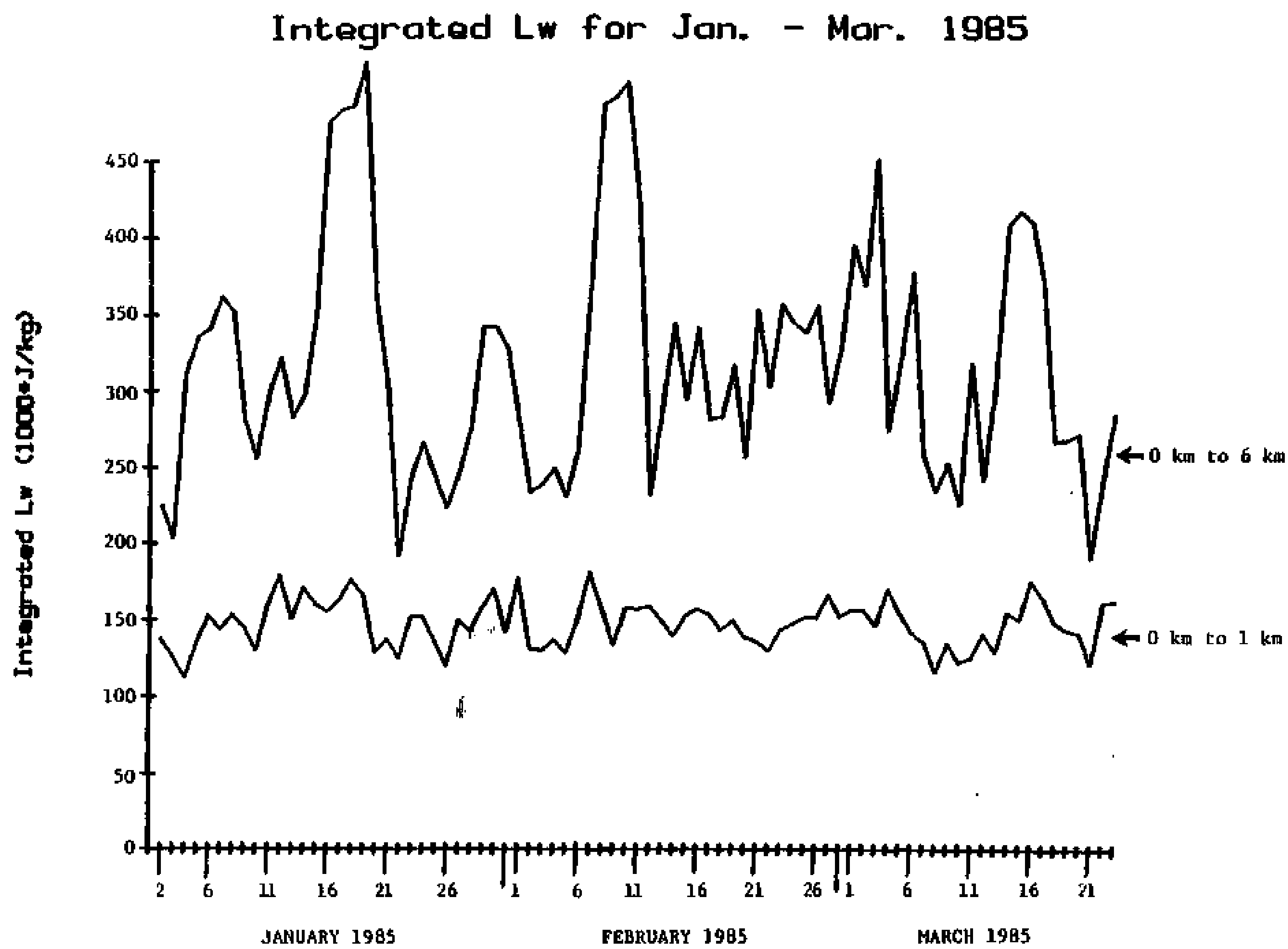

Integrated Lw for Jan. - Mar. 1985
Integrated Lw (1000*J/kg)
450
400
350
300
250
200
150
100
50
0
0 km to 6 km
0 km to 1 km
2
6
11
16
21
26
1
6
11
16
21
26
1
6
11
16
21
JANUARY 1985
FEBRUARY 1985
MARCH 1985

Fig. 4.1.1 (b)

Integrated Lw for Oct. - Dec. 1985

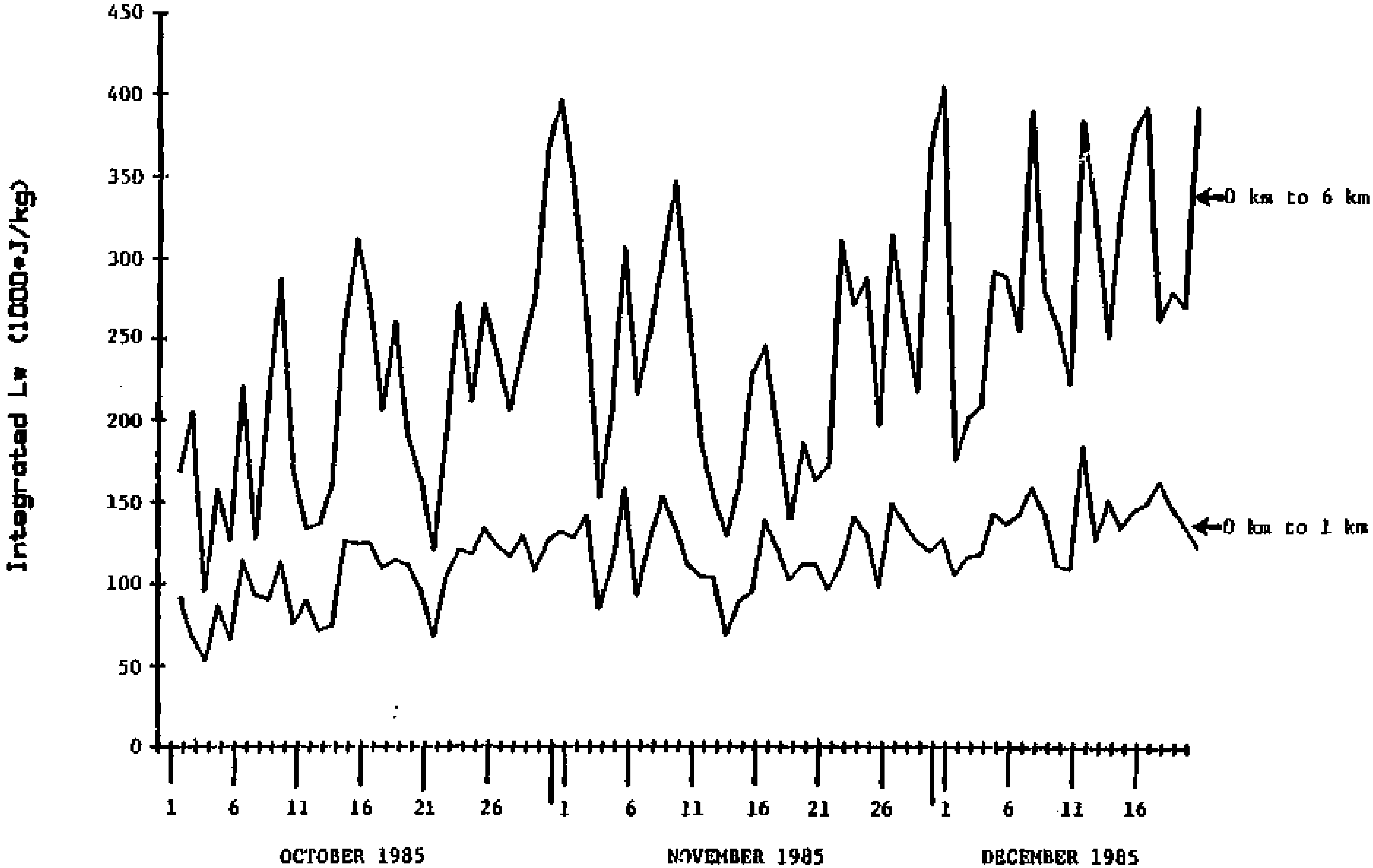

Fig. 4.1.1(c)

Integrated Lw for Jan. - Mar. 1986

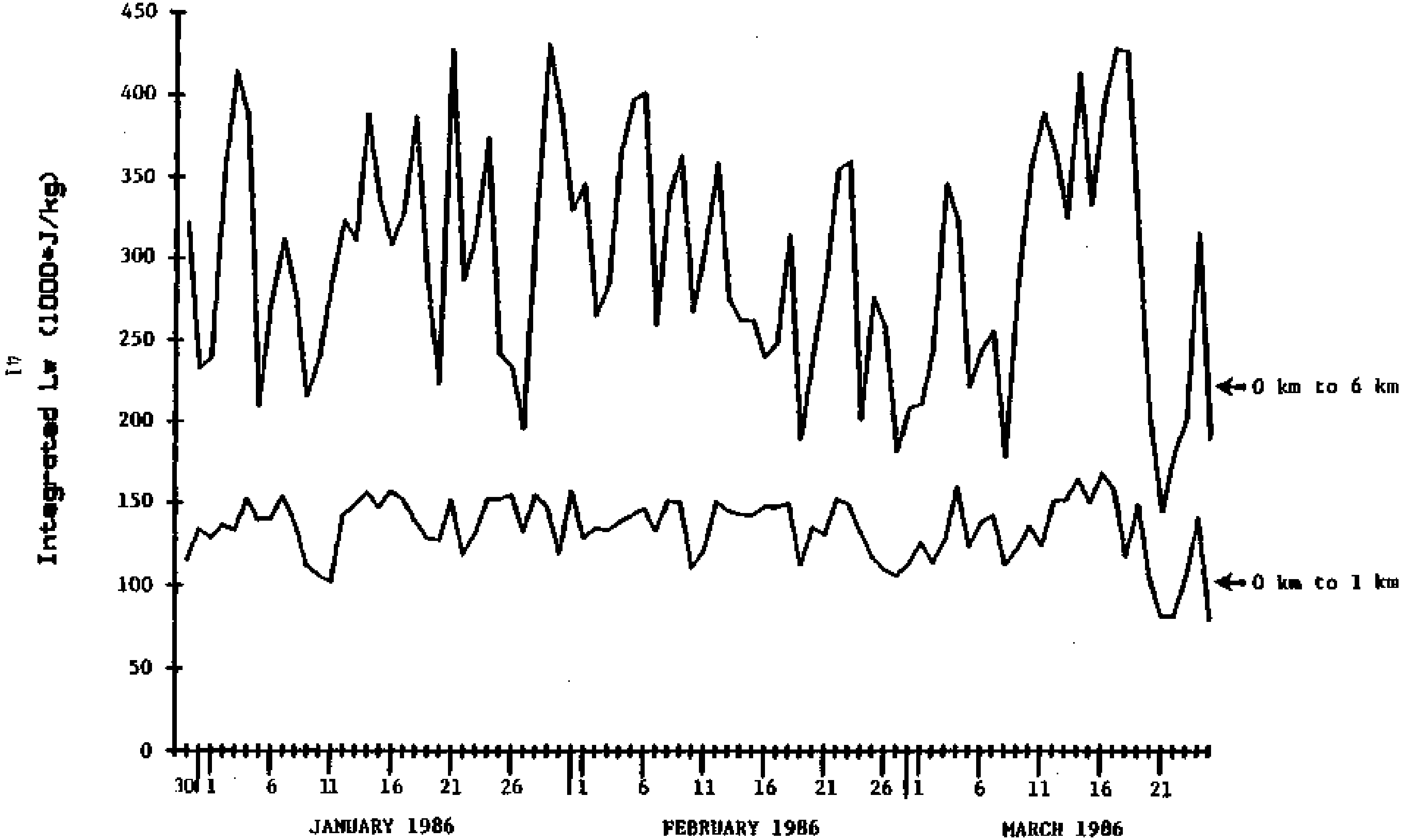

Fig. 4.1.1.(d)

Synoptic Category	Percent Frequency*	Total rain Over Network (mm)	Avg. rain per Reporting Station (mm)	Contribution to Total* Rainfall (%)
COASTLOW	11	1463	4.9	16.8
TROPLINK	9	2891	9.6	33.2
HPRIDGE	13	1312	4.4	15.1
HPESTAB	32	1029	3.5	11.8
SUBTROP	4	2013	6.6	23.1

* some days were not classified due to missing discriminating variables, and hence the total is less than 100%.

Table 4.1. Rainfall characteristics of synoptic categories

Synoptic class	Rainfall Characteristics
COASTLOW	Midlatitude in origin. Cyclonic curvature of isobars, steepening of pressure gradient, pre-frontal warning, upper air subsidence causing lowering of inversion height.
HPRIDGE	Rising pressure, advection of cool moist air resulting in cool, unstable conditions.
HPESTAB	Weak surface pressure gradients. Little thermal advection. Dominant upper air ridge with its attendant subsiding motion and stable stratification.
SUBTROP	No apparent mid-latitude influence. Low pressure systems usually extended southwestwards over subcontinent with unstable conditions to E of this axis.
TROPLINK	Trough apparent over E part of country. Aligned in NW/SE direction, linking tropical disturbances with those originating in westerlies.

rainfall total. The remaining 27% of the seasonal rainfall is associated with high pressure systems (designated HPRIDGE and HPESTAB) with HPESTAB containing some 68% of the no rain days.

4.3 Synoptic-mesoscale interaction (Garstang, Kelbe and Martin)

The interaction between synoptic scale systems and mesoscale features such as the escarpment have been investigated by Kelbe and Garstang (1983) and Garstang et al. (1986). Storms along the escarpment of the eastern Transvaal are shown to be associated with mid-tropospheric troughs of temperate origin which interact with low level easterlies of tropical origin and with the major topographic boundary between the Highveld and Lowveld.

Figure 4.3.0 shows that 68% of all storm and hail days over a 5 year period (1972-1977) occurred when the 850 mb wind was westerly (260 degrees) to northerly (20 degrees). Only a quarter of the non-storm days occur with N-W 850 mb flow. The probability of storm occurrence for each wind direction is shown in Fig. 4.3.0. When summed over the Northwesterly 850 mb wind directions the probability for storms is 51%. Conversely, there is only an 8% probability of severe storms occurring with the 850 mb wind between 170 and 50 degrees.

Synoptic scale troughs produce northwesterly flow over the escarpment. Fig. 4.3.1 shows that these troughs interact with local influences which control the time of occurrence of maximum westerly flow at 850 mb across the escarpment. The timing of this event is shown to be critical with respect to four other local or mesoscale processes:

a. local heating

b. formation of a subsidence inversion east of the escarpment

c. intensification of the inversion east of the escarpment by advection of the mixed layer air off the elevated heat source of the escarpment

d. influx of moist low level air.

Fig. 4.3.2 is a schematic representation of these processes and Fig. 4.3.3 provides evidence of the role played by the low level inflow.

Convective storms on and near the escarpment are thus a product of a number of different scales of motion which interact to reinforce or interfere with each other. Timing as well as location become critical. We have developed evidence which bears both upon the question of timing and upon the question of preferred location. Answers to these questions involve scales of

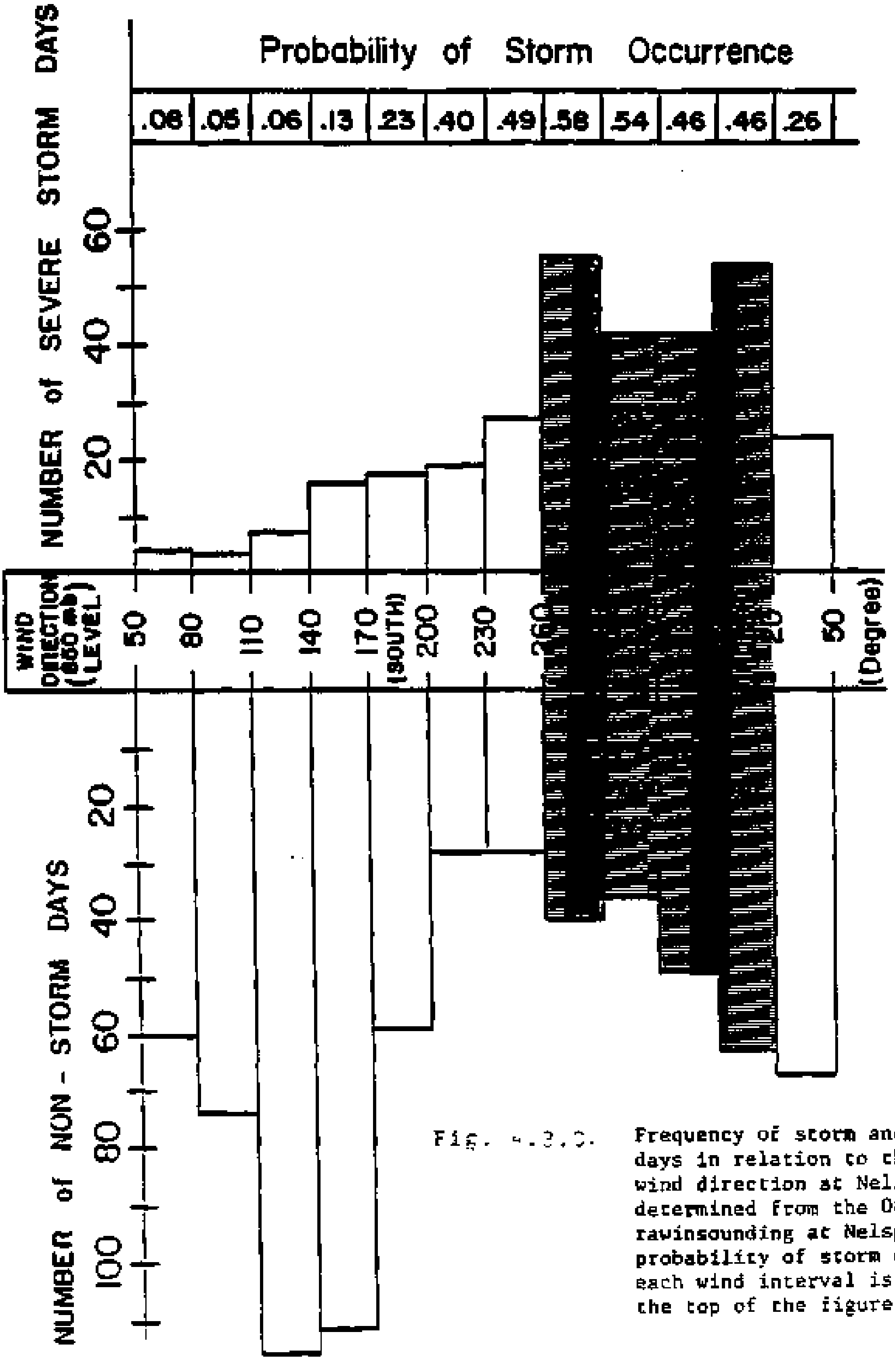

Fig. 4.3.3. Frequency of storm and non-storm days in relation to the 850 mb wind direction at Nelspruit as determined from the 0800 SAST rawinsounding at Nelspruit. The probability of storm occurrence for each wind interval is shown along the top of the figure.

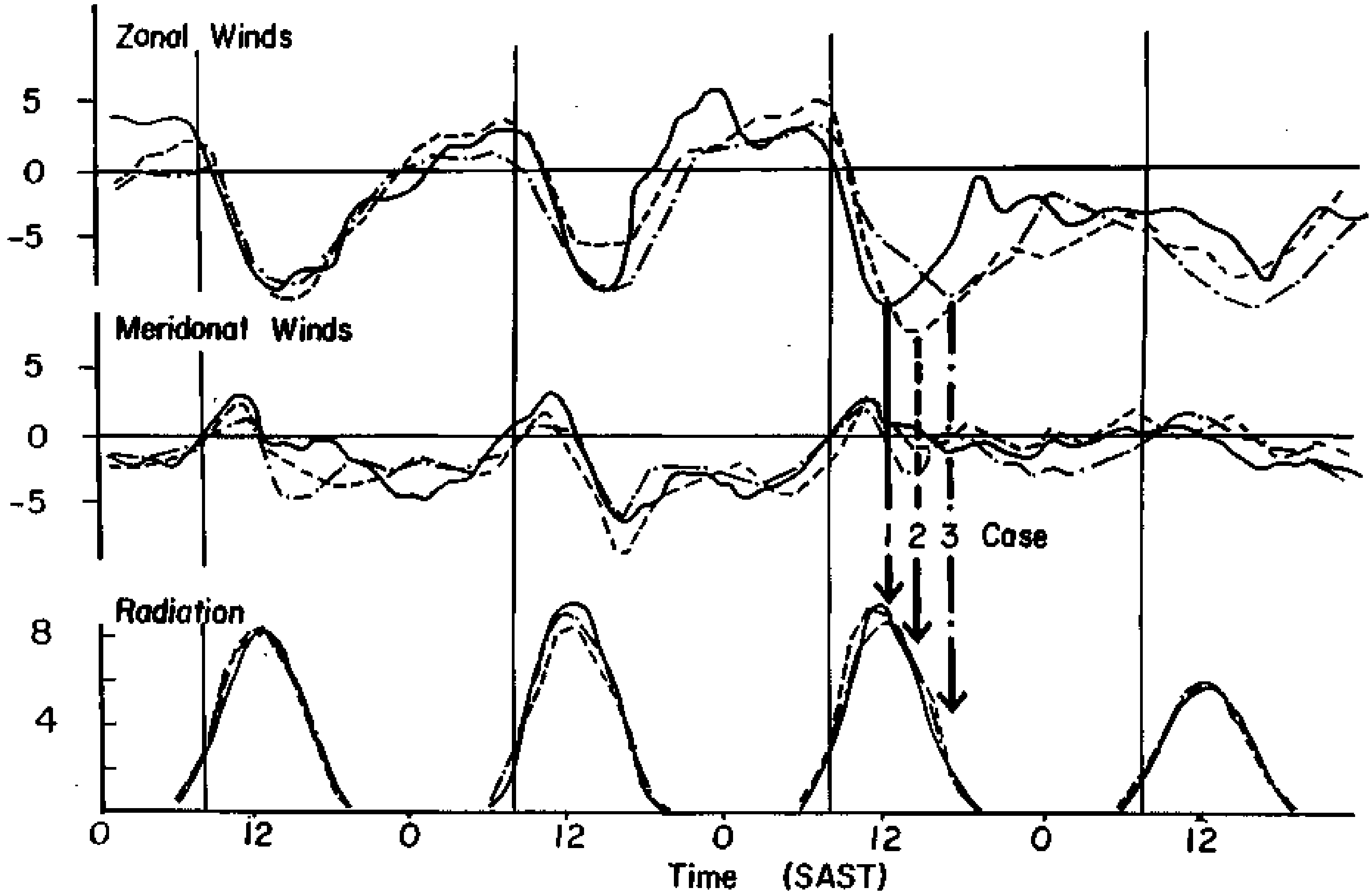

Fig. 4.3.1. Mean hourly values of the surface wind components (m s^{-1}) and global radiation at Nelspruit for all three cases during the four day synoptic sequence. Radiation is in W m^{-2} x 100.

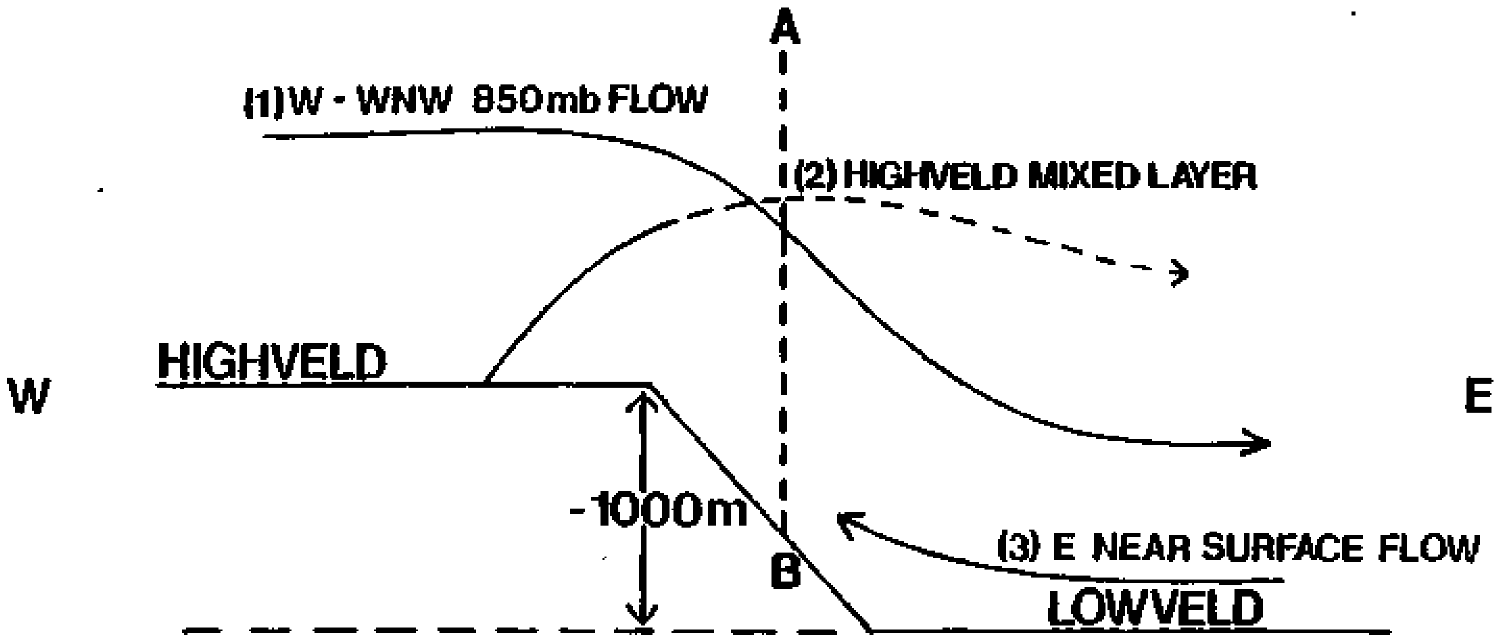

Fig. 4.3.2. Schematic of flows over the eastern Transvaal escarpment. A--B is an arbitrary vertical plane parallel to the escarpment.

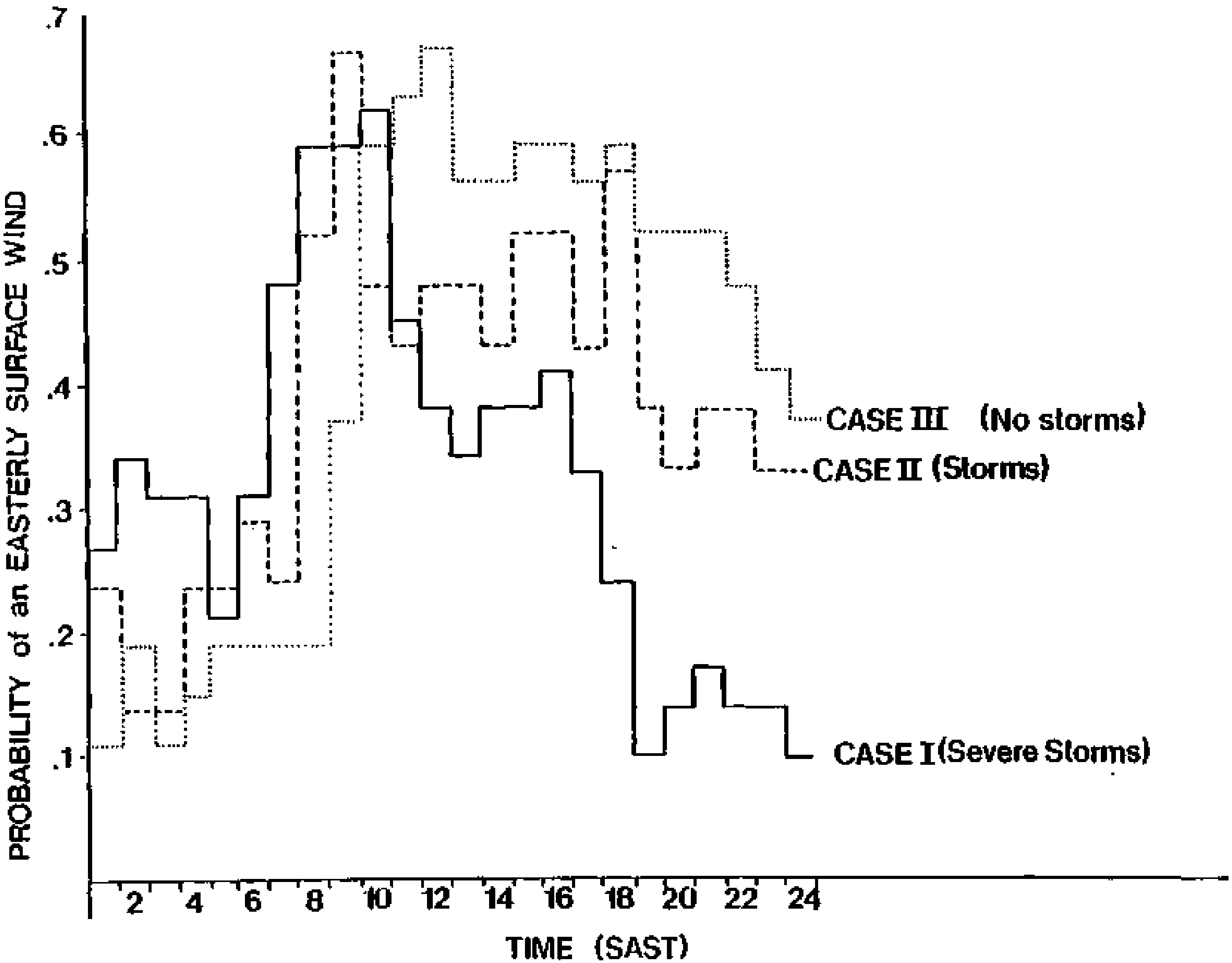

Fig. 4.3.3. Probability of occurrence of easterly surface winds at Friedenheim 5 km east of Nelspruit for each of the three cases shown in Fig. 4.4 as a function of time of day during the summer months for the period 1973-1977.

motion smaller than the synoptic. We deal with these scales in the next two sections.

4.4 Mesoscale controls

A mesoscale network of nine 10 m meteorological towers described in Volume IV was established across the escarpment in 1984. The purpose of these measurements was to determine whether the mesoscale forcing of convective rainfall can be detected in terms of low level mass divergence, vertical mass transports and surface horizontal moisture flux divergence. If such relationships exist then the purpose is to classify the magnitude of surface mesoscale forcing for given days and times. Once the magnitude of the mesoscale forcing is determined then both the natural response (as measured in rainfall or by radar signal responses) as well as the modified response can be characterized in terms of that forcing.

Details of the surface meteorological procedures are given in Volume IV. Figure 4.4.0 gives mean hourly seasonal (October-March) statistics for temperature, moisture, and equivalent potential temperature. Figure 4.4.1 shows the monthly values for the same variables. These figures illustrate

a. that there is little diurnal variation in the mean for moisture as opposed to temperature;

b. January and February are considerably moister (by about 20%) in the mean then the other months.

Figure 4.4.2 shows the mean and standard deviation divergence as a function of time of day for no-rain days and for rain days. No-rain days are defined as those days on which no rain was reported at any of the 9 surface network stations. Rain days are defined as days on which at least one station in the network reported rain. The mean network (9 station) rainfall for the rain days considered in Fig. 4.4.2 is 39.4 mm. No-rain days show little diurnal variation in divergence with the network remaining divergent through the twenty four hours. Rain days, in contrast, show a clear diurnal signal with network showing convergence between about 0900 and 1700 hours LST. The magnitude of the standard deviation of the mass divergence is about 2.5 x 10^{-5} S^{-1} on the no-rain days. This increases somewhat on rain days during the afternoon and early night. The undisturbed standard deviation of around 2.5 x 10^{-5} s^{-1}, however, is accepted as the limit on the resolution of this estimate for the network, i.e. any values outside of those limits are accepted as significant. Figure 4.4.3(a) shows a typical divergence signal, moisture flux divergence and associated rainfall for a rain day. Figure 4.4.4 shows the corresponding signals for a no-rain day.

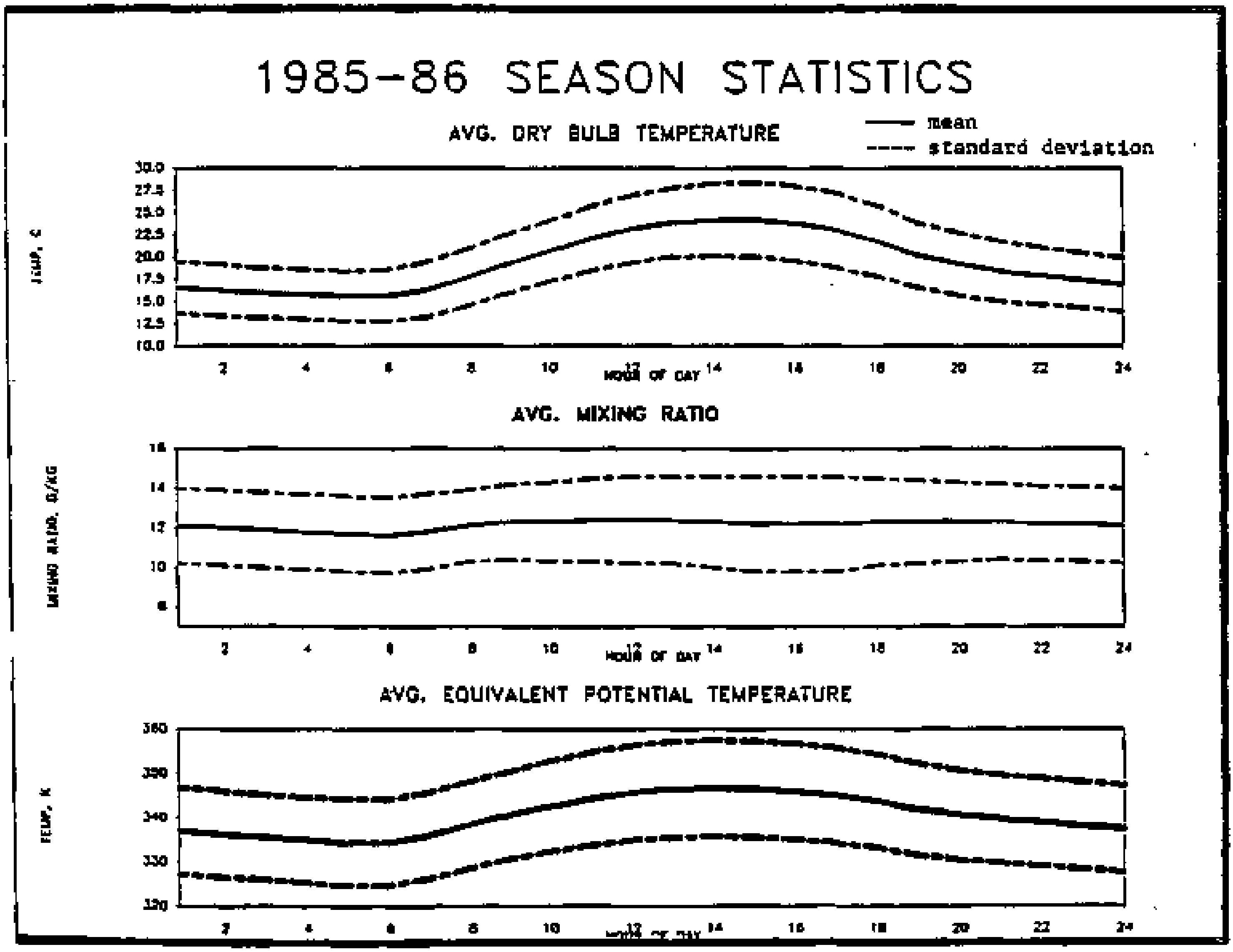

1985-86 SEASON STATISTICS
AVG. DRY BULB TEMPERATURE
mean
standard deviation
AVG. MIXING RATIO
AVG. EQUIVALENT POTENTIAL TEMPERATURE
HOUR OF DAY

Fig. 4.4.0.

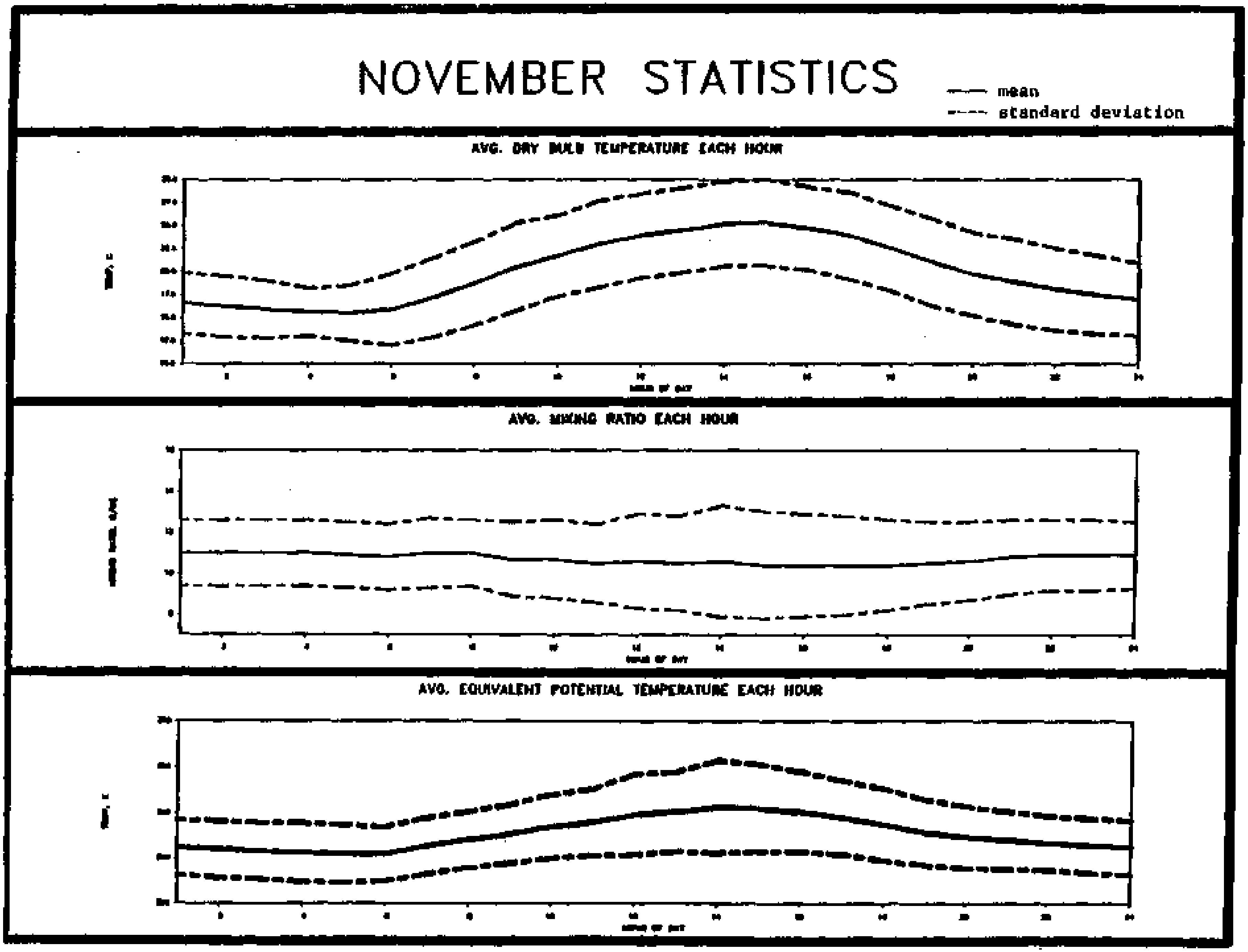
NOVEMBER STATISTICS
mean
standard deviation
AVG. DRY BULB TEMPERATURE EACH HOUR
AVG. MIXING RATIO EACH HOUR
AVG. EQUIVALENT POTENTIAL TEMPERATURE EACH HOUR

Fig. 4.4.1(a)

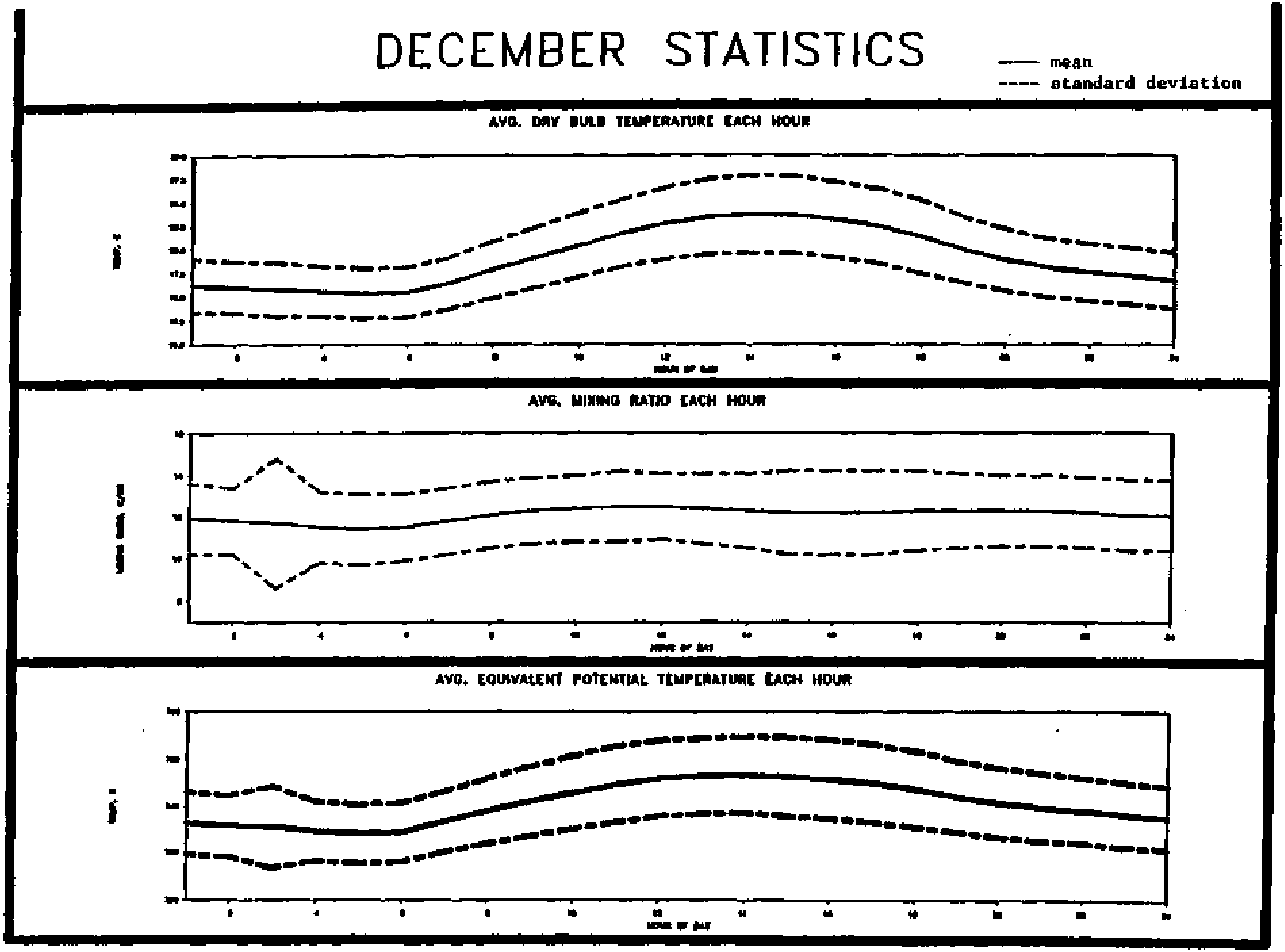
DECEMBER STATISTICS
mean
standard deviation
AVG. DRY BULB TEMPERATURE EACH HOUR
AVG. MIXING RATIO EACH HOUR
AVG. EQUIVALENT POTENTIAL TEMPERATURE EACH HOUR

Fig. 4.4.1 (b).

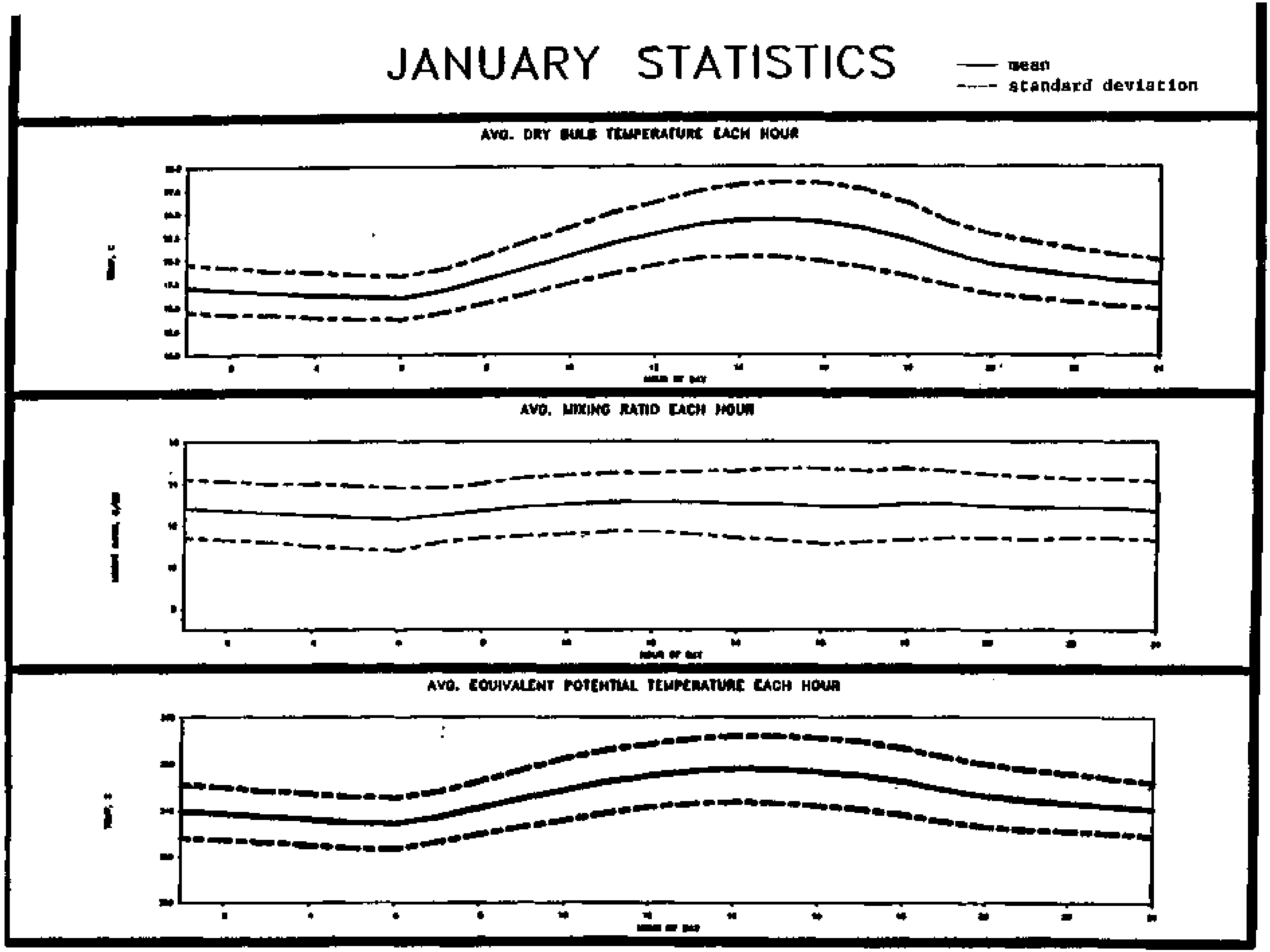
JANUARY STATISTICS
mean
standard deviation
AVG. DRY BULB TEMPERATURE EACH HOUR
AVG. MIXING RATIO EACH HOUR
AVG. EQUIVALENT POTENTIAL TEMPERATURE EACH HOUR

Fig. 4.4.1 (c).

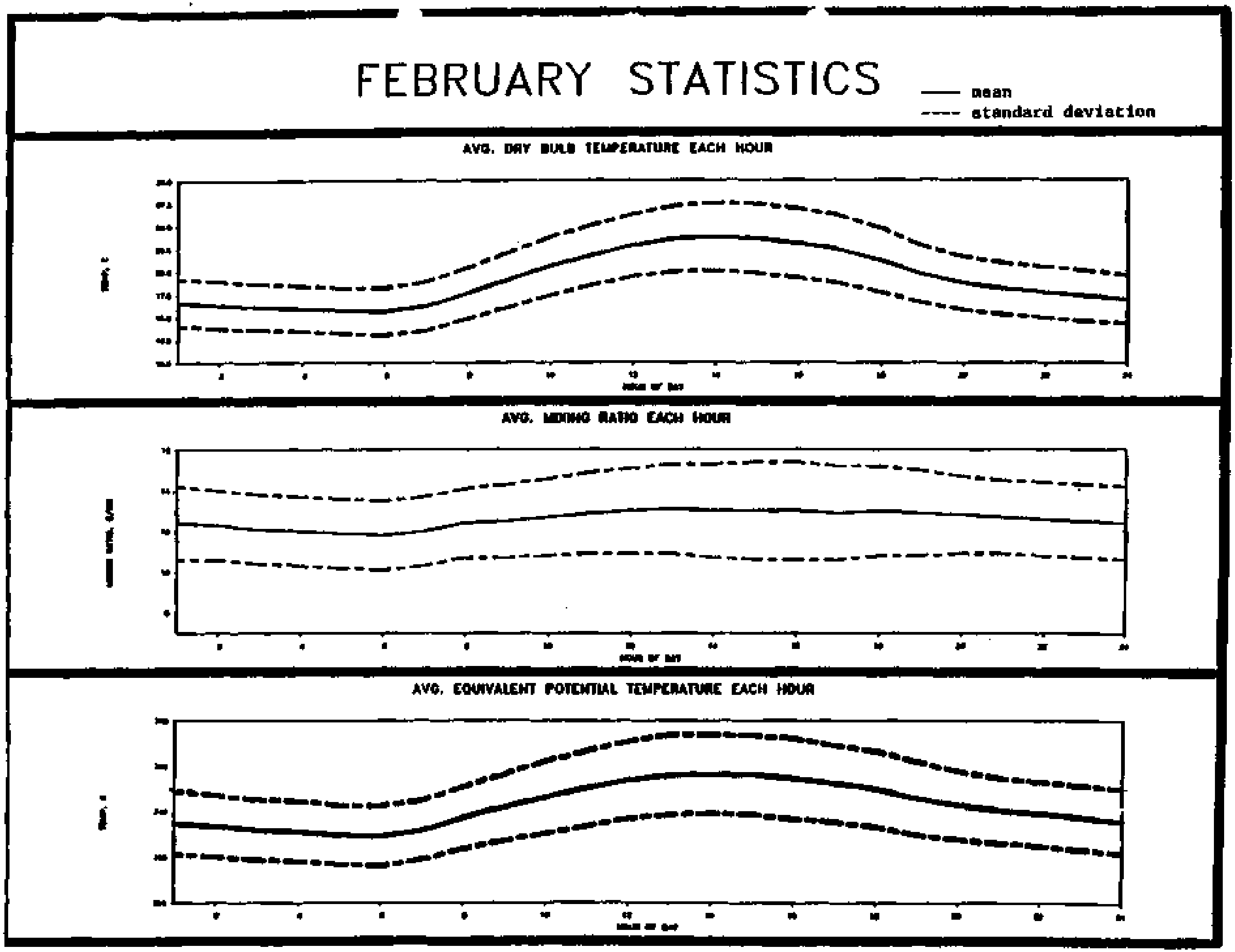
FEBRUARY STATISTICS
mean
standard deviation
AVG. DRY BULB TEMPERATURE EACH HOUR
AVG. MIXING RATIO EACH HOUR
AVG. EQUIVALENT POTENTIAL TEMPERATURE EACH HOUR

Fig. 4.4.1 (d).

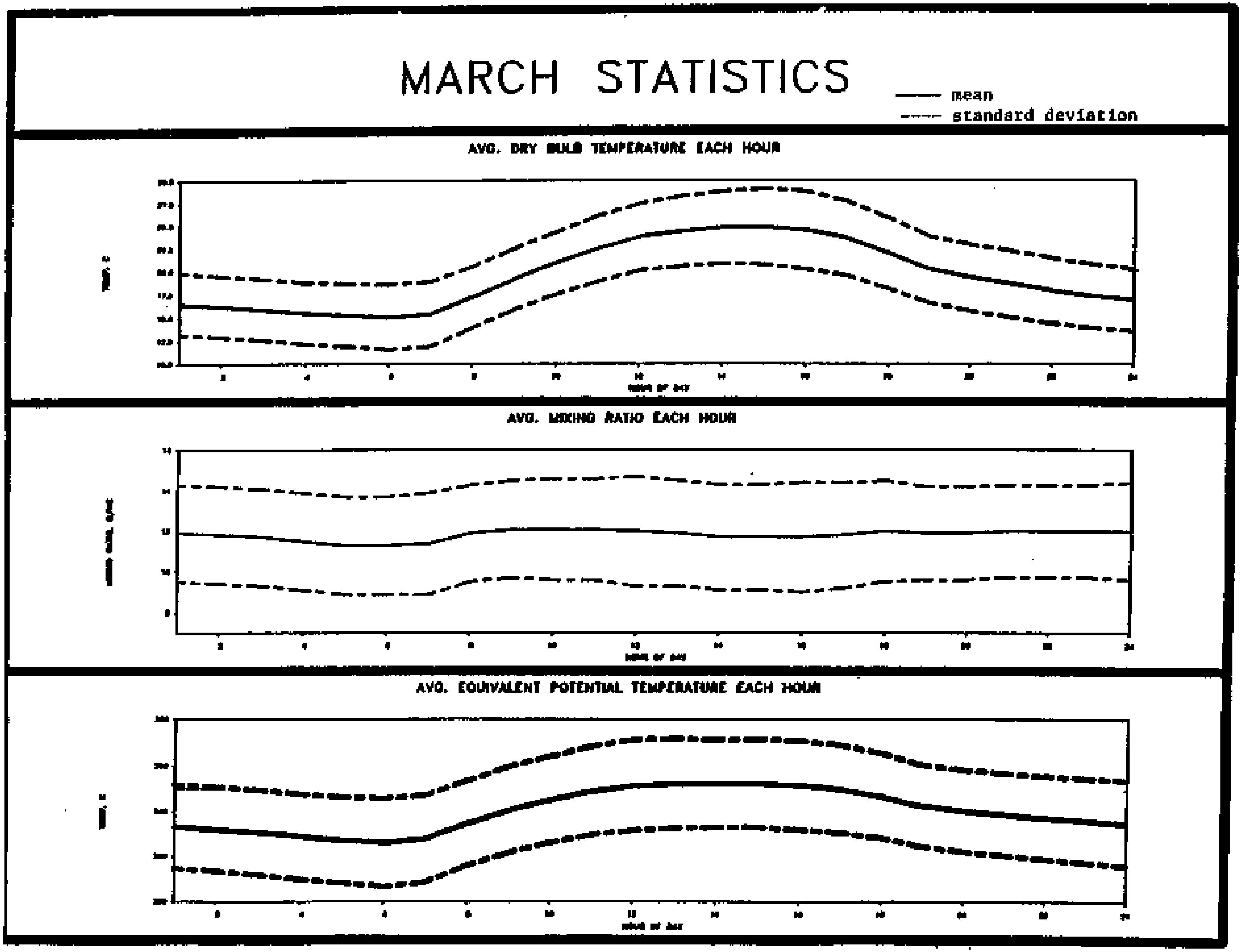
MARCH STATISTICS
mean
standard deviation
AVG. DRY BULB TEMPERATURE EACH HOUR
AVG. MIXING RATIO EACH HOUR
AVG. EQUIVALENT POTENTIAL TEMPERATURE EACH HOUR

Fig. 4.4.1 (e).

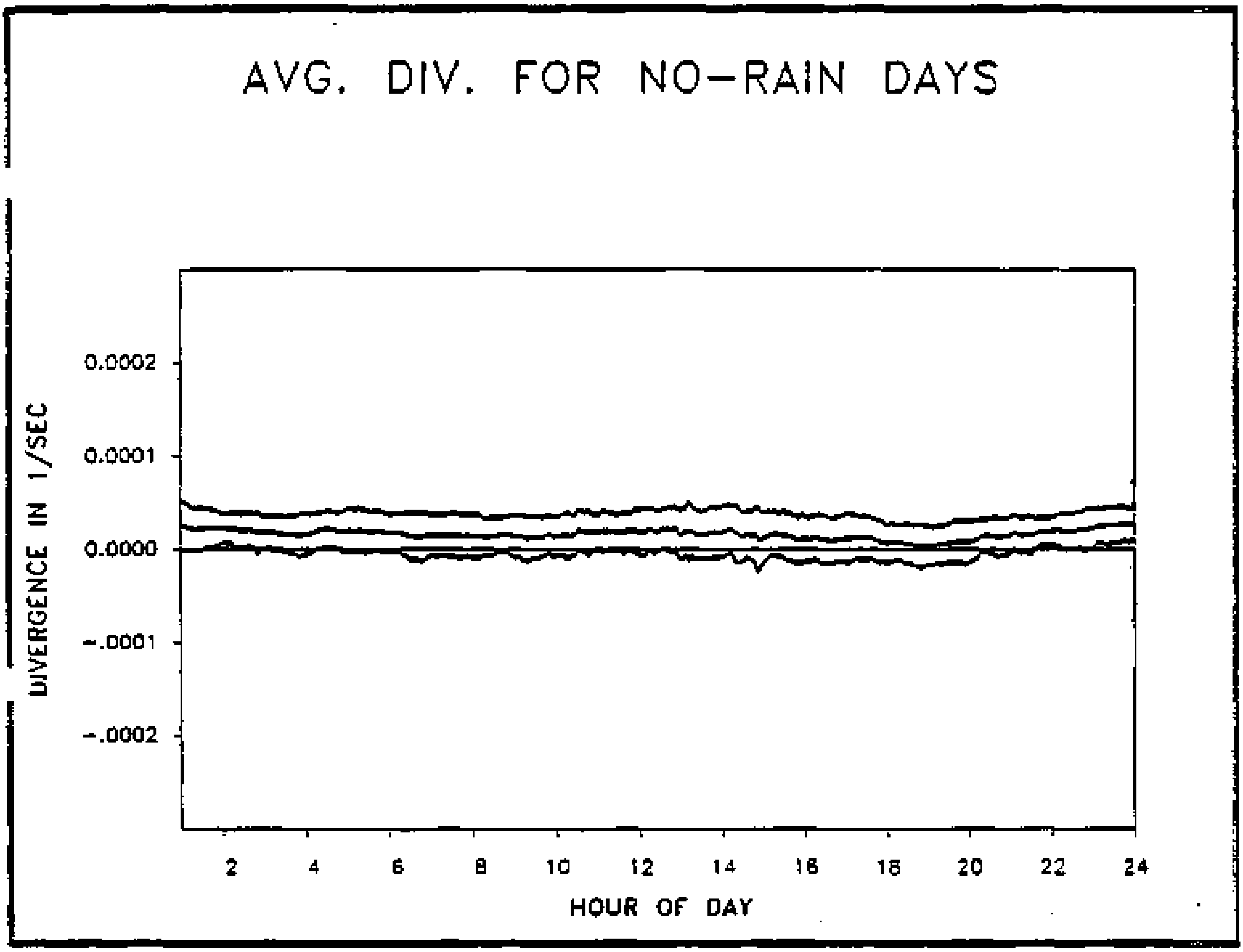

Fig. 4.4.2. The standard deviation is shown on either side of the mean.

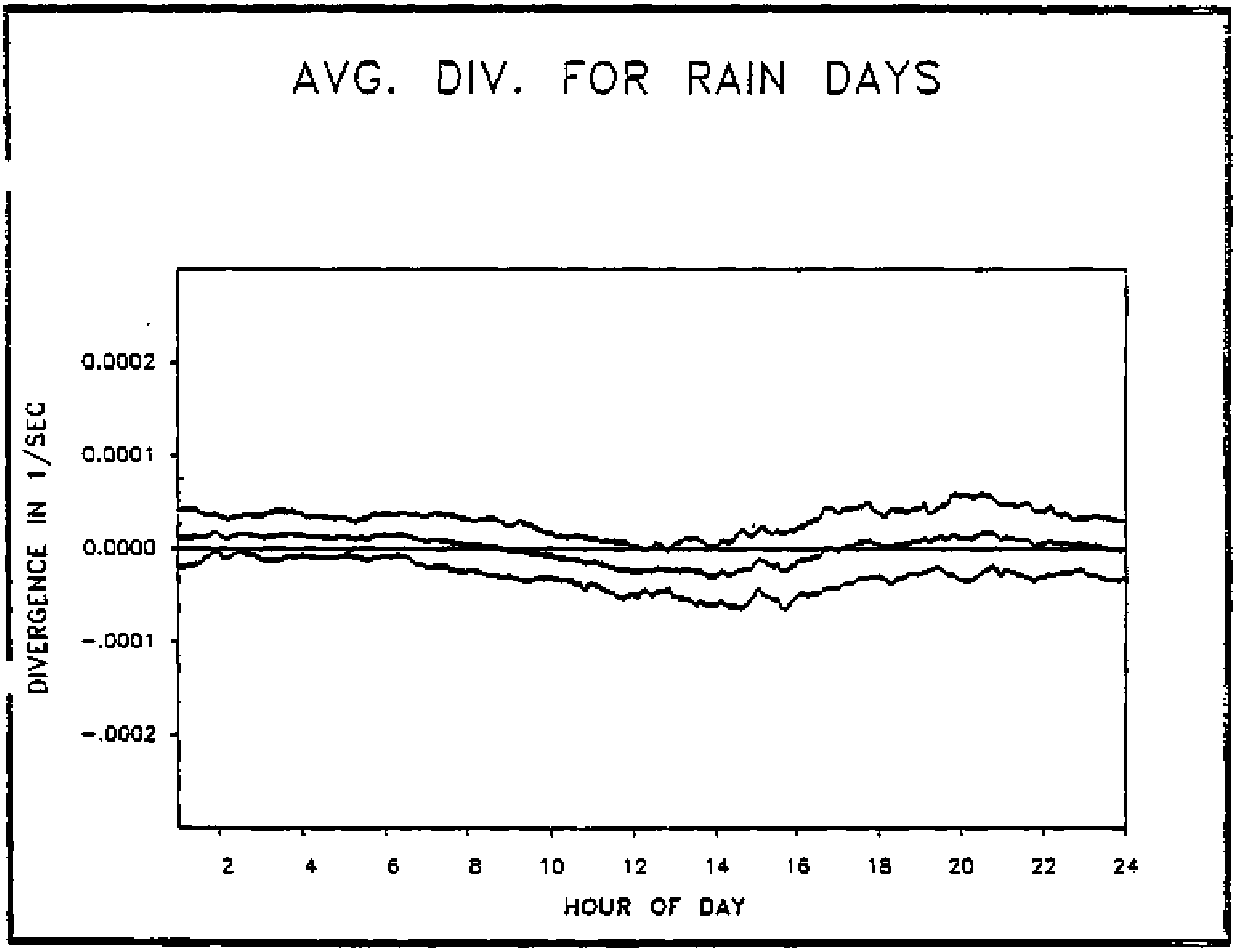

Fig. 4.4.2.(b) Same as for Fig. 4.4.2.(a)

Figure 4.4.3. The upper panel shows the divergence (center trace) and standard deviation (on either side) for the network every 5 mins.

The middle panel shows the net transport every 5 mins and the integrated mass transport starting at 0600 hrs. The lower panel shows the hourly mean station rainfall (bars) and the total Badplaas network rainfall in mm.

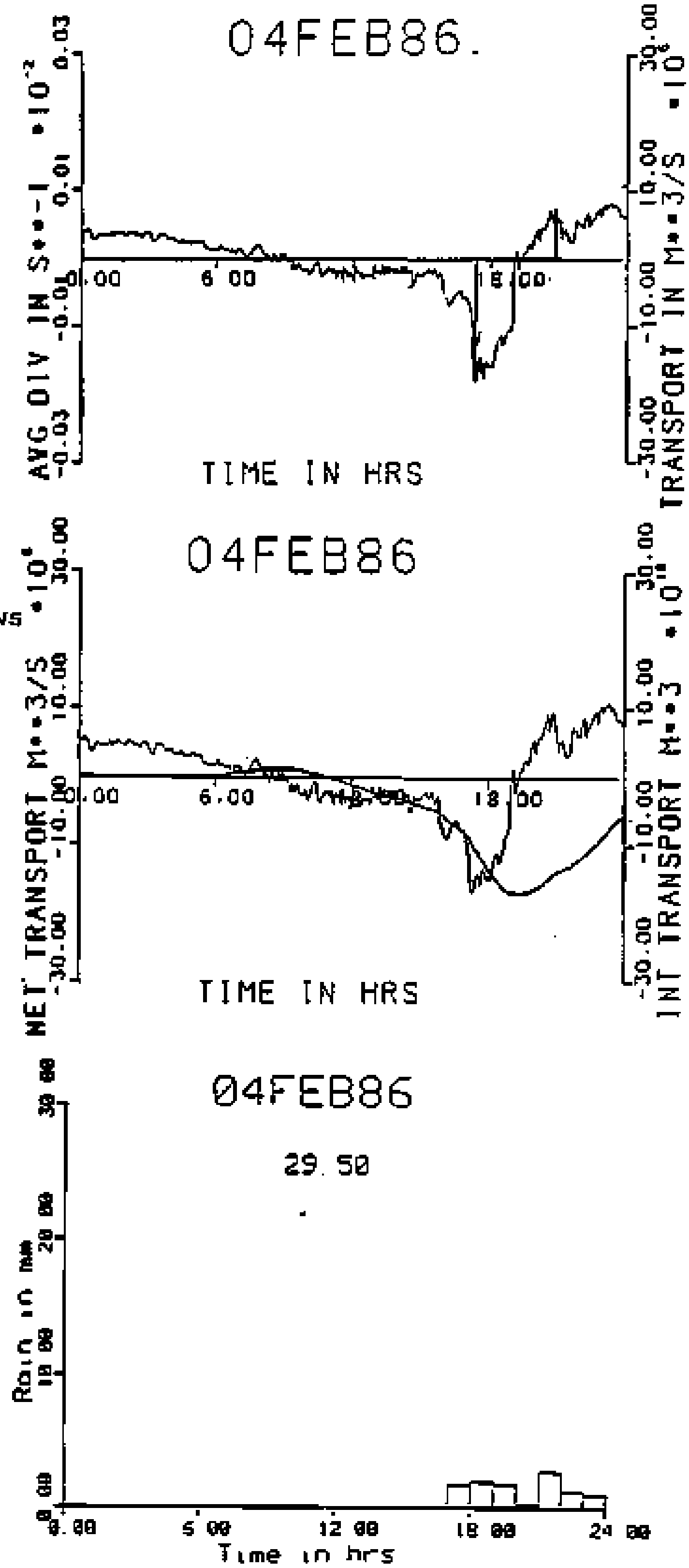

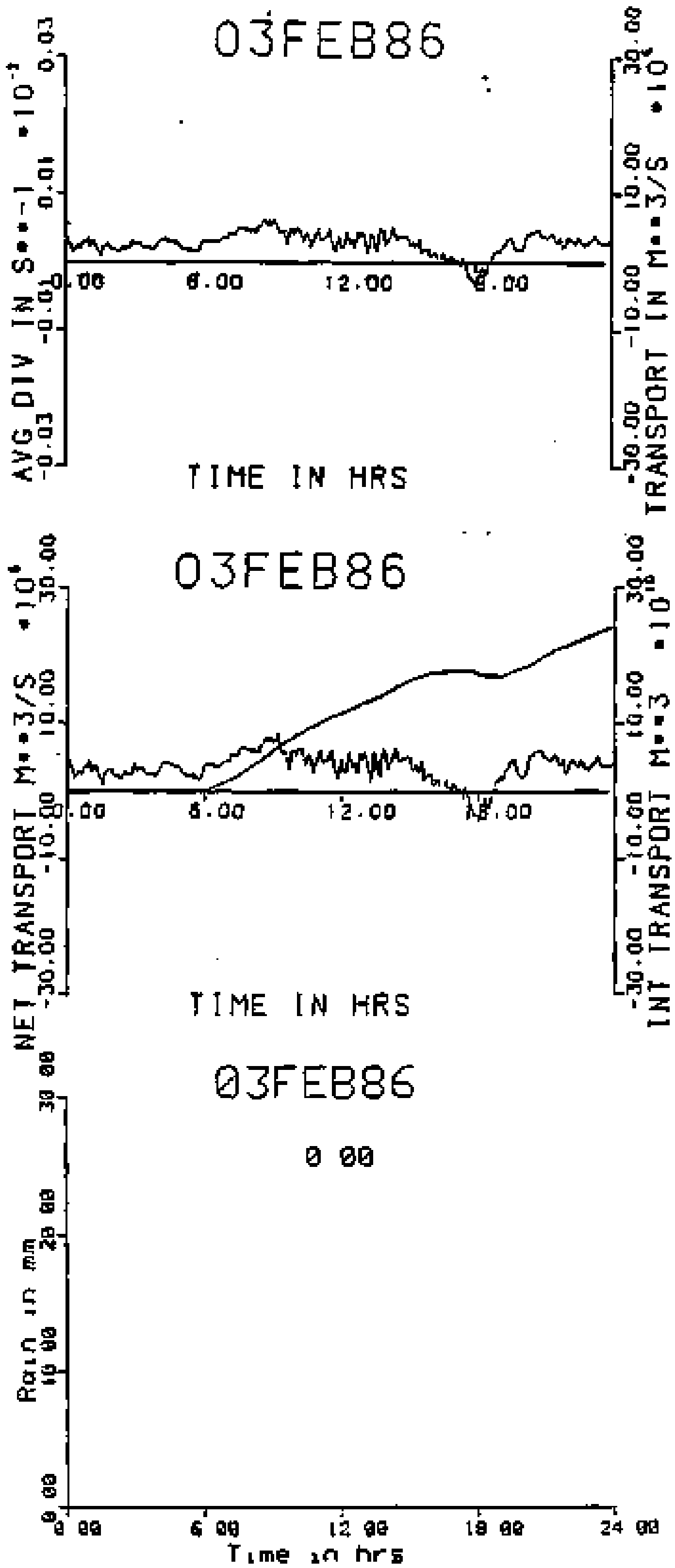

Figure 4.4.4. Same as for Fig. 4.4.3 but for a day with no rain.

The amplitude of the divergence signal for the network can be determined and tabulated. Table 4.2 gives the time of occurrence, magnitude and amplitude of the divergence signal for 50 days during the 1984/85 and 1985/86 seasons. Figure 4.4.5 shows the distribution of the time for occurrence of maximum convergence and divergence. The time of occurrence of maximum convergence is well ordered, centred around 1400 to 1500 hour LST. The time of occurrence of maximum divergence on the other hand, is not simple, suggesting a bimodal distribution with the first maximum around 1600-1700 and a second peak just before midnight. The diurnal distribution of rainfall as measured in the 16 gauge Badplaas network reflects the divergence distribution.

The well ordered nature of the convergence signal suggests a single mesoscale pulse which initiates convection. The subsequent divergence signal represents initial response to the mesoscale forcing followed by a subsequent pulse which can be interpreted as the outflow response to the initial convection. Outflow interactions are addressed in the section below.

Figure 4.4.6 using the numbers provided in Table 4.2, shows the relationship between total network mean daily rainfall and the amplitude of the divergence signal. Twenty days fall in the first 11 ranks with a mean daily network rainfall of 53.6 mm, while the remaining 30 days fall in ranks 12 to 23 with a mean daily rainfall of 39.1 mm.

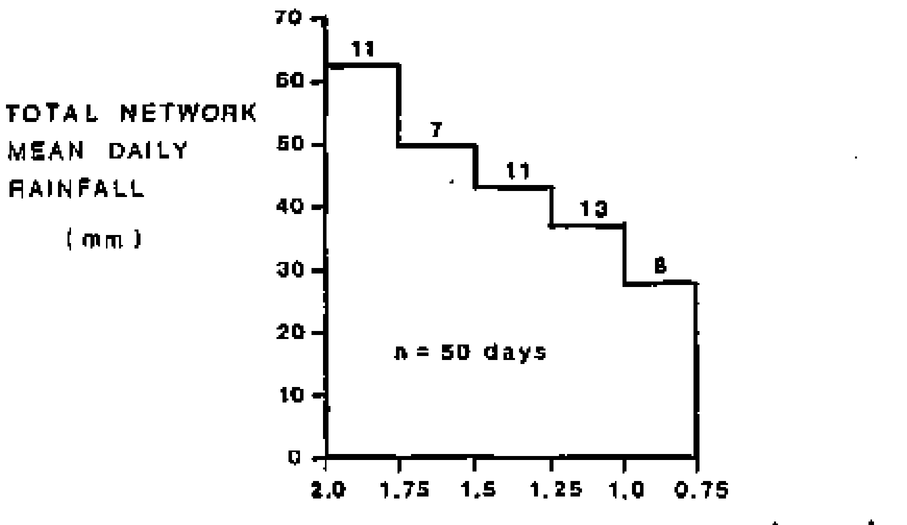

Figure 4.4.6. Maximum amplitude of the network divergence signal (maximum absolute convergence + maximum absolute divergence) for the same 50 days used in Fig. 4.4.5 compared against total Badplaas mean daily rainfall on those 50 days.

Table 4.2

Surface Divergence: Maximum Convergence/Divergence

Date	Time Max Con (LST)	Mag Max Con 10^{-4} s^{-1}	Time Max Div (LST)	Mag Max Div 10^{-4} s^{-1}	|DIV| 10^{-4} s^{-1}	Rank	Rainfall
1 Nov 84	1540	-1.0	1750	+0.5	1.5	10	96.2
12 Nov 84	1350	-1.0	1620	+1.2	2.2	2	148.0
16 Nov 84	1330	-1.2	2030	+0.2	1.45	11	37.8
27 Nov 84	1100	-0.8	1800	+0.5	1.3	14	63.0
28 Nov 84	1405	-0.8	1805	+0.2	1.0	19	101.0
29 Nov 84	0940	-1.0	1235	+0.2	1.2	16	96.8
10 Dec 84	1200	-0.8	1605	+0.5	1.3	14	24.2
12 Dec 84	1020	-0.8	1740	+0.6	1.35	13	160.2
13 Dec 84	1230	-0.2	1825	+1.1	1.3	14	83.8
14 Dec 84	1415	-0.7	1645	+0.8	1.5	10	46.0
16 Oct 85	1555	-1.3	2230	+0.2	1.55	9	2.0
29 Oct 85	1830	-1.9	2245	+0.7	2.6	1	186.0
2 Nov 85	1330	-0.9	--	--	0.9	21	8.2
8 Nov 85	1200	-0.9	1440	+0.9	1.8	6	45.0
9 Nov 85	1140	-1.5	2040	+0.6	2.1	3	122.5
22 Nov 85	1540	-0.9	2155	+0.4	1.3	14	0
26 Nov 85	1845	-0.6	2250	+0.4	1.0	19	58.5
3 Dec 85	1000	-0.4	1745	+0.4	0.8	22	0
6 Dec 85	1540	-0.8	2210	+0.2	1.05	18	5.2
7 Dec 85	1655	-0.9	2220	+0.8	1.7	7	14.5
11 Dec 85	0820	-1.1	1405	+0.8	1.85	5	4.0
14 Dec 85	1345	-0.9	1650	+0.9	1.8	6	2.8
30 Dec 85	1620	-0.4	1905	+0.6	1.0	19	11.8
3 Jan 86	1445	-0.8	1845	+0.5	1.3	14	32.0
7 Jan 86	1415	-0.2	2105	+0.8	1.05	18	1.2
12 Jan 86	1855	-0.6	2150	+1.0	1.6	8	18.5
13 Jan 86	1615	-0.3	1820	+0.9	1.2	16	49.5
14 Jan 86	1715	-0.2	1935	+1.0	1.25	15	23.5
15 Jan 86	1536	-0.6	1750	+1.3	1.9	4	38.5
18 Jan 86	1430	-0.7	1705	+0.5	1.2	16	20.5
29 Jan 86	1445	-0.6	2110	+0.4	1.0	19	58.0
4 Feb 86	1715	-1.3	1845	+0.8	2.1	3	29.5
5 Feb 86	1520	-0.7	1945	+0.2	0.95	20	49.2
6 Feb 86	1440	-0.2	1635	+0.5	0.75	23	58.0
7 Feb 86	1710	-1.4	2030	+0.7	2.1	3	41.5
8 Feb 86	1320	-0.6	2230	+0.3	0.9	21	24.5
9 Feb 86	1300	-0.6	1455	+0.5	1.1	17	26.2
10 Feb 86	1405	-0.5	1600	+0.7	1.2	16	20.2
11 Feb 86	1540	-0.8	2215	+0.9	1.7	7	75.8
12 Feb 86	1800	-0.6	1815	+1.2	1.8	6	34.5
13 Feb 86	1155	-0.4	1415	+0.4	0.8	--	15.8
21 Feb 86	1050	-0.8	1645	+0.3	1.1	17	40.0

Date	Time Max Con (LST)	Mag Max Con 10^{-4} s^{-1}	Time Max Div (LST)	Mag Max Div 10^{-4} s^{-1}	|DIV| 10^{-4} s^{-1}	Rank	Rainfall
22 Feb 86	1300	-0.8	2100	+1.0	1.8	6	32.8
3 Mar 86	2000	-1.2	0005	+0.5	1.7	7	0.8
6 Mar 86	1900	-0.8	--	--	--	--	0
10 Mar 86	1425	-0.5	1645	+1.0	1.5	10	96.5
12 Mar 86	1555	-0.6	2030	+0.3	0.9	21	69.8
13 Mar 86	1345	-0.7	2200	+0.7	1.4	12	4.0
14 Mar 86	1200	-0.5	1440	+0.8	1.3	14	12.5
24 Mar 86	1330	-1.0	1900	+0.2	1.2	16	0

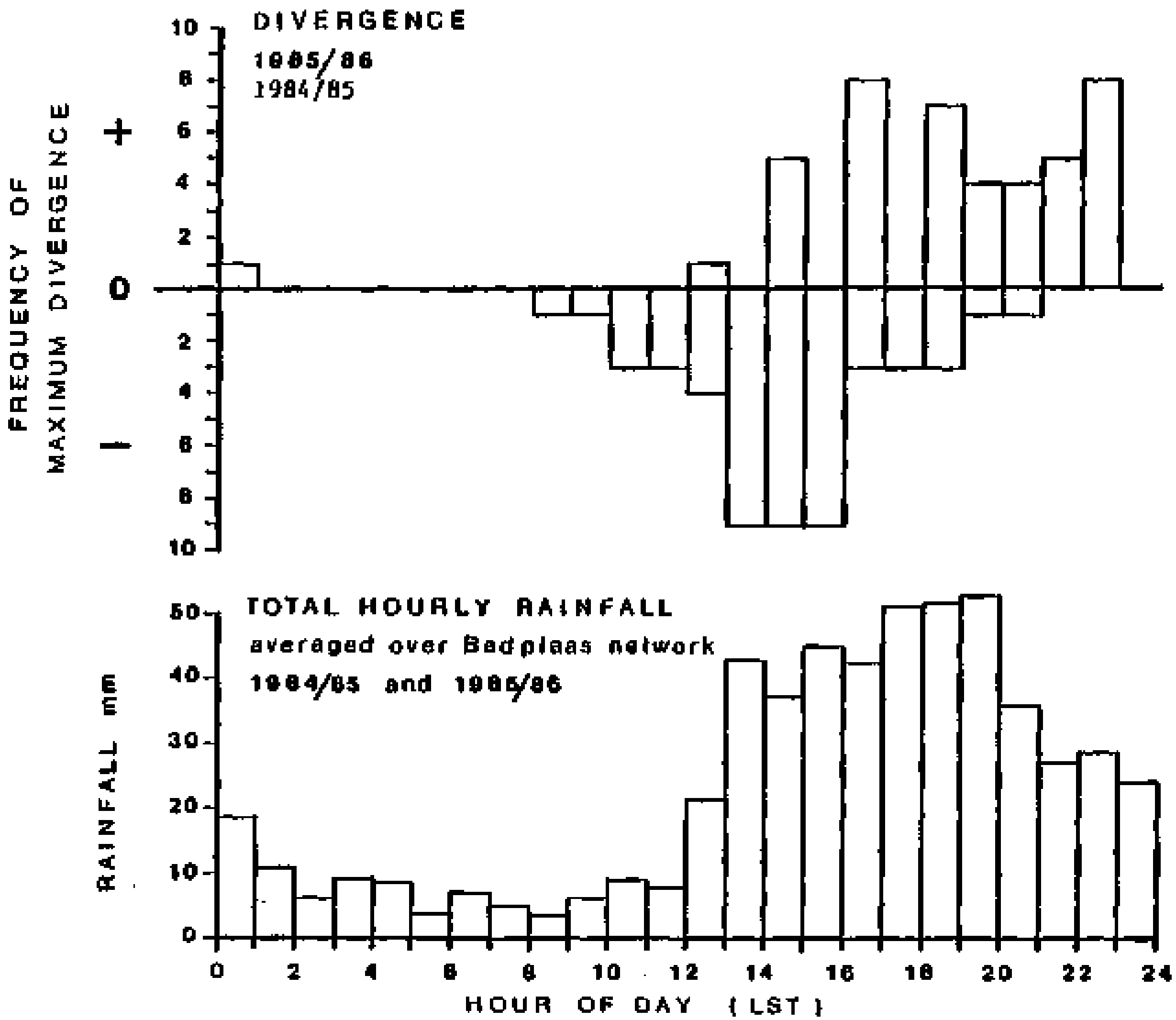

Fig. 4.4.5. Frequency of occurrence by hour of day on 50 days of the time of maximum convergence and time of maximum divergence for the 1984/85 and 1985/86 seasons compared with the mean total hourly rainfall measured over the Badplaas network for the same seasons.

On the basis of the above results three classes of mesoscale forcing can be established:

Strong mesoscale forcing: amplitude of DIV $> 1.5 \times 10^{-4}$ s $^{-1}$

Weak mesoscale forcing : amplitude of $0.5 >$ DIV $< 1.5 \times 10^{-4}$ s^{-1}

No mesoscale forcing : amplitude of DIV $< 0.5 \times 10^{-4}$ s $^{-1}$

The mean network total daily rainfalls corresponding to these three classes of surface mesoscale forcing are approximately 55 mm, 40 mm and less than 25 mm rainfall with large standard deviations of 50.37, 36.92 and 19.63 mm respectively.

The relationship between divergence as calculated from the mesoscale network and rainfall may be improved by including the areal extent of the maximum convergence as parameterized by Ulanski and Garstang (1978) and by including a measure of the horizontal moisture flux at the surface. Figure 4.4.7 shows an attempt to measure the advection of moisture into the Lowveld, escarpment and Highveld. Figure 4.4.7 (a) and (b) show contrasting situations in rainfall production. Figure 4.4.7 (a) for 10 March 1986 shows a well defined convergence/divergence pair with high equivalent pontential temperatures (356°K) contained within the divergence pair. Figure 4.4.7 (b) for 22 November 1985 shows a very similar divergence pattern (magnitude and size) but with Theta-e only reaching 332°K. On March 10 a total of 96.5 mm of rain was recorded by the surface network stations. On November 22 no rain was recorded.

4.5 A description of the meteorology of Nelspruit rainfall based on practical observing and forecasting experience (Mather and Morgan)

Our knowledge of the meteorology of storms and rainfall derives from attempts to forecast storm occurrences, types and intensities. Forecasting is a skill acquired through experience, with occasional assistance from science. In Nelspruit the main body of experience has come from the many years of hail suppression activities.

During the PAWS years the facilities for manipulating and archiving meteorological data at Nelspruit have been brought to a high level. With the new computer system and the fund of data that has been accumulated, it is now possible to begin producing more objective storm forecasts, using past experience as a guide. A collection of forecast studies appears in Vol. IV of this Report.

The subjective forecasting methods applied at Nelspruit are quite successful in predicting daily weather for operational purposes. Though surprises do occur, the forecasting is useful in terms of scheduling varying levels of maintenance on aircraft and

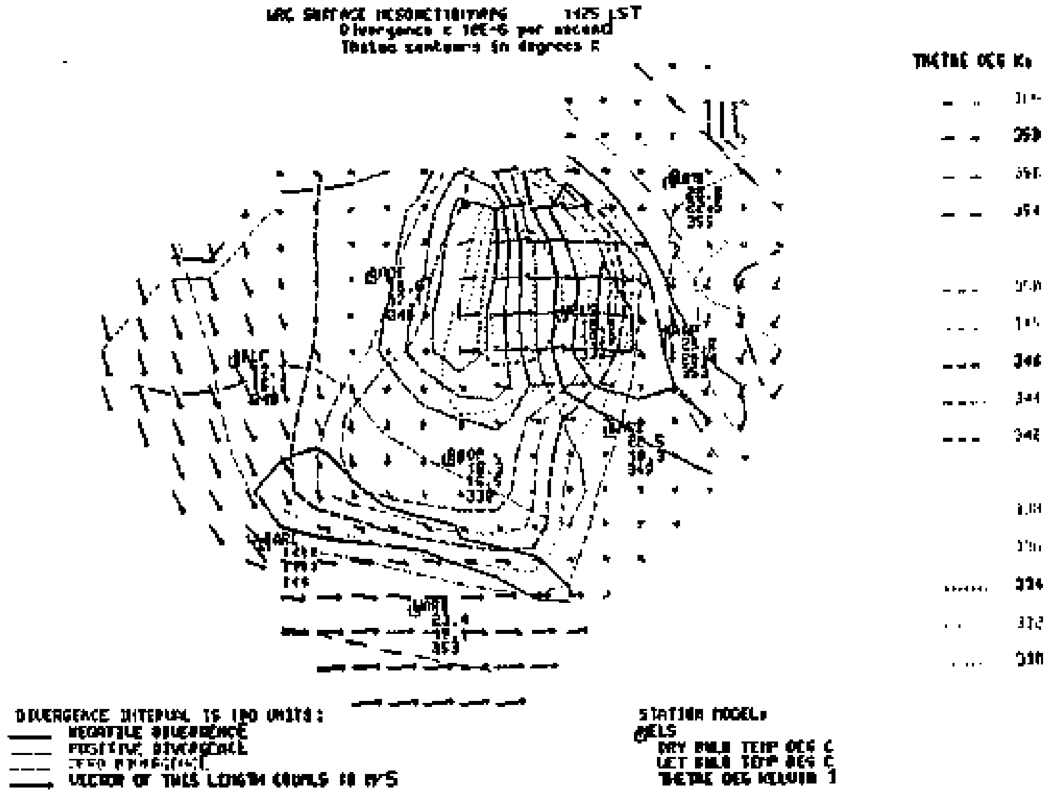

(a)

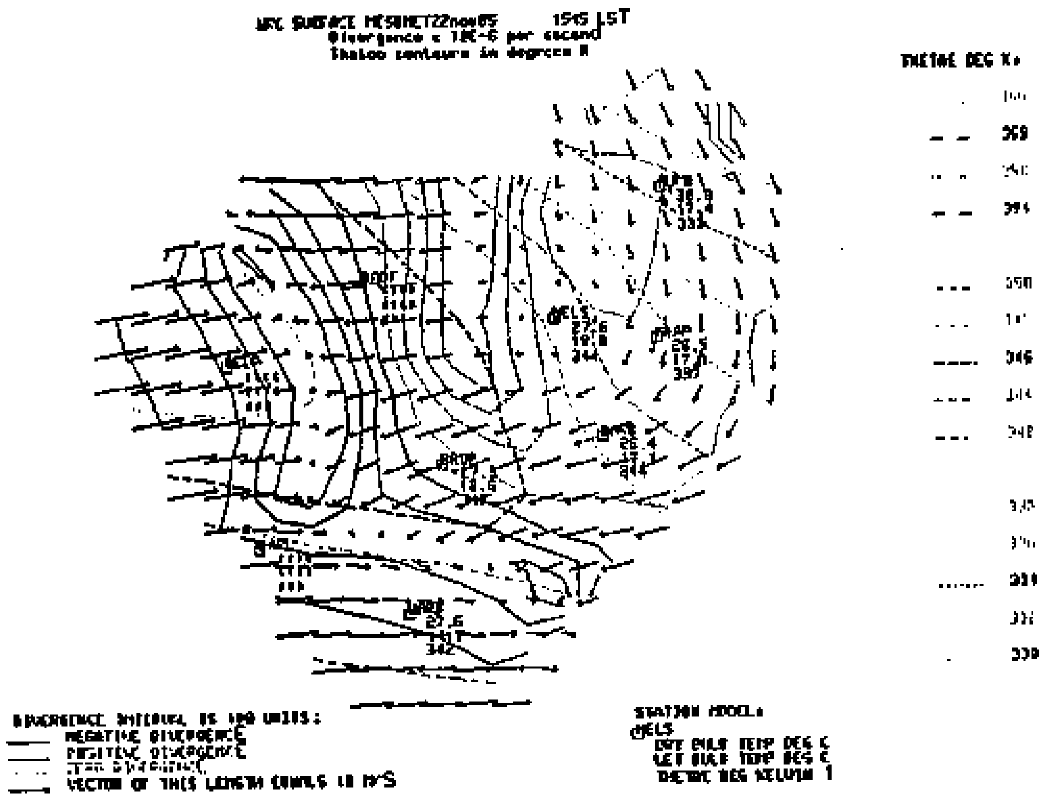

(b)

Figure 4.4.7 Surface meteorological network with divergence, 10 m surface winds and the equivalent potential temperatures shown at the time of maximum convergence on (a) 18 March 1986 when a total of 85.8 mm of rainfall was recorded in the network gages, and (b) 22 November 1985 when no rainfall was recorded.

other important systems and establishing daily priorities for data reduction and analysis. It would be difficult to conceive of carrying out a personnel-limited field programme such as PAWS, without it.

4.5.1 Forecasting.

The information that is used to prepare the daily forecast at Nelspruit comes from the following sources:

a. the Nelspruit 0600Z radiosonde ascent, which measures vertical profiles of temperature, humidity and wind velocity

b. the 0600Z surface data obtained from the Weather Bureau by interrogating their computer via telex

c. the 0000Z radiosonde ascents from eight South African upper air stations

d. recordings of the satellite images of the 0730 and 0800 infrared and visual Meteosat transmissions.

The 0600Z surface data is fed into the project computer and 9 maps of surface variables are computed. One of the most useful variables plotted is the equivalent potential temperature (Theta-e). Since this temperature is conservative with respect to dry and pseudo-adiabatic processes (such as lifting caused by airmass traverses over higher terrain), maps of Theta-e are free from terrain effects that mask essential differences in air mass properties when only surface temperatures are plotted. More simply, Durban and Johannesburg will exhibit the same Theta-e temperatures despite their differences in height provided they are both under the influence of the same airmass.

Other maps of considerable interest are 24 hour difference plots. These provide a good indication of the rate of movement of synoptic systems across the country.

Maps of country-wide stability indices and their 24 hour tendencies are also plotted and displayed in colour on the visual display unit. Examples of these maps and some forecasts prepared from them are given in Volume IV.

A detailed analysis of the local stability is prepared by plotting the Nelspruit 0600Z and the Pretoria 0000Z sounding on the same thermodynamic diagram, then constructing an interpolated sounding from the two for the escarpment west of Nelspruit. Experience has shown a conditionally or neutrally stable Nelspruit sounding can be de-stabilized by storms that form along the escarpment, then move into the Lowveld. Cold air from their outflows can undercut and lift the neutrally stable Lowveld air to its level of free convection (LFC), setting off convection that would not have been forecast on the basis of the Nelspruit sounding alone.

4.5.2 Weather types and their attendant rainfall

The types of weather affecting the rainfall in the PAWS area are divided into four general categories:

- airmass
- frontal
- post frontal
- tropical

a. Airmass

Isolated to occasional scattered storms occur in airmasses undisturbed by synoptic events. The extent of these generally isolated storms depends upon the moisture content of the airmass and the surface heating available. Airmass storms are most frequent in the mid-summer months of November to February when moist airmasses are almost always present in the area. Rain that falls from these storms is erratically distributed and concentrated mainly along the escarpment. This is due to a mesoscale "sea breeze" that begins between 0900 and 1000 local time. This airflow is relatively cool, but is laden with moisture. The high terrain west of Nelspruit is the first area to reach its convective temperature and the easterly breeze supplies the necessary moisture for convection. On a classical airmass thunderstorm day, the escarpment area as seen by radar or satellite is delineated by convective storms, the highest area showing first activity.

The extent to which the Lowveld benefits from these outbreaks is dependent upon two factors; the strength and direction of the storm steering winds (the 500 mb flow) and the temperature of the low level easterly flowing air. If the 500 mb flow is absent or even easterly, the escarpment storms will remain stationary or move westward from their points of initiation. Good westerlies will drive the storms into the Lowveld where they will survive. as long as the temperature of the low level easterlies is not too low (the Lowveld airmass unconditionally stable).

These stationary escarpment storms may also throw extensive anvils over the Lowveld which cut off heating, effectively damping convection in the Lowveld.

These escarpment storms are almost always present during the summer months and while augmenting rainfall from these storms would not benefit the Lowveld directly, additional water would benefit stream flow and natural and artificial water storage systems in this area.

b. Frontal systems

Cold fronts, which sweep into the area from the south and the southeast, are major rain events in the Lowveld. These systems are clearly visible on the images from satellites as they approach and pass the Cape and sweep up the southeast coast through Natal. Two factors which substantially affect the rainfall produced by these systems are their timing and the extent of upper air support.

A cold front that arrives in the area in the early morning or late evening may undercut air that is too cool to release convection. A cold front, whose arrival coincides with the daytime heating maximum, can set off some of the most severe weather witnessed in the area. The arrival of a cold front coincident with the approach of a strong upper air trough brings some of the best and most widespread rains to the Lowveld. The rate of movement of the upper air trough eastward also determines how long rain events persist in the area.

c. Post-frontal weather

Post-frontal weather is characterized by cool overcast conditions with intermittent drizzle. The rainfall from these events comprises less than 5 percent of the annual total. It is an important condition for the near Highveld, however, as the extent of the westward push of the cool moist airmass determines where storms will first break out on the Highveld. Satellite images clearly show storms forming along the western edge of the cloudy post frontal air. Their subsequent trajectories are again dependent on the upper level flow and on the rate at which the cool moist air pushes westward. Experience in the PAWS area suggests that these storms might possess considerable modification potential.

d. Tropical weather events

The weather described above in (i),(ii) and (iii) is most prevalent in the early summer (October through December) and can be ascribed to mid-latitude forcing (easterly movement of weather systems driven by the subtropical jet stream). While infrequent, there are two other weather events that can profoundly affect the Lowveld seasonal rainfall.

The first occurs when a tropical cyclone drifting down the Mocambique channel makes landfall east of Nelspruit. Such a cyclone at the end of January 1983 accounted for 25 percent of that season's rainfall. Another event similar to the cyclone event occurs when a deep low over Zimbabwe and a strong Indian Ocean high pressure area converge causing strong easterly flow at all levels above the Lowveld. This event, which leads to general rainfall over the area, often for several days, can produce more rainfall than a cyclone. An analysis of summertime rainfall (see RAIN II report) indicates that the presence or absence of these two events may mean the difference between below or above average summer rainfall.

Modification attempts in these two situations are not even contemplated since these systems are already efficient rain producers and because of the flood risk.

5.0 A PHYSICAL DESCRIPTION OF NELSPRUIT CLOUDS (Morgan, Morrison and Mather)

5.1. Introduction

Rain is produced over the Eastern Transvaal Escarpment mostly by cumuliform clouds, and it is these that PAWS has been studying. Cumulus clouds are distinguished primarily by their shapes, (looking like heaps or piles of cloud), but the processes going on in them are also very particular to them and are the key to stimulating them to enhance their rain production. Cumulus clouds exist over a wide range of sizes, from small, fair-weather cumulus to giant cumulonimbus. The aircraft investigations of PAWS are carried out in growing cloud turrets on the flanks of convective complexes.

In the following, the characteristics of the cloud turrets which have been sampled by the PAWS Learjet are presented, to give the reader a quantitative picture of the clouds which are being studied and seeded.

Measurements are presented here without a discussion of measurement techniques. The interested reader will find measurements discussed in Vol. IV, Sections 2,9 and 10.

5.2 Vertical Velocities and Condensation Rates

Perhaps the most important single physical characteristic of cumulus clouds is the rate at which condensation is taking place in them and this depends primarily on their vertical velocities. The same vertical velocities determine the cloud's ability to hold water drops and ice particles in suspension long enough to grow to the large sizes characteristic of convective rainfall. Fig. 5.2.0 summarizes the updraft measurements made during the past 5 years by the instrumented Learjet.

The average maximum vertical velocity is almost twice the average minimum, an almost universal characteristic for cumulus clouds and thunderstorms. The mean of the average vertical velocities is only 3.1 m sec^{-1}, and a significant percentage of cases had negative average vertical velocities. These correspond to encounters with dead or dying clouds. It is for this reason that for many purposes we restrict our attention to clouds with average vertical velocities greater than 2.5 m sec^{-1}. Dying clouds often fill rapidly with ice particles and have depleted cloud liquid water.

The Cloud Sample Database also contains the average updraft and average downdraft. These are averages over only the upward moving and downward moving portions of the cloud pass, respectively. They are summarized in Table 5.1. Sample sizes differ between Fig. 5.2.0 and Table 5.1 because of definitions; some clouds have no updraft, some no downdraft, but all have a *maximum* and a *minimum* vertical velocity. Sample sizes are large for both displays because the calculations required that only the

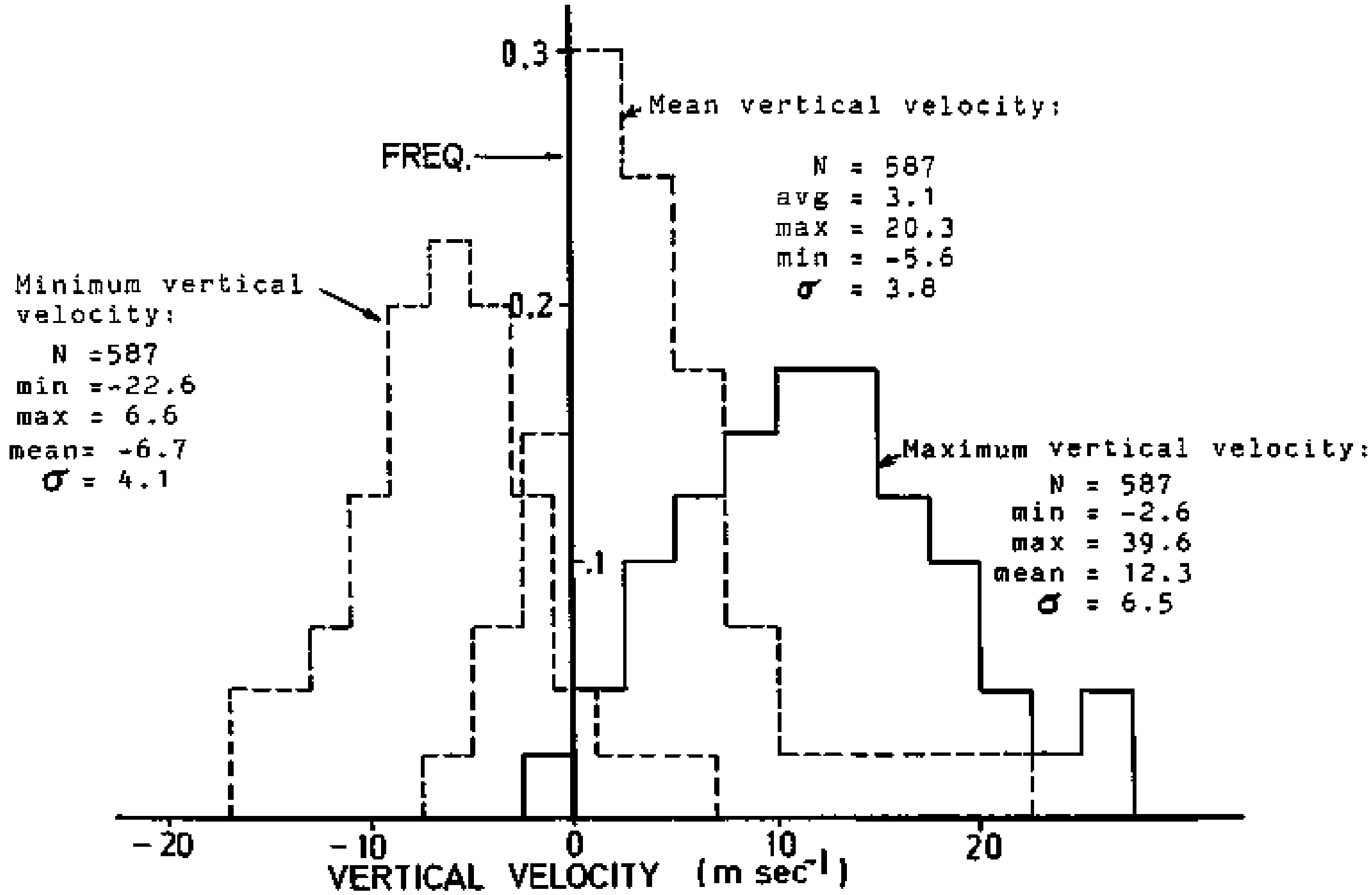

Fig. 5.2.0. The average maximum and minimum vertical velocities for all first passes in the cloud sample database with good vertical velocity data.

vertical motion system be functioning.

Table 5.1 Means, extremes and standard deviations for average updraft and average downdraft (all speeds in m sec^{-1})

	minimum	average	maximum	std.dev.	N
average updraft	0	5.5	23.0	3.3	583
average downdraft	-10.4	-2.7	0	1.4	568

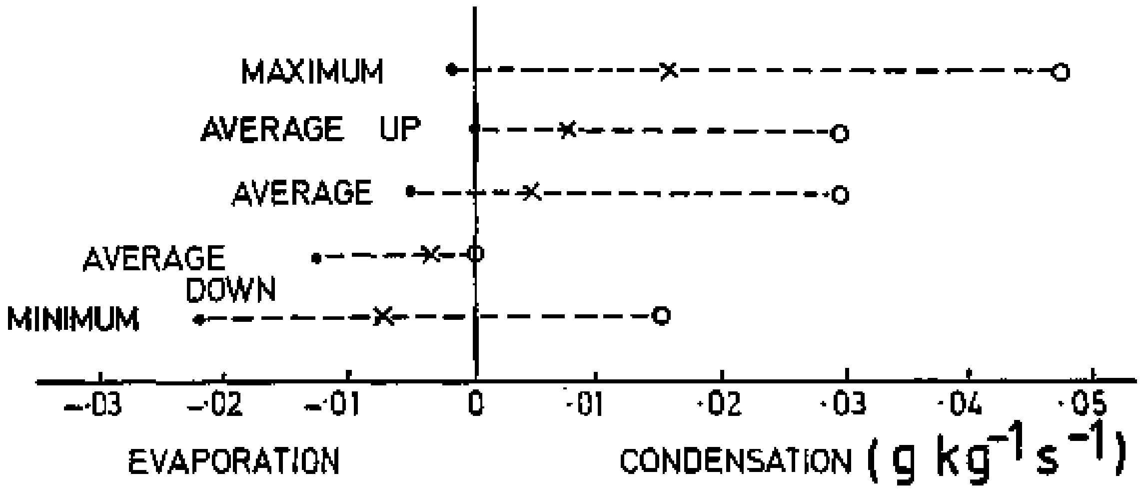

Figure 5.2.1. The condensation rate in Nelspruit clouds, 1984/85 season. Averages indicate computations performed over the upward and downward moving portions of the clouds.

Fig. 5.2.1 shows condensation rates estimated at flight level for clouds examined during the 1984-85 PAWS field season, calculated as described in Vol. IV Section 10.3. The updraft condensation rates are at times quite high, reflecting not only strong updrafts but also the warm, moist subcloud air frequently encountered in the region.

5.3 Fluxes

Cumulus clouds can be viewed as the visible part of a very special type of airmass mixing. They transport large amounts of warm air from near the earth's surface through very deep layers of the atmosphere. With some simple assumptions (discussed in Vol. IV Section 10.4) it is possible to look at the magnitude and variability of air and water vapour fluxes in the clouds.

Table 5.2 gives the means, extremes and variability of the air and vapour fluxes in a large number of clouds (first penetrations only).

The average airmass flux in turrets is in the neighbourhood of 20 kton sec^{-1}, or 20×10^{9} g sec^{-1}. This is an order of magnitude or two less than the flow estimated in mature thunderstorms or hailstorms. The vapour flux is three orders of magnitude less than the mass flux, since vapour density bears that relationship to air density. An additional view of the overall sizes of the cloud turrets is given in Table 5.3 which summarizes measurements of outside dimensions of cells. Cloud width estimates are based on time in cloud and true air speed. Cloud cross-sectional area is simply the area of a circle whose diameter is the cloud width. Cloud top heights were calculated based on video measurements (see Vol. IV Section 10.11). The sample size is determined by equipment status, cloud width measurements requiring that the FSSP and JW be working, for determining cloud boundaries.

5.4 Mixing

The fluxes have been divided into their upward and downward components. The cloud turrets investigated by PAWS often contain both up and downdrafts. The existence of downdrafts in rising clouds is a well known manifestation of mixing. To isolate this phenomenon, we have established for each traverse the percentage of the distance flown in cloud which was updraft. Fig. 5.4.0 shows that, the stronger the updraft, the greater the percentage of the cloud it occupies.

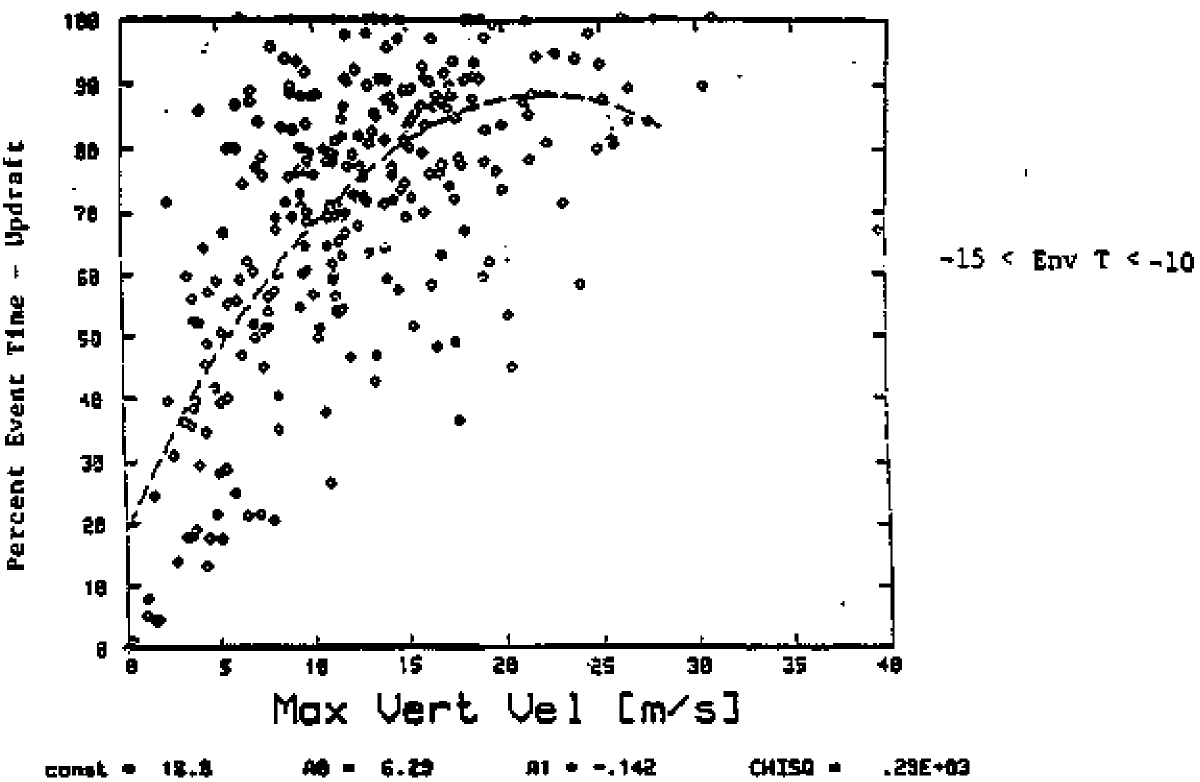

Fig. 5.4.0. The percent of cloud pass which contained upward motion vs the maximum vertical velocity encountered for cloud passes between -5 and -15°C.

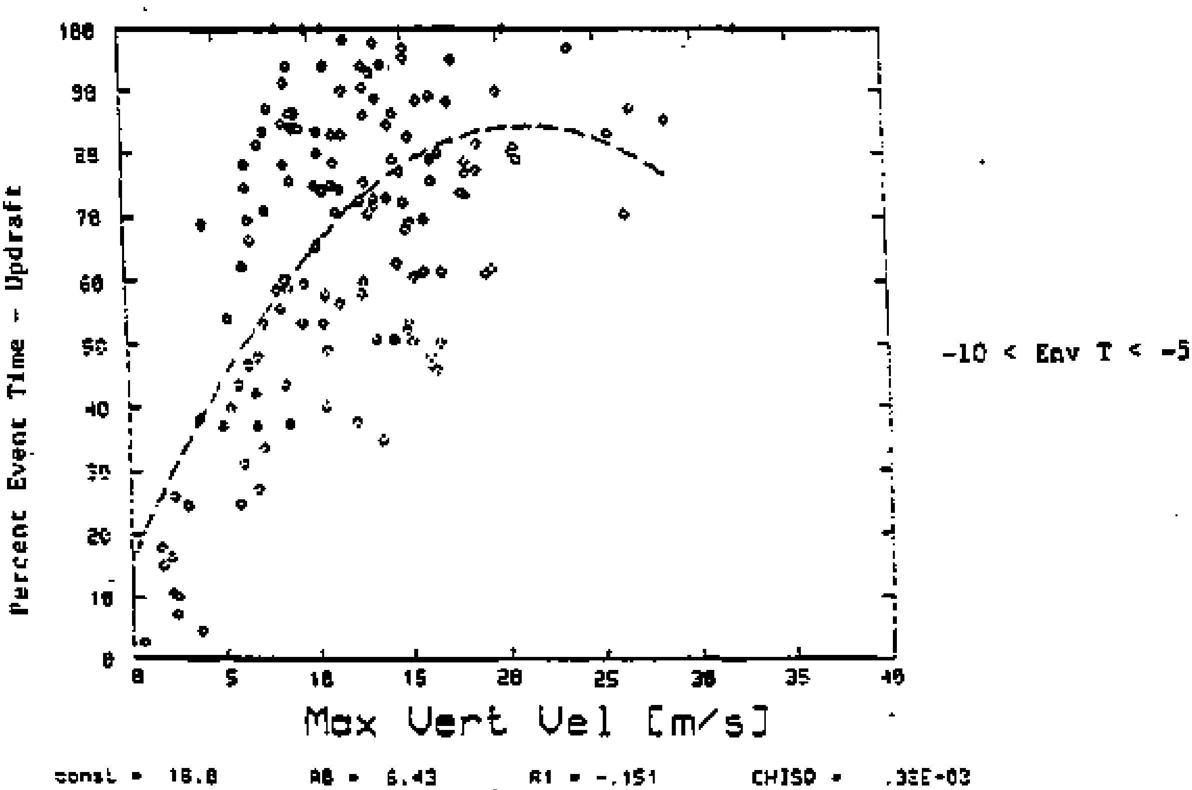

Table. 5.2 Summary of the fluxes of air and water vapour in cloud turrets, first passes only.

	min	avg	max	std.dev.	N
air mass flux kton sec^{-1}	-29.7	18.85	282.6	35.0	587
air mass upflux kton sec^{-1}	0	22.9	291.7	35.5	587
air mass downflux kton sec^{-1}	-55.7	- 4.0	0	6.32	587
Vapour flux ton sec^{-1}	-92.9	56.4	1027.6	113.4	585
Vapour upflux ton sec^{-1}	0	67.4	1056.8	114.9	585
Vapour down-flux ton sec^{-1}	-95.3	-10.2	0	15.5	580

Table 5.3 A summary of cloud dimensions (first passes only)

	min	avg	max	std.dev.	N
cloud width (km)	0.5	2.9	9.4	1.4	439
cloud cross sectional area (km^2)	0.17	8.1	70.9	8.2	439
Video cloud tops (m asl)	6000	7259	9200	642	32

The influence of mixing on Nelspruit clouds is better shown by looking at its effect on the thermodynamics. It has been possible to show, with the Total Water Content Instrumentation on board the Learjet (Vol. IV Section 9.1) that at least some portions of the interiors of clouds, around the -10°C level, are close to being unmixed. That is, the innermost cores (at least), are adiabatic; the peak measured values of Total Water Mixing Ratio lie very close to the water vapour mixing ratio averaged over the lowest layers above the ground. That in itself is a very satisfying result, and of considerable consequence to our understanding of the clouds. A better way to show the net effect of mixing on the clouds is to consider the percentage of the flux of air in the cloud which contains various fractions of the adiabatic Total Water Mixing Ratio (TWMR) value. Fig. 5.4.1

shows the cumulative frequency of upward flux versus the ratio between TWMR and the adiabatic value, for 25 clouds with little or no precipitation content and adiabatic Total Water Contents as estimated by the Engine-Vapour method. It is clear that sizeable percentages of the upward flux in these clouds are close to being adiabatic.

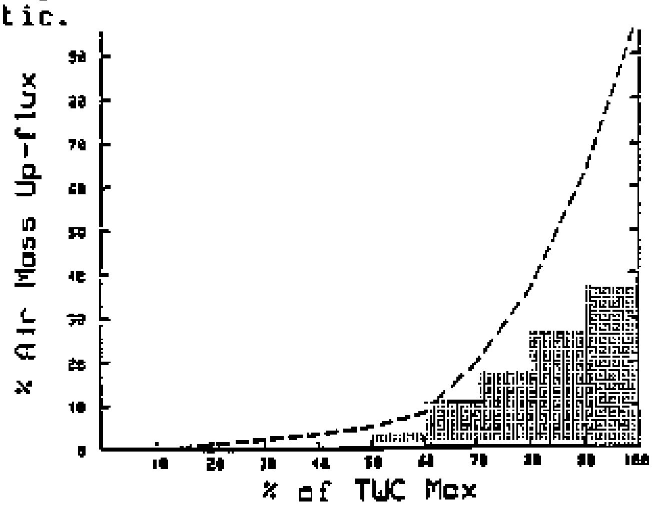

Figure 5.4.1. The distribution of upward air flux as a function of the Total Water Mixing Ratio (TWMR) divided by its maximum value in each cloud, for 25 clouds with little or no precipitation and adiabatic peak values of TWMR. Dashed curve is cumulative, the shaded histogram is frequency.

5.5 Buoyancy

The motions within cumulus clouds, whose dimensions and magnitude have just been shown, are driven by non-hydrostatic forces and inertia, opposed by drag. These are rather complex both theoretically and practically. It is conventional in discussing cumulus cloud motions to simplify the cloud dynamics to very few elements. Kinetic energy is put into the base of the cloud (cloud base updraft) presumably by some impulse or lifting mechanism and subsequent changes in energy are predicted based on the concept of buoyancy. This is expressed as the temperature difference between the cloud and its environment.

The buoyancy in clouds can be estimated from the temperature measurements of the Lear. The buoyancy is really the difference in density between cloud and environment and density is proportional to the virtual temperature, which takes account of the water vapour in the air.

More important is the effect of the condensed water in the cloud on the air density. For this we have calculated the Cloud Virtual Temperature (Vol. IV Section 10.9) which includes a correction term based on the Condensed Water Content measured by the Engine-Vapour technique. This correction lowers the buoyancy significantly in many cases.

Fig. 5.5.0 shows histograms of excess temperature (average in-cloud temperature minus environmental temperature) and excess cloud virtual temperature (average T_{cv} in cloud minus environmental temperature) averaged across the width of the cloud. The excess temperature distribution shows a mean value of zero with 48 % of the sample being buoyant and the rest not. The excess T_{cv} distribution seems shifted to the left by about a degree (the mean is -0.9°C) and results in only 13% of the sample being buoyant.

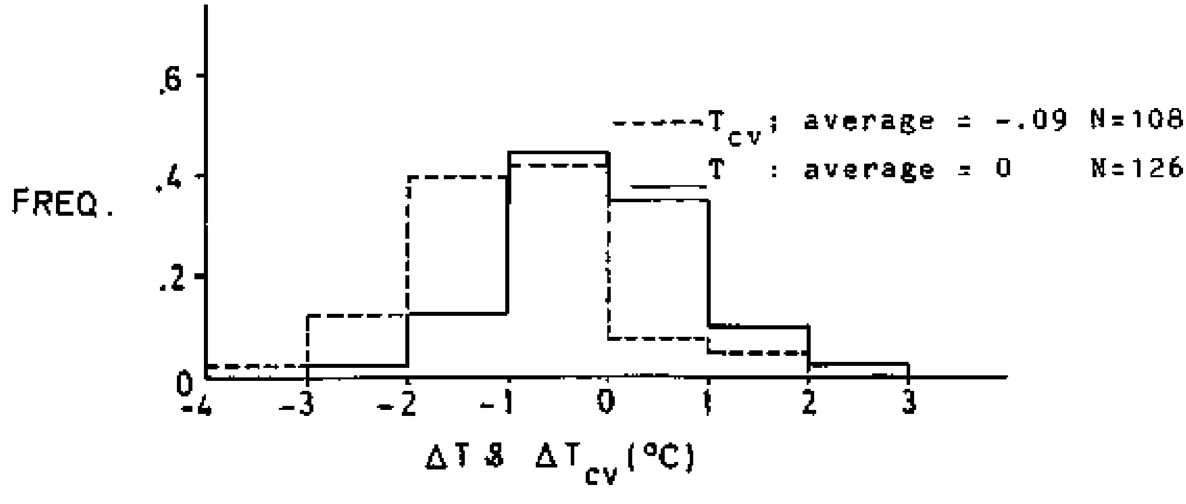

Figure 5.5.0. The excess temperature (T) and the excess Cloud Virtual Temperature (T_{cv}) distributions.

This is a very important point. Whichever way one summarizes the buoyancy, and even allowing for a slight negative biasing effect due to the random occurrence of wetting of the element of the Rosemount temperature probe, the buoyancies are not large. Though buoyancy is a contributor to updraft development in turrets on convective complexes in Nelspruit, other forces are equally or more important. What is required is convergence at cloud turret scale, not only below cloud base, but through deep layers of the lower cloud. The low buoyancies shown here suggest that the modest increases in cloud temperature which are shown to be possible by freezing liquid water (see Vol. IV Section 9.11 and 10.7) in Nelspruit clouds are potentially important to the Nelspruit cloud seeding hypothesis.

5.6 Hydrometeors in Nelspruit Clouds

Nelspruit clouds exhibit a very characteristic range of hydrometeor sizes and types. At cloud penetration altitudes the cloud droplet concentrations are fairly low due to the modified maritime character of the boundary layer airmass and the high degree of coalescence which often takes place in the lower part of the cloud. Mean cloud droplet sizes are large, due to the high condensation rates. Precipitation sized particles (diameters 100 um, visible on the 2D-C records) can be water drops, graupel or a mixture of both. Pristine crystal shapes are rarely seen except occasionally at cloud edges in the -15^{o}C region and in anvils. Aggregates of indiscernible types are seen occasionally at colder temperatures.

5.6.1 Cloud droplets and coalescence products

It is difficult to discuss the cloud droplets alone because they are in constant interaction with the larger particles in the hydrometeor spectrum. This will become evident later on when coalescence is discussed. Here we will just display some magnitudes.

The concentrations of cloud droplets have been described above as low. The range of concentrations is given in Table 5.4 for several subsets of the cloud-sample database.

Table 5.4 Statistical summary of measurements of cloud particle concentrations and mass weighted mean diameters (MWMD)

	min	avg	max	std.dev.	N
average FSSP concentration (cm^{-3})	47.2	318.3	676.6	88.6	439
max FSSP concentration (cm^{-3})	61.0	421.2	895.3	104.3	439
average FSSP MWMD	8.8	21.5	26.3	2.1	439

The sizes of cloud droplets are also summarized in Table 5.4.

The concentrations and average sizes of cloud droplets are not independent. They bear an inverse relationship to each other, as shown in Fig.5.6.0. The data points on this graph are storm averages.

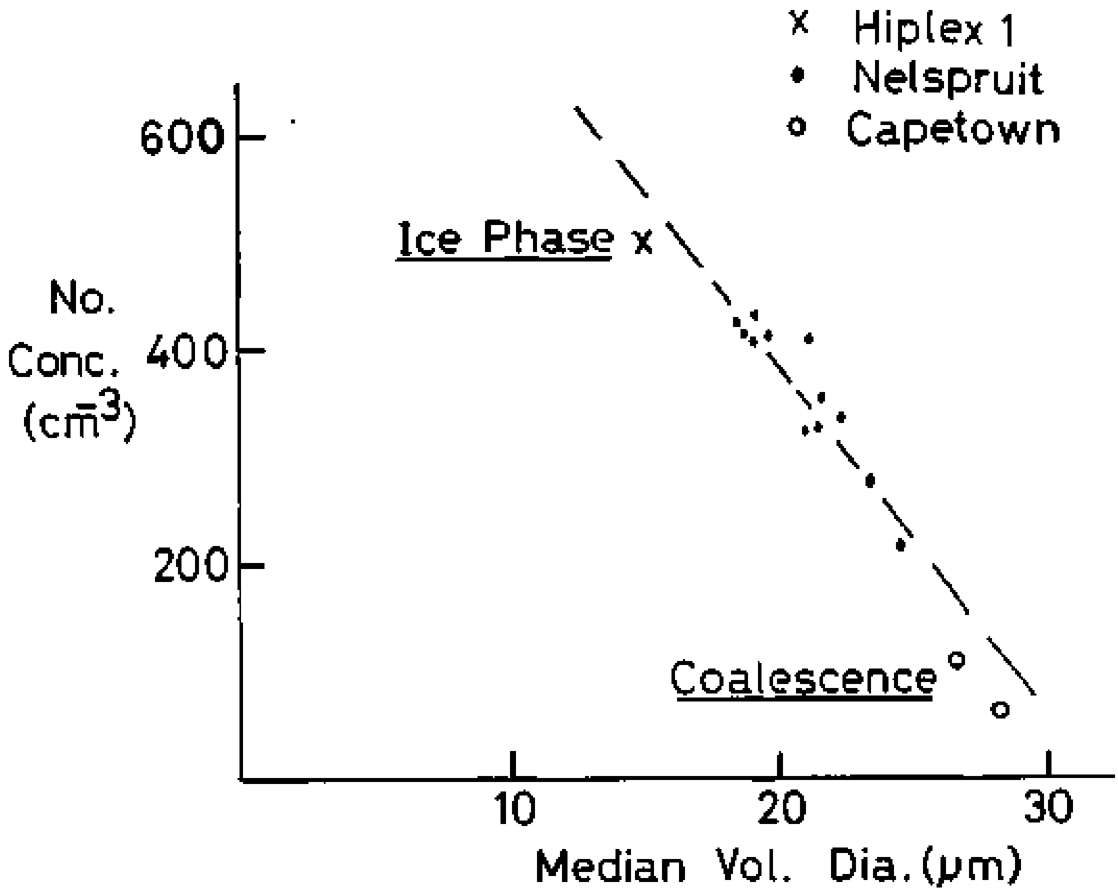

Figure 5.6.0. A relationship between number concentration and median volume diameter used to classify and compare Nelspruit clouds.

The liquid water content in clouds is measured by three techniques. Two are hot wire devices, the Johnson-Williams (JWD) Liquid water meter and the King liquid water meter. The other is the FSSP cloud droplet spectrometer. The hot wires give liquid water content (g m^{-3}) as a direct output; the FSSP presents a size spectrum which must be integrated over all sizes to estimate the LWC.

The King hot wire has been a very important instrument for our research. In fact, since it has been mounted on the aircraft we have decided to remove the JW. The measurements of the King instrument, however, require judgement on the part of the analyst due to a saturation which occurs in most clouds so it will not be used here to describe cloud LWC values.

The liquid water content in the cloud diameter range is shown in Table 5.5, measured by two instruments, the Johnson-Williams hot wire and the FSSP.

Table 5.5 A summary of measurements of cloud liquid water content (LWC) by two techniques, the Johnson-Williams hot wire (JW) and the Forward Scatter Spectrometer Probe (FSSP), first passes only.

	min	avg	max	std.dev.	N
average JW LWC (g m^{-3})	0	0.9	2.32	0.42	439
max JW LWC (g m^{-3})	0	1.57	3.03	0.6	439
average FSSP LWC (g m^{-3})	.08	1.07	2.82	0.4	439
max FSSP LWC (g m^{-3})	.09	1.56	4.52	0.5	439

At cloud penetration altitude, the process of precipitation formation in active clouds is already well underway, but not always observable by our conventional instruments. The reason for this is discussed in Vol. IV Section 9.1. In clouds in which no precipitation particles are revealed by the 2D-C probe, the cloud liquid water contents are markedly less than the adiabatic values. The Engine-vapour instrumentation, however, shows the presence of roughly adiabatic values of condensed water. The additional water thus revealed consists of drops which are the products of coalescence. We are unable to measure their sizes, but expect them to lie in the 50 - 150 um diameter range. (Since this was written, a King hot wire device has been installed on the Learjet. In the absence of 2-D activity, there is excellent agreement between cloud liquid water contents measured by the King and the Engine-Vapour instruments. Both the FSSP and JW instruments considerably underestimate the liquid water content in most clouds in the Nelspruit area). Fig. 5.6.1 (discussed further in Vol. IV Section 9.6), shows that, in clouds with little or no precipitation (2D-C average concentration less than 10 l^{-1}), the number of cloud particles is inversely proportional to the mass of the coalescence products. This demonstrates the important interaction between the cloud particles and the rest of the particle spectrum. The data of Fig. 5.6.1 are averages over cloud passes, not core or parcel measurements. The negative regression shows up well in spite of the averaging and in spite of other factors' variations, indicating that the effect of the coalescence is a strong one.

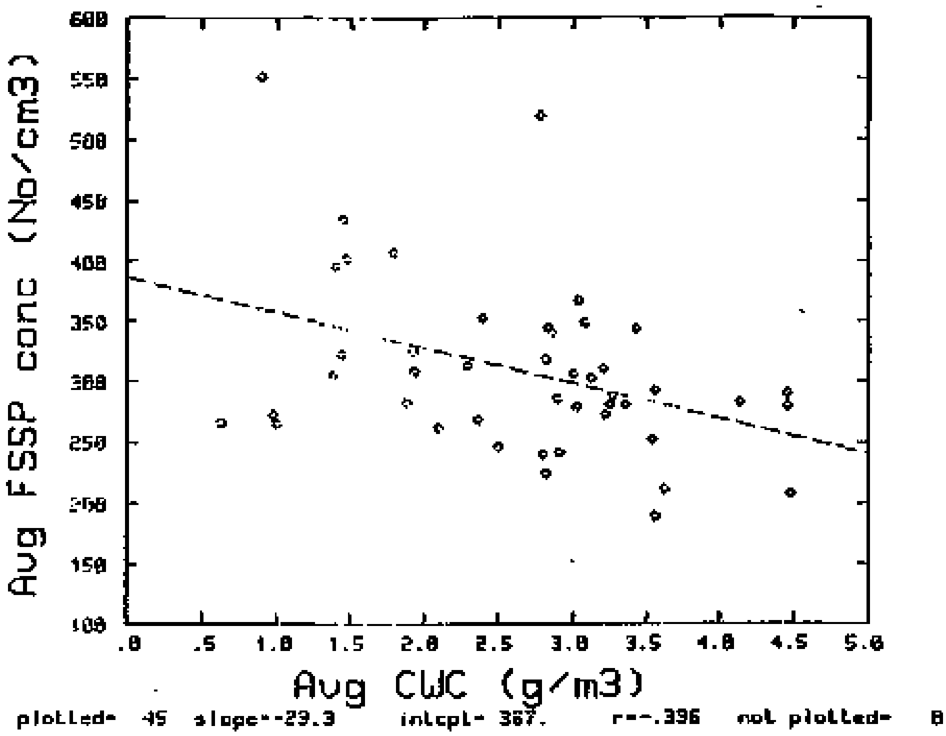

Figure 5.6.1. The dependence of FSSP cloud particle concentrations on Condensed Water Content measured by the E-V technique in clouds between -8 and -12°C which contain little or no precipitation.

The coalescence products contain a considerable portion of the condensed water in the clouds. We are able to estimate the total Condensed Water Content (CWC) with the newly developed Engine-Vapour technique (Vol. IV Section 9.1) and Table 5.6 allows comparison of those estimates with the estimates of (JW and FSSP) cloud water only. The CWC is on average more than twice the cloud water, indicating that the coalescence products contribute a major portion of the total CWC.

Table 5.6 Comparison of Mean Condensed Water Contents (measured by the Engine-Vapour technique) with Cloud Liquid Water Content (measured by JW and FSSP) in clouds containing no precipitation particles.

	LIQUID WATER CONTENT (g m^{-3})								
	0-1	1-2	2-3	3-4	4-5	5-6	6-7	Avg	Std.Dev
Engine-Vapour system	0	1	4	2	11	1	1	4.02	1.10
J-W hot wire	1	13	6	0	0	0	0	1.71	0.42
FSSP	0	14	6	0	0	0	0	1.91	0.44

5.6.2 Liquid Precipitation Particles

The first precipitation particles to appear in a cloud at the -10°C level, as revealed by the 2D-C, are often water drops. This is just an advanced stage of development of the coalescence process described just above. Often, a mixture of ice (graupel) and water particles appear. In those cases, the ice particles are quite round in shape and are probably rimed frozen drops of fairly high density. Coalescence is the precipitation generation mechanism in these clouds and probably plays a strong role in most Nelspruit clouds.

A published study (Mather et al., 1986) has shown that the appearance of precipitation in the form of large drops or large drops and graupel is predictable by parameters from the environmental sounding. Fig. 5.6.2 shows the excellent discrimination between drops and no drops on a plot of cloud base temperature versus buoyancy at 500 mb. The appearance of large drops appears to be favoured by a deep layer between cloud base and the -10°C level, and by a long time of passage of the cloud air parcel between those levels. This conforms to theoretical considerations.

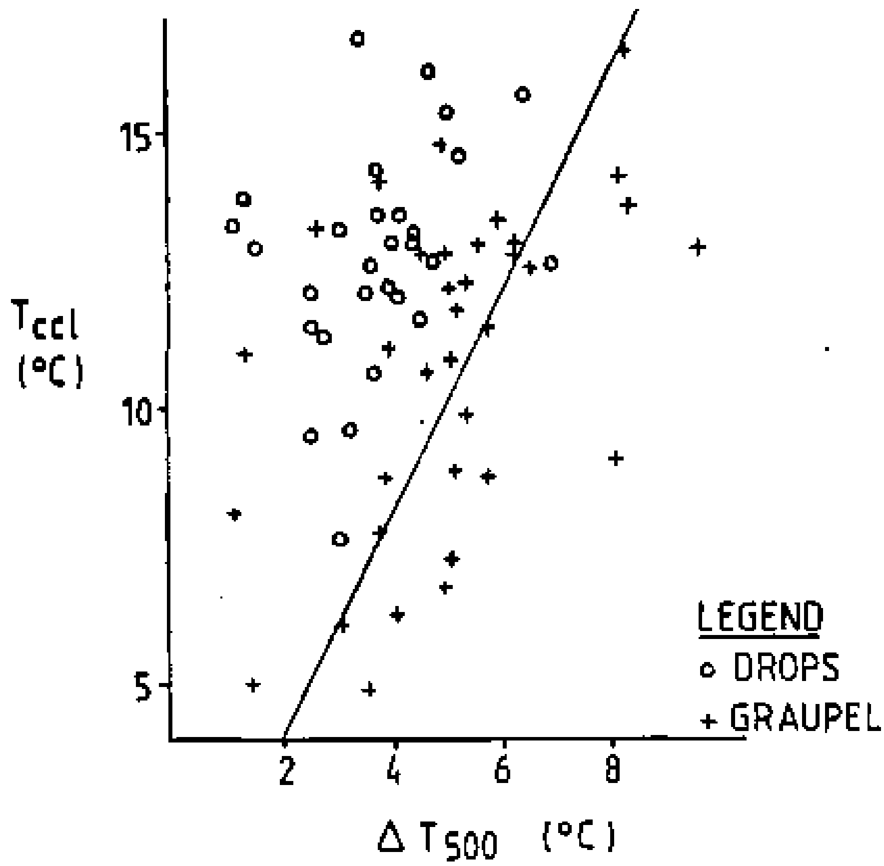

Figure 5.6.2. Plot of convective condensation levels (CCL) temperatures versus buoyancies at 500 mb for the storms in this study. Circles represent those storms containing some images of drops. Crosses represent those storms in which graupel images only were detected.

5.6.3 Ice (Graupel) Precipitation Particles

At times the first precipitation in clouds at -10°C is in the form of graupel particles or a mixture of graupel particles and water drops. This is due to ice nucleation, which is a difficult phenomenon of great theoretical and practical importance to the field of cloud physics.

The variability of ice concentrations in Nelspruit clouds shows an important component of the precipitation process. It also underlines the importance of understanding and predicting the degree of ice formation. An exploratory study of the variations of ice nucleus concentrations was carried out in February-March 1986 at Nelspruit and is described in Vol. IV Section 12.

A study of the occurrence of ice in vigorous (mean vertical velocity$>$2.5 m sec^{-1}) clouds (see Vol. IV Section 9.8) between the levels of -3°C and -22°C has shown that large liquid drops can be found in clouds even at -20°C, and ice particles can be found even at -5°C. Also, a fraction of clouds can be found at all the heights considered with no detectable precipitation sized particles in them. Fig. 5.6.3 summarizes the fractions of clouds with and without ice and with and without drops as a function of temperature. Fig. 5.6.4 shows the percent of clouds which contained ice only and water only, over the same temperature range.

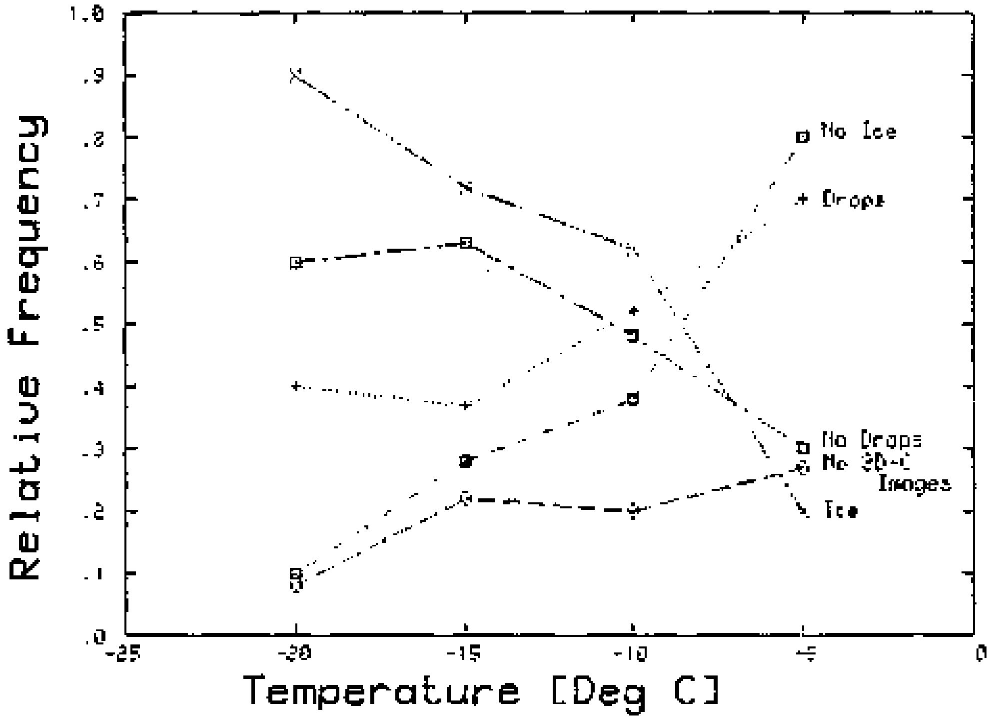

Figure 5.6.3. Summary of the frequency of occurrence of clouds with ice particles and water drops, or no precipitation, as a function of the environmental temperature at penetration level.

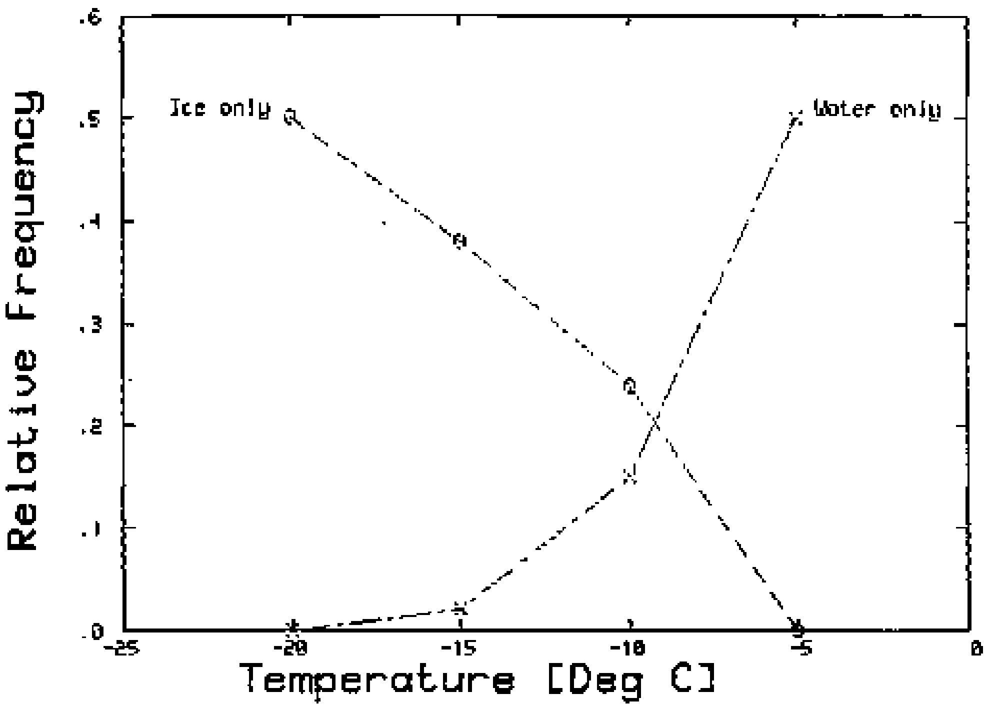

Figure 5.6.4. Summary of the frequency of occurrence of clouds which contained precipitation particles which were ice only or water drops only.

A study was made of the concentrations of ice particles in those clouds of the study just described which contained ice particles only. It was necessary to determine these for the entire layer between -8°C and -17°C. These are shown in Table 5.7. The sample sizes are smaller in the last two rows because zeros were not used in the calculations.

Table 5.7 The variability of ice concentrations in clouds with average updraft speeds greater than 2.5 m sec^{-1}, with 2D-C image classifications graupel and ice.

	avg	max	std.dev	N
2D-C concentration averaged over cloud (l^{-1})	20.3	137.1	29.3	52
maximum 2D-C concentrations (l^{-1})	78.4	684.5	140.9	52
avg zero image concentration (l^{-1})	6.1	50.3	10.8	52
max zero image concentration (l^{-1})	21.7	196.7	38.3	52
avg D<128 um concentration (l^{-1})	10.4	79.0	17.2	52
max D<128 um concentration (l^{-1})	41.3	438.6	80.2	52
avg D>128 um conc (l^{-1})	10.5	61.7	12.9	52
max D>128 um conc (l^{-1})	44.2	455.0	79.8	52
avg D>1067 um conc (l^{-1})	.247	1.145	.285	38
max D>1067 um conc (l^{-1})	1.8	16.9	3.6	38

5.6.4 Radar Reflectivity in Cloud Turrets

The reflectivity from a single range gate of the Learjet's airborne radar is recorded as part of the digital data set, on magnetic tape. The range gate is situated 1.5 km (about 10 sec of flight) straight ahead of the aircraft and the data are time shifted during processing to bring them into coincidence with the rest of the data set.

Radar reflectivity interpretation is very complex, and always subject to many uncertainties. Reflectivity is however a good general index of the state of development of the precipitation in clouds. In most cases radar is the only view one has of this. Our recorded airborne radar reflectivities are thus a proper component of this physical description of Nelspruit cloud turrets.

Fig. 5.6.5 shows the histograms of average and peak radar reflectivities from a large sample of clouds studied during the 1984-85 and 1985-86 seasons. They show that most frequently the clouds examined have weak reflectivities. Many times, however, the radar indicates advanced precipitation development. On a few occasions, reflectivities corresponding to very heavy rain were encountered.

This description of the clouds at Nelspruit is a synopsis of observations and analyses carried out through the 1985-86 season. Further analyses and more observations can be expected to further sharpen our comprehension of the precipitation mechanisms that are active in Nelspruit clouds.

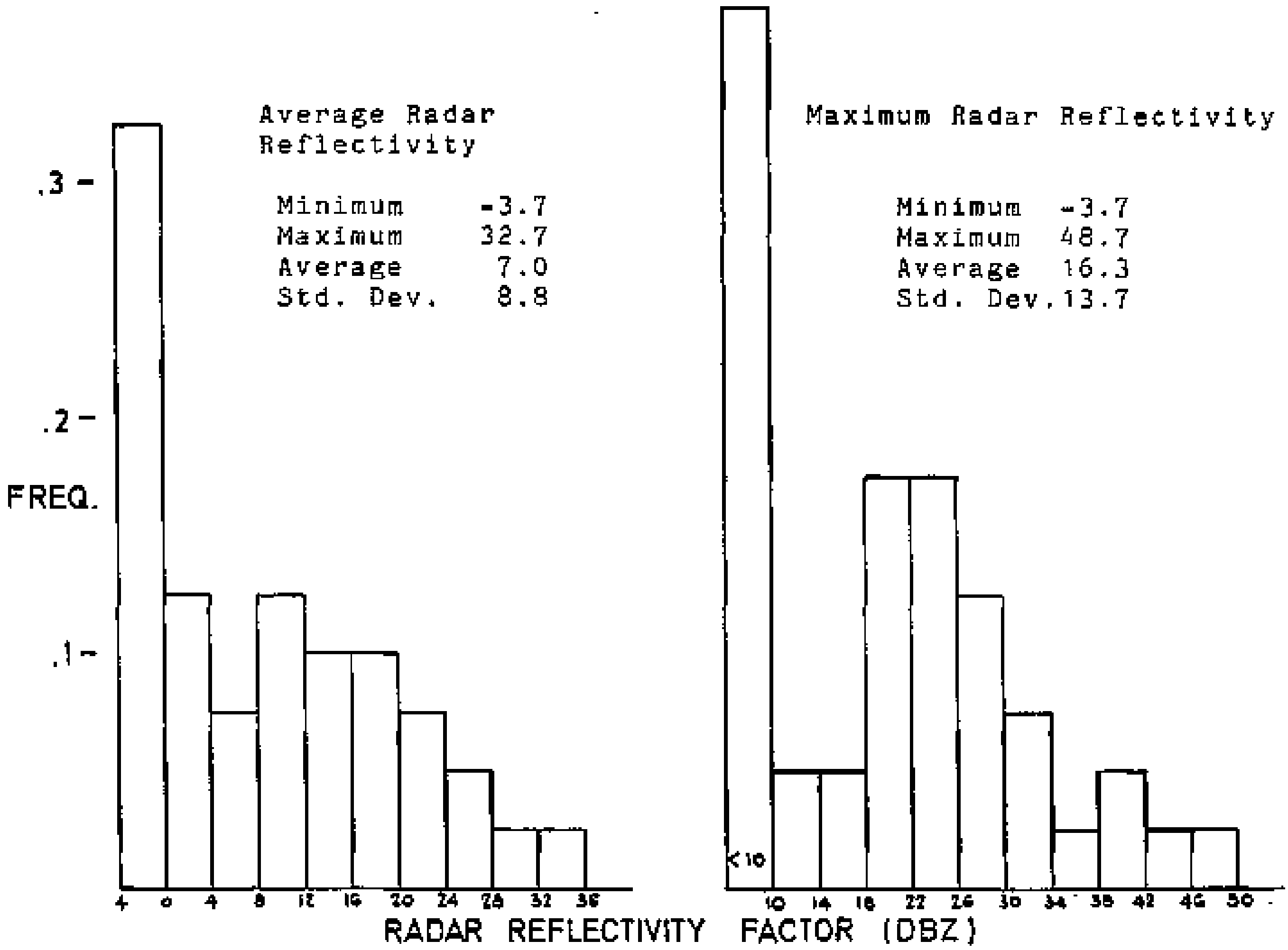

Figure 5.6.5. Histograms of average and peak radar reflectivities from a large sample of clouds studied during the 1984/85 and 1985/86 seasons. All data are from first passes through turrets rising on the flanks of multicell storms.

5.6.5 The Precipitation Efficiency of Cloud Turrets in the Nelspruit Study Area (Morgan and Morrison)

Precipitation efficiency is an important concept in the fields of cloud physics and weather modification. In fact, it is the very concept which gives rise to some of the modern concepts for enhancing rainfall by artificial means.

Perhaps the most common definition of the precipitation efficiency of a cloud system is the sum total of the precipitation reaching the ground during the system's lifetime divided by the sum of all the water vapour entering its base during the same period. Such a definition is not very useful because of the difficulty of measuring the required quantities.

For the study of Nelspruit clouds we have employed a definition of efficiency which is suited to the measurements made by the instrumented Learjet. With the Learjet we measure quantities within the cloud which allow an estimate of the local and instantaneous efficiency. Vol. IV, Sect. 9.5 gives the details underlying two indeces of local efficiency, the conversion efficiency and the reservoir effect.

The conversion efficiency is the rate at which cloud water is being converted into precipitation (through capture by precipitation and through coalescence to form new precipitation particles) divided by the condensation rate (the rate at which cloud water is being replaced). A value of one would indicate that precipitation was growing (by capturing cloud droplets) exactly as fast as cloud was being made available by the condensing of vapour.

Fig. 5.6.6 shows the cumulative distributions of conversion efficiency index as measured in 299 unseeded cloud turrets in four temperature ranges. The warmest clouds (-4 to -8°C) clearly have lower efficiences than the colder ones. The curves for the colder temperature intervals are grouped together, and indicate a wide range of efficiencies, with over 50 percent of clouds having index values of less than 1.0.

Another important factor is the reservoir of cloud water which is available for the growth of precipitation. If there is a high liquid water content, precipitation will continue to grow for some time, even if the condensation rate is low and this, called the Reservoir Effect Index, is computed by dividing the precipitation growth rate by the cloud liquid water content. It indicates the fraction of the cloud water content which is being converted to precipitation each second, and has dimensions sec^{-1}. A value of 10^{-3} indicates that a thousandth of the cloud liquid water content (ingorning condensation) is being converted to precipitation each second, and that a time of the order of 1000 seconds (15 minutes) would be required to completely consume the cloud. An index value of 10^{-1} indicates that a tenth of the cloud water is being converted each second, and that the cloud will disappear in about ten seconds. The inverse of the Reservoir Index is similar to, but not the same as, the depletion time discussed in Knight et al., (1982).

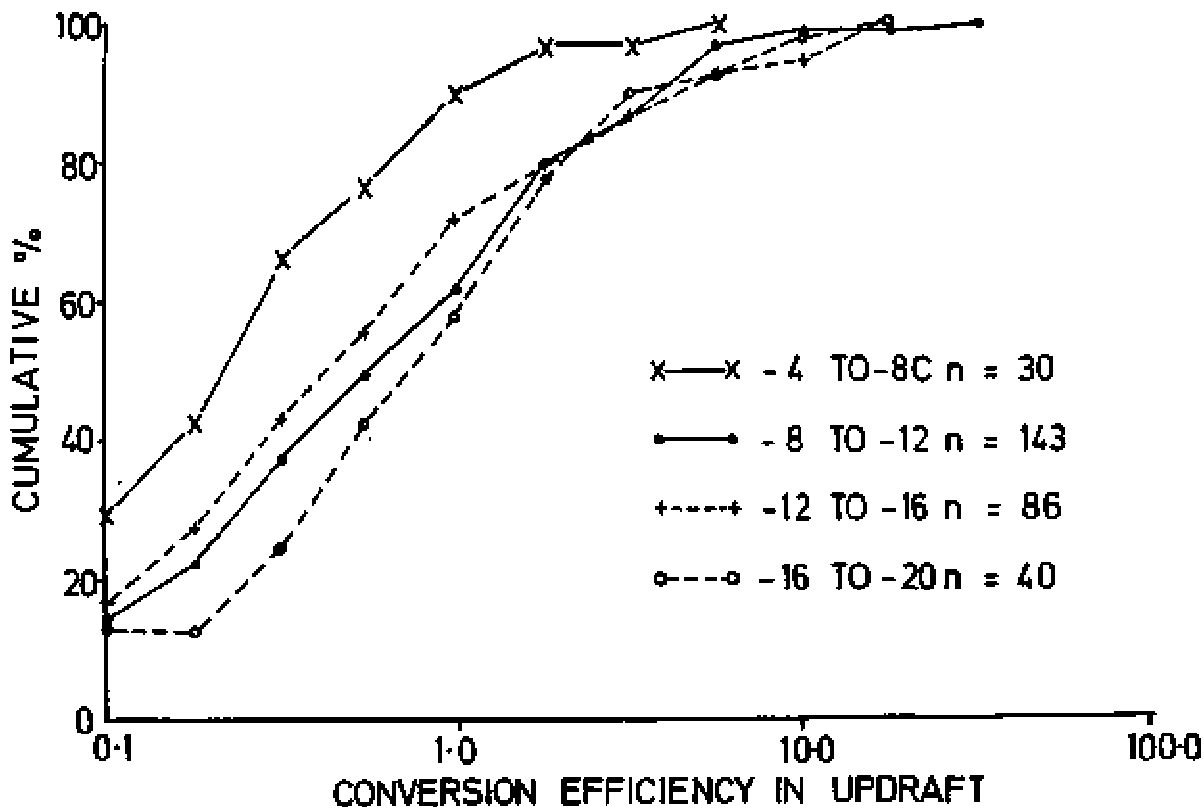

Fig. 5.6.6. Conversion efficiencies (CE) over four temperature ranges computed for all "first pass" cloud turrets (untreated).

Fig. 5.6.7 shows cumulative distributions of the Reservoir Effect Index for 299 unseeded turrets in four temperature intervals. Again, the warmest clouds show different behaviour from the colder ones, with low values of the reservoir index indicating an excessive cloud water content relative to the precipitation content. The colder clouds exhibit a wide range of index values, with roughly half having values less than 3×10^{-3} (consumption time, scale of 300 seconds or 5 minutes).

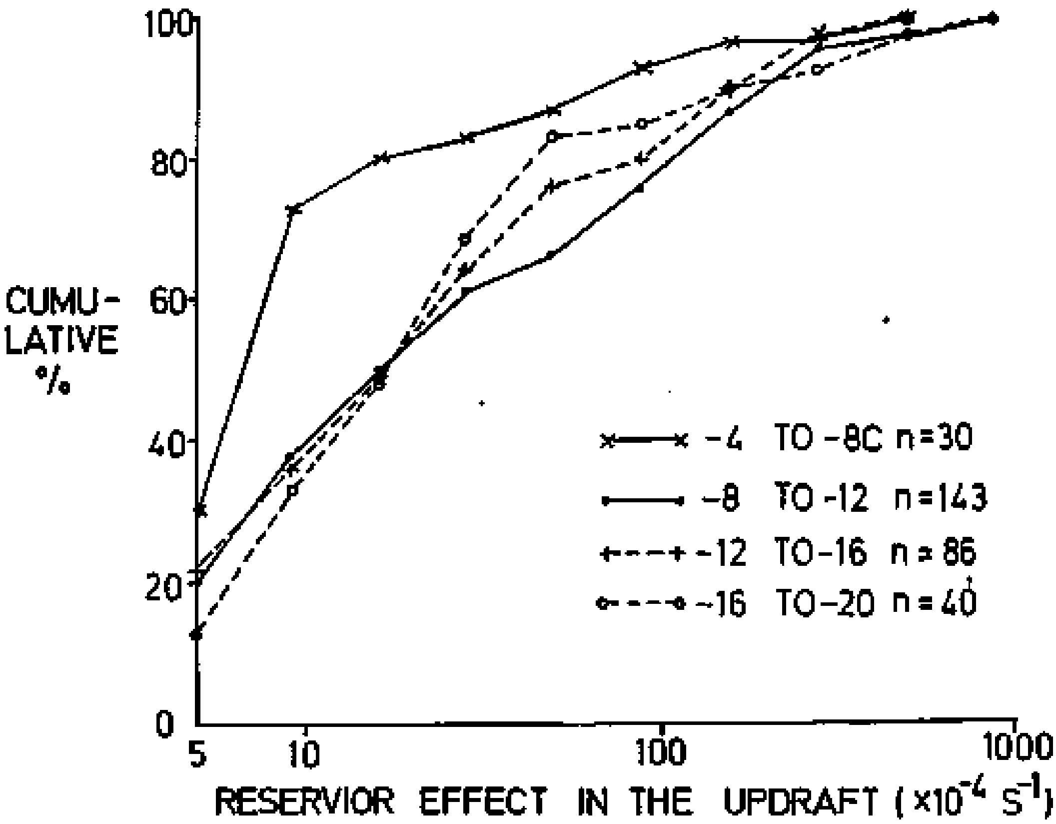

Fig. 5.6.7. Reservoir effects (RE) over four temperature ranges for all first pass cloud turrets.

6.0 REFERENCES

Byers, H.R., and R.R. Braham, Jr., 1949: The Thunderstorm. Washington, D.C., Government Printing Office.

Diab, R., and M. Garstang, 1985: Wind power dependence upon weather systems. Internat. J. Amb. Energ., 6, 89-100.

--------, and -------, 1986: Classification of synoptic weather regimes in South Africa by discriminant analysis. Proc. of the 2nd Internat. Conf. on Southern Hemisphere Meteorology, 1-5 December, Wellington, New Zealand.

Gabriel, K.R., 1972: Analysis of meteorological data by means of canonical decomposition and biplots. J. Appl. Meteor., 11, 1071-1077.

Garstang, M., and G.D. Emmitt, 1983: Anatomy of drought. Symposium on Atmospheric Sciences in South Africa, 18-20 October, Pretoria, South Africa.

--------, G. Brier, B. Kelbe and R. Diab, 1983: Synoptic controls and long term periodicity in southern hemisphere rainfall. Proc. of 1st Internat. Conf. on Southern Hemisphere Meteorology, 31 July - 6 August, Sao Jose dos Campos, Brazil.

--------, B. Kelbe, G.D. Emmitt and W. London, 1986: Generation of convective storms over the escarpment of northeastern South Africa. To be published in Mon. Wea. Rev.

Harrison, M.S.J., 1984: A generalized classification of South African summer rain-bearing synoptic systems. J. Climat., 4, 547-560.

--------, 1986: A synoptic climatology of South African rainfall variations. Ph.D dissertation, University of the Witwatersrand, Johannesburg, South Africa, 341 pp.

Kelbe, B., and M. Garstang, 1983: The initiation of deep convection over northeastern South Africa and Swaziland. Proc. 1st Internat. Conf. on Southern Hemisphere Meteorology, 31 July -6 August, Sao Jose dos Campos. Brazil.

-------, M. Garstang and G. Brier, 1983: Analysis of rainfall variability in the northeastern region of South Africa. Arch. Met. Geoph. Biocl., Ser. B. 32, 231-252.

Kessler, E., 1969: On the distribution and continuity of water substance in atmospheric circulation. Meteor. Monogr., 32, 84 pp.

Knight, C.A., W.A. Cooper, D.W. Breed, I.R. Paluch, P.L. Smith and G. Vali, 1982: Microphysics, in Hailstorms of the Central High Plains, Vol I The National Hail Research Experiment, Knight and Squires, eds., Colorado Associated University Press, Boulder, Colorado, pp 151-193.

Mather, G.K., B.J. Morrison and G.M. Morgan, Jr., 1986: A preliminary assessment of the importance of coalescence in convective clouds of the Eastern Transvaal. J. Climate Appl. Meteor., 25, 1780-1784.

PAWS, 1984: Annual report on the Program for Atmospheric Water Supply by Simpson Weather Associates, Inc., Charlottesville, Virginia, and Cansas International Corporation, Nelspruit, South Africa to the Corporation for Atmospheric Water Supply, Pretoria. South Africa.

RAIN, 1983: Rain augmentation in Nelspruit: Phase II final report. Prepared by Simpson Weather Associates, Inc., Charlottesville, Virginia, 148 pp.

Tyson, P.D., 1980: Atmospheric circulation changes and the occurrence of extended wet and dry spells over southern Africa. I.G.U Working Group on Desertification in and Around Arid Lands, Fujinomiya, Japan.

-------, 1984: The atmospheric modulation of extended wet and dry spells over South Africa, 1958-1978. J. Climat., 4, 621-635.

Ulanski, S.L., and M Garstang, 1978: The role of surface divergence and vorticity in the life cycle of convective rainfall, Part I: Observations and analysis. J. Atmos. Sci., 35, 1047-1062.

Woodley, J.C., J. Jordan, A. Anthony, J. Simpson, R. Biondini and J. Flueck, 1982: Rainfall results of the Florida area cumulus experiment, 1970-76, J. Appl. Meteor., 21, 139-164.